

MICROCOPY RESOLUTION TEST CHART  
NATIONAL BUREAU OF STANDARDS-1963-A

//

DOT/FAA/CT-82/29

# Correlation of Flammability Test Data on Antimisting Fuels

AD A127142

Levelle Mahood  
Robert L. Talley

Falcon Research & Development Co.  
109 Inverness Drive East  
Englewood, Colorado 80112

December 1982

Final Report

APR 25 1983  
A

This document is available to the U.S. public through the National Technical Information Service, Springfield, Virginia 22161.

DTIC FILE COPY



U.S. Department of Transportation  
**Federal Aviation Administration**  
Technical Center  
Atlantic City Airport, N.J. 08405



83 04 22 076

#### NOTICE

This document is disseminated under the sponsorship of the Department of Transportation in the interest of information exchange. The United States Government assumes no liability for the contents or use thereof.

The United States Government does not endorse products or manufacturers. Trade or manufacturer's names appear herein solely because they are considered essential to the object of this report.

1. Report No. DOT/FAA/CT-82/29		2. Government Accession No. AD-A127142		3. Recipient's Catalog No.	
4. Title and Subtitle CORRELATION OF FLAMMABILITY TEST DATA ON ANTIMISTING FUELS				5. Report Date December 1982	
				6. Performing Organization Code	
7. Author(s) Levelle Mahood and Robert L. Talley				8. Performing Organization Report No. Falcon TR-364010	
9. Performing Organization Name and Address Falcon Research and Development Company 109 Inverness Drive East Englewood, Colorado 80112				10. Work Unit No. (TRAVIS)	
				11. Contract or Grant No. DTFA03-80-C-00061	
12. Sponsoring Agency Name and Address U.S. Department of Transportation Federal Aviation Administration-Technical Ctr Atlantic City Airport, New Jersey 08405				13. Type of Report and Period Covered FINAL August 1980-August 1981	
				14. Sponsoring Agency Code	
15. Supplementary Notes					
16. Abstract As a part of a comprehensive FAA program to minimize post-crash fire hazards of jet transport aircraft, a correlation study was conducted on flammability test data of neat Jet A fuel, and the same fuel with various antimisting additives. The data were from full-scale aircraft crash tests, large-scale fuel spillage/ignition tests, and several small-scale flammability tests. Various rheometric tests were also considered. The ability of certain antimisting fuels to eliminate large fireballs during occupant-survivable aircraft crashes was amply supported. Large-scale crash simulations were found to be highly developed, and provide essential credibility on a given antimisting fuel near the end of its development. Small-scale flammability test rigs used for screening antimisting fuels were found generally effective, but with some conflicting data between rigs, and with some deviations from large-scale results. Methods have been defined which can provide higher confidence and resolution for selected test rigs. Enhanced correlation requires characterization of the fuel droplets and flows produced by a given test rig, and application of semi-empirical liquid breakup and ignition/combustion models. Liquid breakup correlation is provided in a limited case--for a Newtonian fuel at small-scale.					
17. Key Words Flammability            Ignition Turbine Fuels        Liquid Breakup Antimisting Fuels Test Apparatus			18. Distribution Statement Document is available to the U.S. public through the National Technical Information Service, Springfield, Virginia 22151		
19. Security Classif. (of this report) Unclassified		20. Security Classif. (of this page) Unclassified		21. No. of Pages	22. Price

## METRIC CONVERSION FACTORS

### Approximate Conversions to Metric Measures

Symbol	When You Know	Multiply by	To Find	Symbol
<b>LENGTH</b>				
in	inches	2.5	centimeters	cm
ft	feet	30	centimeters	cm
yd	yards	0.9	meters	m
mi	miles	1.6	kilometers	km
<b>AREA</b>				
in <sup>2</sup>	square inches	6.5	square centimeters	cm <sup>2</sup>
ft <sup>2</sup>	square feet	0.09	square meters	m <sup>2</sup>
yd <sup>2</sup>	square yards	0.8	square meters	m <sup>2</sup>
mi <sup>2</sup>	square miles	2.6	square kilometers	km <sup>2</sup>
	acres	0.4	hectares	ha
<b>MASS (weight)</b>				
oz	ounces	28	grams	g
lb	pounds (2000 lb)	0.45	kilograms	kg
		0.9	tonnes	t
<b>VOLUME</b>				
tsp	teaspoons	5	milliliters	ml
Tbsp	tablespoons	15	milliliters	ml
fl oz	fluid ounces	30	milliliters	ml
c	cups	0.24	liters	l
pt	pints	0.47	liters	l
qt	quarts	0.95	liters	l
gal	gallons	3.8	liters	l
ft <sup>3</sup>	cubic feet	0.03	cubic meters	m <sup>3</sup>
yd <sup>3</sup>	cubic yards	0.76	cubic meters	m <sup>3</sup>

### TEMPERATURE (exact)

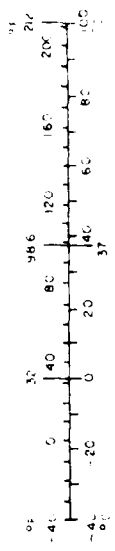
Fahrenheit temperature	5/9 after subtracting 32	Celsius temperature
------------------------	--------------------------	---------------------

### Approximate Conversions from Metric Measures

Symbol	When You Know	Multiply by	To Find	Symbol
<b>LENGTH</b>				
mm	millimeters	0.04	inches	in
cm	centimeters	0.4	inches	in
m	meters	3.3	feet	ft
m	meters	1.1	yards	yd
km	kilometers	0.6	miles	mi
<b>AREA</b>				
cm <sup>2</sup>	square centimeters	0.16	square inches	in <sup>2</sup>
m <sup>2</sup>	square meters	1.2	square yards	yd <sup>2</sup>
km <sup>2</sup>	square kilometers	0.4	square miles	mi <sup>2</sup>
ha	hectares (10,000 m <sup>2</sup> )	2.5	acres	
<b>MASS (weight)</b>				
g	grams	0.035	ounces	oz
kg	kilograms	2.2	pounds	lb
t	tonnes (1000 kg)	1.1	short tons	
<b>VOLUME</b>				
ml	milliliters	0.03	fluid ounces	fl oz
l	liters	2.1	pints	pt
l	liters	1.06	quarts	qt
l	liters	0.26	gallons	gal
m <sup>3</sup>	cubic meters	35	cubic feet	ft <sup>3</sup>
m <sup>3</sup>	cubic meters	1.3	cubic yards	yd <sup>3</sup>

### TEMPERATURE (exact)

Celsius temperature	9/5 then add 32	Fahrenheit temperature
---------------------	-----------------	------------------------



## PREFACE

This final technical report was prepared under contract number DTFA03-80-C-00061 with the U.S. Department of Transportation, Federal Aviation Administration Technical Center, Atlantic City, New Jersey. Mr. Thomas Rust, Jr., of the Aircraft Safety Development Division, Engine/Fuel Safety Branch (ACT-3), was the FAATC Project Manager.

The contractor was Falcon Research and Development Company, a subsidiary of Whittaker Corporation. The Contract Project Manager at Falcon's Englewood, Colorado, facility was Mr. Levelle Mahood, who also served as principal investigator in the areas of aircraft fuel fires and explosions, and related large-scale testing. Mr. Robert L. Talley of Falcon's Buffalo, New York, facility served as principal investigator in the areas of liquid breakup, fuels rheology, and related small-scale testing. The invaluable contributions of Dr. William A. Sirignano, who acted as a consultant to Falcon R&D in the area of combustion technology, are gratefully acknowledged.

The authors are indebted to many key participants in antimisting fuel research and development, who gave so generously of their time and insights. These include: (1) FAATC--Mr. Eugene P. Klueg, Mr. Thomas Rust, Jr., Mr. Robert F. Salmon, Dr. Thor I. Eklund, Mr. Augusto Ferrara, and Mr. Thomas M. Gustavino; (2) UK/RAE--Dr. S. P. Wilford, and Dr. E. A. Timby; (3) JPL--Dr. V. Sarohia; (4) NAEC--Mr. John Schaible; and (5) Southwest Research Institute--Dr. R. J. Mannheimer.

The authors also wish to acknowledge the contributions of others at Falcon R&D, including A. Stein, R. K. Miller, J. M. Otto, D. M. Taylor, H. H. Iwata, J. O. Duggan, and D. R. Ludwick.



## TABLE OF CONTENTS

	Page
I. INTRODUCTION	1
Purpose	1
Background	1
II. DISCUSSION	3
General	3
Air Flow	3
Liquid Flow	10
Liquid Breakup	10
Droplet Dispersion	14
Heating and Ignition	17
Propagation	18
Pass/Fail Criteria	22
Sustained Fuel Fire	23
References	24
III. ANALYSIS OF FLAMMABILITY TESTS	27
General	27
Full-Scale Crash Tests	27
Fuel and Air Flow	27
Liquid Breakup	33
Wing Fuel Spillage Tests	41
FAA Wing Fuel Spillage Facility	41
NWC Wing Spillage Facility	43
RAE Rocket Sled Test Facility	43
RAE Minitrack Test Facility	45
JPL Mini-Wing Shear Facility	46
FAA Flammability Comparison Test Apparatus	48
Analysis	48
SWRI Spinning Disc	50
Analysis	50
Correlation of Flammability Tests	52
Enhancing Correlations	64
Aerodynamics	66
Fuel Jets	66
Droplet Diagnostics	66
References	68
IV. ANTIMISTING FUELS RHEOLOGY	70
References	78

	Page
V. LIQUID BREAKUP	81
Rationale	81
Liquid Breakup Mechanisms	83
Oscillatory Breakup	83
Stripping and Taylor Breakup	92
Antimisting Fuels Breakup	92
Liquid Breakup Model	107
References	129
VI. CONCLUSIONS	135

## LIST OF ILLUSTRATIONS

Figure		Page
II-1	Antimisting Fuel Test Groupings	8
II-2	Free Turbulent Jet	9
II-3	Three-Dimensional Incompressible Wall Jet	11
II-4	Opposed Fuel and Air Jets	13
II-5	Typical Diameter Ranges for Various Substances	15
II-6	Typical Mass Fraction Versus Droplet Diameter for a Hydrocarbon with Viscoelastic Additive	16
II-7	Droplet Combustion Modes	19
II-8	Variations of Fuel Temperature, Mass Fraction, and Droplet Radius With Time for a Monodisperse Hydrocarbon Spray	21
III-1	Distance, Velocity, and Acceleration Versus Time, SP-2H Crash Test No. 1	29
III-2	Distance, Velocity, and Acceleration Versus Time, SP-2H Crash Test No. 2	30
III-3	Droplet Diameter Versus Cumulative Mass Percent - Time Increment No. 1	34
III-4	Droplet Diameter Versus Cumulative Mass Percent - Time Increment No. 5	35
III-5	Droplet Diameter Versus Cumulative Mass Percent - Time Increment No. 6	36
III-6	Droplet Diameter Versus Cumulative Mass Percent - Time Increment No. 10	37
III-7	Droplet Diameter Versus Cumulative Mass Percent - Time Increment No. 11, High Velocity	38

List of Illustrations (contd.)

Figure		Page
III-8	Droplet Diameter Versus Cumulative Mass Percent - Time Increment No. 11, Low Velocity	39
III-9	Fuel Temperature Versus Fuel-to-Air Relative Velocity	62
IV-1	Viscometer/Rheometer Schemes (Elongational Flow)	75
V-1	Probable Role of Viscoelasticity in Breakup	90
V-2	Breakup Mechanisms	94
V-3	Approximate Shear and Tensile Viscosities for 1.3% AM-1 in JP-8 Fuel	99
V-4	Liquid Breakup in Wing Fuel Spillage Configuration	106
V-5	Breakup Model Prediction Versus Experimental Data	114
V-6	Neat Jet A Droplet Distribution Predictions	131
V-7	Dynamic Pressure and Velocity Decay in Spray Flammability Test Apparatus	117
V-8	Droplet Distribution Decay Predictions for Neat Jet A, 100 psig	118
V-9	Droplet Distribution Decay Predictions for Neat Jet A, 75 psig	119
V-10	Droplet Distribution Decay Predictions for Neat Jet A, 50 psig	120
V-11	Shear Viscosity of 0.3% FM-9 in Jet A	122
V-12	General Shear Strain Rate - Droplet Size Behavior During Stripping Breakup of a Newtonian Liquid	123

List of Illustrations (contd.)

Figure		Page
V-13	Computed Breakup of 0.3% FM-9 in Jet A for Small Jet Experiment of Eklund and Cox	126

## LIST OF TABLES

Table		Page
II-1	Summary of AMF Flammability Test Facilities/Apparatus	4
III-1	Selected Data from SP-2H Crash Test No. 1 (Neat Jet A Fuel)	31
III-2	SP-2H Crash Test No. 1, Liquid Breakup Model Input Velocities and Droplet Data Output	32
III-3	Wing Fuel Spillage Facilities	42
III-4	Fuel Ejection Velocity in Meters/Sec.	44
III-5	Spinning Disc Dynamics	51
III-6	AMF Flammability Test Data Summary	53
III-7	Fuel-to-Air Speed in ft/sec by Facility, FM-9 Concentration, and Flammability	75
V-1	Breakup Model Nomenclature	109

## EXECUTIVE SUMMARY

This flammability correlation analysis compared test data from a large number of flammability tests used to determine the quality of antimisting fuel. These included full-scale aircraft crash tests, large-scale fuel spillage/ignition tests, and small-scale flammability tests. All tests comprised the discharge of the test fuel using various procedures and with various velocities into an environment which included ignition sources of varying intensities. The tests were conducted initially with Jet-A, or equivalent, to obtain a standard or baseline to which the same fuel with various quantities of antimisting additives was compared to give an indication of the antimisting quality of the latter. Various rheometric tests were also considered as a means of determining the effectiveness of the fuel relative to its antimisting properties.

The ability of certain antimisting fuels to eliminate large fireballs during occupant-survivable aircraft crashes was amply supported by the data analyzed during this study. Large-scale crash simulations were found to be highly developed, and provide essential credibility on a given antimisting fuel near the end of its development. Small-scale flammability test rigs used for screening antimisting fuels were found generally effective, but with some conflicting data between rigs, and with some deviations from large-scale results. No reasons could be positively identified for these discrepancies notwithstanding the limited employment of a combustion modeling technique.

Enhanced correlation among the tests studied requires characterization of the fuel droplets and flows produced by a given test rig, and application of semi-empirical liquid breakup and ignition/combustion models. This was not accomplished to the degree necessary due to the limited scope of this program. Liquid breakup correlation is discussed and a solution for a limited case is provided as an example of the use of this analytical tool. This case was for a Newtonian fuel (not antimisting fuel) on a small-scale basis.

## I. INTRODUCTION

### PURPOSE.

The primary purpose of this effort was to perform a correlation study of antimisting fuel (AMF) flammability test data developed by six test groups--the Federal Aviation Administration Technical Center (FAATC), the United Kingdom's Royal Aircraft Establishment (RAE), the U.S. Naval Weapons Center (NWC), the Naval Air Engineering Center (NAEC), the Jet Propulsion Laboratory (JPL), and Southwest Research Institute (SwRI). This effort included study of the applicable test facilities and procedures, test data, and possible improvements, modifications, and additions to the testing to enhance data repeatability and correlation.

### BACKGROUND.

The Federal Aviation Administration has been conducting a comprehensive program to minimize fire hazards of jet transport aircraft in impact-survivable accidents by developing antimisting fuels. As implied by their generic name, AMF's inhibit the misting which occurs when neat kerosene fuel is released at significant velocity relative to the atmosphere. Even at bulk liquid and air temperatures well below the fuel's flash point, the finely divided mist is readily ignitable and propagates flame fronts rapidly. The commonly resulting "crash fireball" heats and ignites pools of spilled fuel at the crash site. Sustained burning of proximate spilled fuel can lead to rapid destruction of an aircraft, and severely reduce occupant survivability. By eliminating the crash fireball, AMF's break this hazardous chain of events.

In the course of development of AMF's, a broad range of test methods, apparatus, and facilities have been essential. The complex polymer chemistry of typical additives involves both standard and specialized test apparatus and procedures which address rheology and other properties of the doped fuels. Small-scale flammability tests have evolved to expose candidate AMF's to idealized crash conditions--including flow, expulsion, breakup, and ignition.

Finally, full-scale crash tests and large-scale flammability tests have been essential for proof-of-concept, phenomenology at adequate scale, and demonstrating full-scale effectiveness of near-term candidate AMF's.

This study has been initiated at an opportune time. A significant body of test data has been developed over the full size spectrum

of AMF flammability testing. A data base of rheometric testing is also available. Equally important, understanding of non-Newtonian flow, liquid breakup, ignition and combustion phenomena has improved significantly in the past few years.

This report presents analyses of the various test methods and data, relates physical parameters and phenomena to them, and defines methods for improving confidence in individual tests and comparability between tests.

## II. DISCUSSION

### GENERAL.

Table II-1 describes the test facility or apparatus, performing organization, and applicable references. Figure II-1 relates the various tests by type (flammability, rheometry), size, and fundamental method. Three methods of correlation are shown, but semi-empirical methods predominated. The various tests are selectively analyzed and compared in subsequent sections of this report. However, it is illuminating to discuss their similarities and differences qualitatively in the context of physical parameters and phenomena.

All AMF flammability tests involve the following phenomenological elements in the sequence presented:

1. Air Flow
2. Fuel Flow
3. Liquid Breakup
4. Droplet Dispersion
5. Heating
6. Ignition
7. Propagation
8. Sustained Fuel Fire

### AIR FLOW.

In the general crash scenario, absolute air flow velocity can be near zero, due solely to wind. The NAEC Crash Tests, RAE Rocket Sled Tests, and the SwRI Spinning Disc, Drop Test, and Air Gun involve (and require) near-quiescent ambient air. The remainder utilize liquid fuel orifices which are fixed in relation to the ground, and move the air to simulate motion relative to the atmosphere. Free air jets are used by the large-scale FAATC Wing Spillage and NWC Wing Spillage facilities and the JPL Mini-Wing apparatus. The FAATC small-scale Flammability Comparison Test Apparatus (FCTA) utilizes air flow within a 1-inch I.D. pipe.

Figure II-2 depicts a free turbulent air jet as described in aerodynamic literature.<sup>24</sup> Note that "potential core" flow is free of entrainment, and maintains a constant velocity over a cross-sectional area which diminishes to zero at a distance of 6.4 nozzle diameters from discharge. The limit of diffusion is defined along a half-angle of 10° from the axis of the jet, extending out about 100 nozzle diameters. Beyond the "established flow" limit is the "terminal region", where the velocity is near zero.

Table II-1. Summary of AMF Flammability Test Facilities/Apparatus

FACILITY AND TITLE	DESCRIPTION	REFERENCES
<p>Naval Air Engineering Center, Lakehurst, N.J.</p>	<p>Specially modified SP-2H test aircraft are accelerated 6,190 feet down the track of Recovery System Track Site No. 4 by a jet car powered by four J-48 turbojet engines. At this point the jet car separates, and aircraft and shuttle proceed 900 feet. The aircraft then separates and travels 200 feet to the crash site. The aircraft impacts a 3° sloped earthen mound and decelerates along a prepared earth surface with an array of 48 open-flame torches. Provisions are made for fuel leakage from the front, top and bottom surfaces of the wing tanks.</p>	<p>1, 2, 3</p>
<p>Full-Scale Crash Tests (SP-2H Aircraft)</p>	<p>Fan discharge air from a TF-33 engine is augmented and exits a 69-inch square duct. Sixteen feet downstream (11.5 feet above ground level) is a replica wing section with a 12-inch pipe, facing upstream, protruding from the leading edge. A variety of fuel discharge orifices can be fitted. Test fuel exits this orifice and is broken up and reversed in flow direction by the free air jet. Three feet below the centerline and 4-1/2 feet past the fuel discharge plane is a large propane torch, facing downstream. The flame is 5 feet long, 18 inches in diameter, and has a nominal temperature of 1100°F. Photographic records are made of resulting combustion phenomena and subsequently evaluated.</p>	<p>4, 5, 6, 7, 8</p>

Table II-1. Summary of AMF Flammability Test Facilities/Apparatus (cont.)

FACILITY AND TITLE	DESCRIPTION	REFERENCES
<p>Naval Weapons Center, China Lake, CA.</p>	<p>The NWC T-Range provides air flow from several storage tanks, which is heated to restore near-ambient conditions and discharged from a modular low velocity diffuser (35-inch square discharge duct). An airfoil (84-inch chord, 14.5 inches maximum thickness) is located 37 inches above the ground and 85.5 inches aft of the diffuser's discharge plane--centered in the air flow. A 6-inch diameter fuel orifice is located in the wing leading edge, looking upstream. At the lower edge of the airstream bound, 27 inches above the ground plane, is an aft-facing propane torch. The torch is ignited at intervals of 1.5 seconds, with burn duration of about 0.1 seconds. The free flame volume (no fuel in airstream) is about 1 liter. In operation, AMF is fed by gravity from an elevated hopper to exit the wing leading edge. The airflow reverses and breaks up the liquid stream, which is subjected at the lower bound to heating and ignition by the torch. Photographic records of combustion phenomena are evaluated.</p>	<p>9</p>
<p>Wing Fuel Spillage/Air Shear Tests</p>	<p>The NWC T-Range provides air flow from several storage tanks, which is heated to restore near-ambient conditions and discharged from a modular low velocity diffuser (35-inch square discharge duct). An airfoil (84-inch chord, 14.5 inches maximum thickness) is located 37 inches above the ground and 85.5 inches aft of the diffuser's discharge plane--centered in the air flow. A 6-inch diameter fuel orifice is located in the wing leading edge, looking upstream. At the lower edge of the airstream bound, 27 inches above the ground plane, is an aft-facing propane torch. The torch is ignited at intervals of 1.5 seconds, with burn duration of about 0.1 seconds. The free flame volume (no fuel in airstream) is about 1 liter. In operation, AMF is fed by gravity from an elevated hopper to exit the wing leading edge. The airflow reverses and breaks up the liquid stream, which is subjected at the lower bound to heating and ignition by the torch. Photographic records of combustion phenomena are evaluated.</p>	<p>10, 11, 12, 13</p>
<p>United Kingdom Royal Aircraft Establishment, Farnborough, England</p>	<p>A replica wing tank (10 or 20 gallons capacity) is accelerated down a track by two or three rockets and then engages an arrester cable. The tank has a slit in its leading edge which is sealed by a weighted rubber plug. Deceleration ejects the plug and fuel is released into an array of 18 kerosene-fueled torches. Resulting combustion phenomena are photographically recorded and evaluated.</p>	<p>10, 11, 12, 13</p>
<p>Rocket Sled Tests</p>	<p>A replica wing tank (10 or 20 gallons capacity) is accelerated down a track by two or three rockets and then engages an arrester cable. The tank has a slit in its leading edge which is sealed by a weighted rubber plug. Deceleration ejects the plug and fuel is released into an array of 18 kerosene-fueled torches. Resulting combustion phenomena are photographically recorded and evaluated.</p>	<p>10, 11, 12, 13</p>

Table II-1. Summary of AMF Flammability Test Facilities/Apparatus (cont.)

FACILITY AND TITLE	DESCRIPTION	REFERENCES
Jet Propulsion Laboratory, Pasadena, CA.	A centrifugal blower provides air flow (260 ft/sec maximum) from an 8-inch diameter orifice over a small replica wing centered in the flow two diameters downstream. The wing has a slit in its leading edge with a vertical dimension of about 0.2 inches, through which fuel is expelled into the opposing airstream. Directly aft of the wing, centered on the airflow, is an oxy-acetylene torch facing downstream which burns continuously. Any resulting combustion is monitored visually, photographically, by thermocouples, and by a radiometer.	14, 15
Federal Aviation Administration Technical Center, Atlantic City, N.J.	The FCTA is a self-contained and semi-automatic test apparatus integrated into a single cabinet, which can be operated indoors given adequate space, ventilation, and safety precautions. Air from a storage tank flows through a sonic orifice and into a 1-inch I.D. pipe. Test fuel is expelled from a cylinder by a mechanically driven piston into a 1/4-inch O.D. stainless steel tube. This tube penetrates the air pipe and expels fuel upstream along its longitudinal axis. The mixed fuel/air stream expands in a diffuser which penetrates the right-hand side of the console. A propane torch is located downstream. Combustion is monitored photographically and by a radiometer.	16, 17, 18, 19, 20, 21
Flammability Comparison Test Apparatus		

Table II-1. Summary of AMF Flammability Test Facilities/Apparatus (cont.)

FACILITY AND TITLE	DESCRIPTION	REFERENCES
<p>Southwest Research Institute, San Antonio, Texas</p>	<p>A metal disc about 2.5 inches in diameter is mounted horizontally on the shaft of a variable speed motor. An integral cup is centered in the top of the disc, into which fuel flows from a static tube overhead. Four integral (closed) radial flow channels (2mm diameter by 10mm long) located in angular increments of 90° (viewed from above) extend from the cup to the disc's outer edge. About 3.9 inches from the disc's edge is a continuously burning propane torch. The test fuel flows down from the supply line into the cup, and is forced outward into the flow channels by centrifugal action (e.g., 30,000 RPM). The liquid fuel is flung from the four orifices in the disc's edge, which then breaks up and encounters the torch. Resulting combustion is monitored visually, photographically, and by radiometer.</p>	<p>22, 23</p>
<p>Spinning Disc Tests</p>		

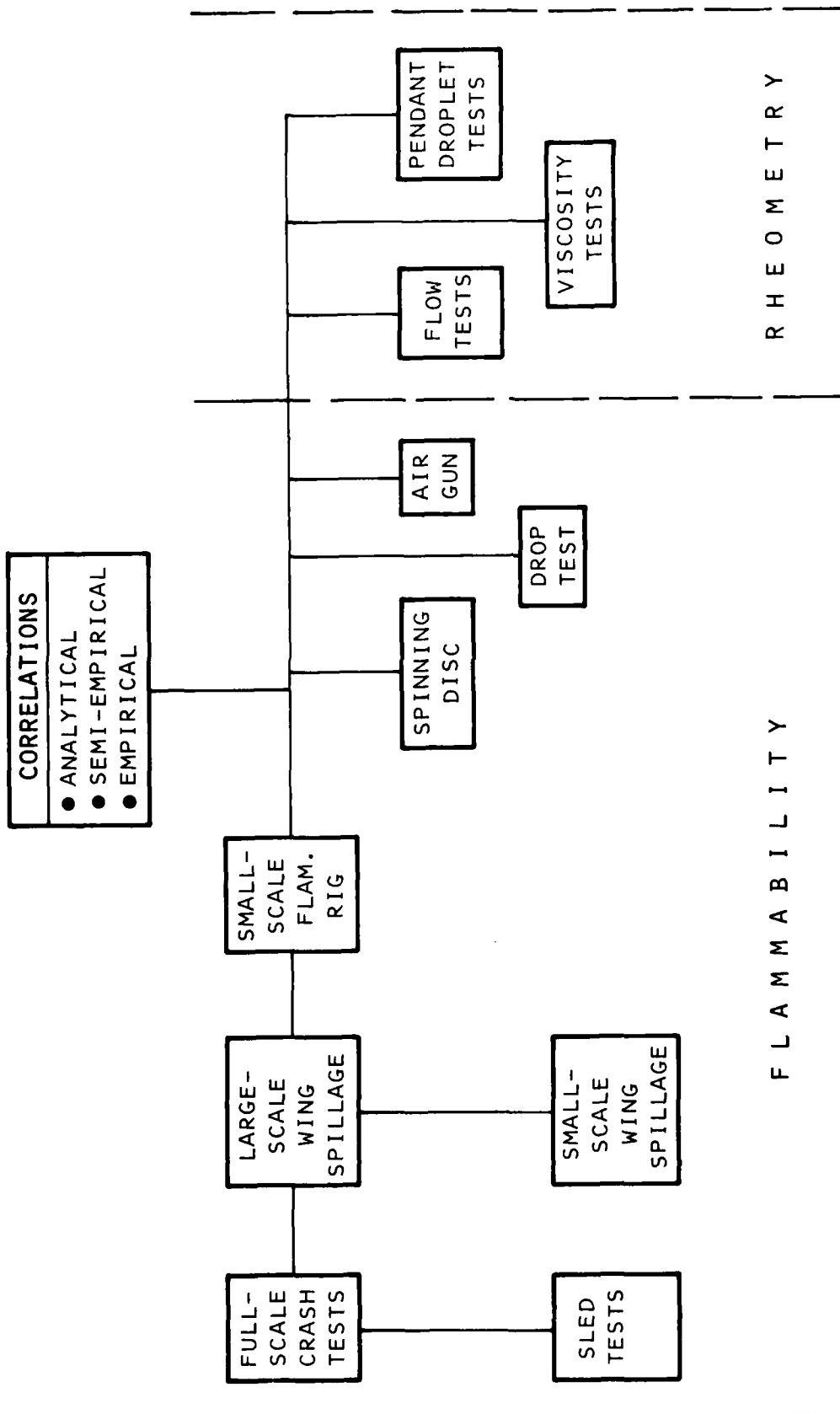


FIGURE II-1. ANTIMISTING FUEL TEST GROUPINGS

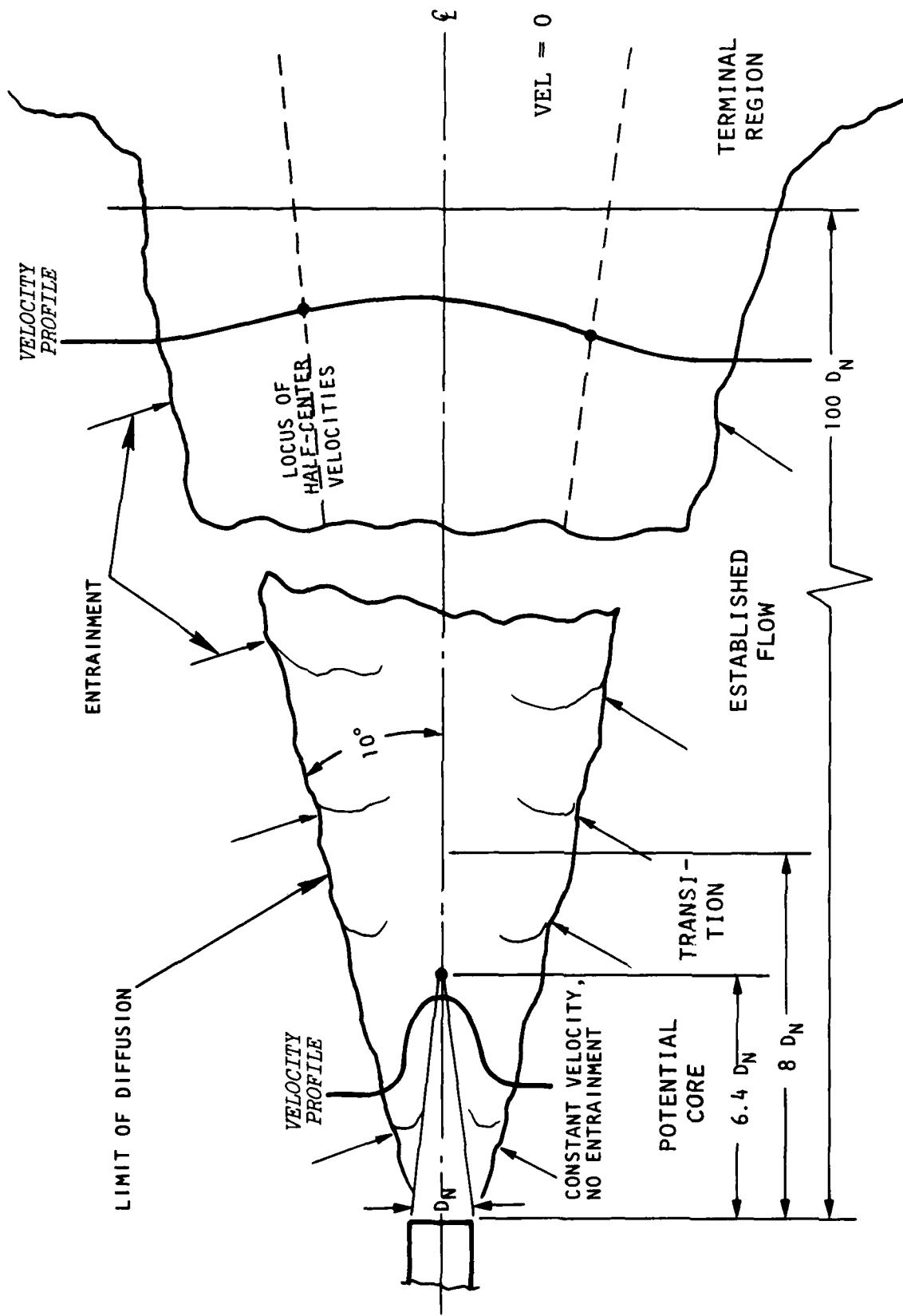


FIGURE II-2. FREE TURBULENT JET

The NWC report<sup>9</sup> provides data on velocity profile decay and turbulence within the jet. The data show a significant range of variability of air velocity. Profile data were obtained on the large-scale FAATC Wing Spillage facility from the plane of discharge out to 93 inches. Hence, velocities other than those in the "potential core" were not available to compare with the free air jet depicted.

An interesting variation is the introduction of a "ground plane" to the FAATC Wing Spillage facility. This simulates a crash scenario with a mid- or low-wing aircraft, and the considerable influence of "ground effect". Figure II-3 is an isometric view of a free air jet from a rectangular orifice<sup>25</sup> (as at the FAATC facility), depicting the modified velocity profile due to ground effect, as contrasted to Figure II-2. No velocity mapping data were available to correlate with this generalized flow configuration.

#### LIQUID FLOW.

In the crash scenario, liquid fuel flow is induced through breaches in fuel tank walls primarily by the relatively high transient accelerations and decelerations incident to the impact(s); or, in their absence, by the gravity head of the fuel. In the NAEC Full-Scale Crash Tests, breaches are deliberately generated in the leading edges, tops, and bottoms of several wing fuel tanks of the SP-2H aircraft.

Large orifices are typically involved, so that even with a high volumetric rate of spillage, relatively low stress is placed on the fuel during transport to and through the openings in the tanks. This is particularly important because AMF's are generally susceptible to loss of a degree of their antimisting property with exposure to excessive shear. The RAE Rocket Sled Tests share with the NAEC Crash Tests the use of deceleration to induce fuel flow from a tank. The FAATC and NWC wing spillage rigs and the FAATC FCTA are carefully designed to avoid shear stress on the AMF's tested. The FAATC Wing Spillage rig uses a gas pressure cap in the holding tank to induce fuel flow to the orifice, whereas the NWC rig uses gravity flow from an elevated storage tank. The FCTA uses positive expulsion from a cylinder by a mechanically-driven piston. The SwRI Spinning Disc utilizes acceleration of the liquid through four radial flow channels connecting a center chamber to orifices on the outer edge of the spinning disc.

#### LIQUID BREAKUP.

The crux of the post-crash fire hazard with high flash point turbine fuel, such as Jet A, at nominal ambient temperature is liquid break

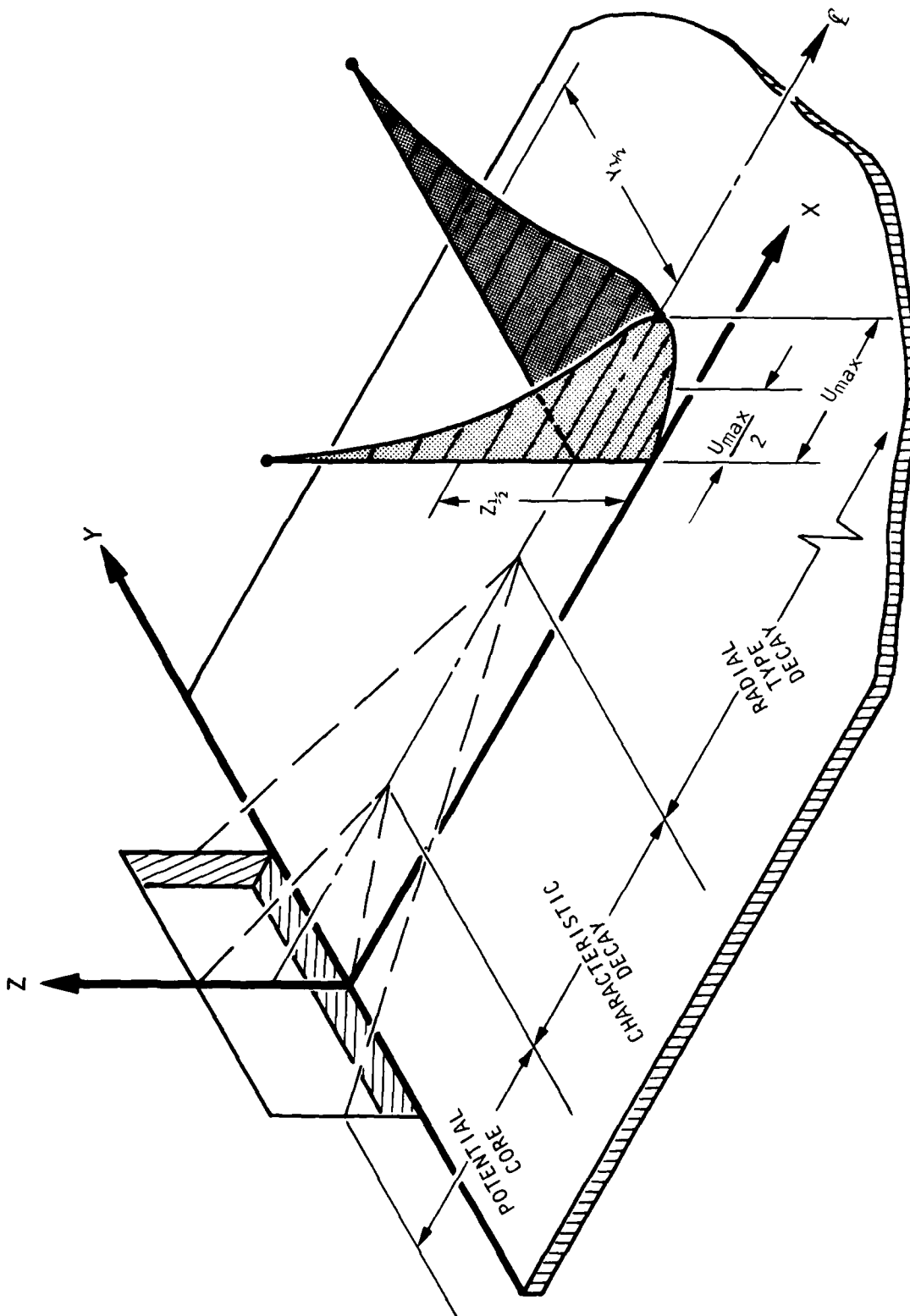


FIGURE II-3. THREE-DIMENSIONAL INCOMPRESSIBLE WALL JET

up, i.e. conversion of the fuel from a relatively low surface area, high volume and low ignitability configuration to a very high surface area and, hence, flammable mist. This conversion is due to relative motion between ejected fuel and the atmosphere. In a crash scenario, the air is at low or zero velocity, whereas the fuel is being ejected from an aircraft which is itself moving at significant speed. The highest relative velocity between the air and the fuel is typically achieved (1) at high aircraft deceleration while still at relatively high speed, and (2) with fuel ejecting through the forward wall(s) of the tank(s). The maximum relative velocity is significant in that it places the maximum demand upon the performance of AMF in suppressing mist formation.

Fuel is ejected a considerable distance ahead of the decelerating fuel tanks in both the NAEC Crash and the RAE Rocket Sled tests. The FAATC, NWC and JPL Wing Spillage rigs simulate this critical encounter with a free air jet flowing against a directly opposed fuel stream exiting from an orifice in a fixed airfoil's leading edge. The opposed fuel and air jets are schematically illustrated by Figure II-4. It is a highly desirable feature of the FAATC Wing Spillage facility that breakup occurs in the "potential core" region, Figure II-2.

The FAATC FCTA uses a fuel jet opposed to air flow within a 1-inch I.D. pipe. In cases where the average plume diameter,  $D_p$ , is greater than one inch (Figure II-4), impingement on the pipe's interior surface will occur.

The SwRI spinning disc ejects the fuel from four peripheral orifices, while rotating at rates as high as 30,000 rpm. Hence, the ejected liquid "sees" an initial velocity relative to the air which is the vector sum of its radial and tangential velocities at that point.

Liquid breakup is discussed in detail in subsequent sections of this report. Suffice it to say that the localized relative fuel/air velocity is considered crucial to resulting droplet size spectra, and configurations vary with AMF type from compact (e.g., near-spherical) droplets to long filaments. If a significant change in flammability occurs for a given AMF and test apparatus at the same relative fuel/air velocity because absolute air and fuel velocities have been varied, the possible influence of undefined and/or uncontrolled variations in the dynamic conditions must be considered.

Liquid breakup is sensitive to scale. Over the range of fuel jet diameters of the tests analyzed, significantly different phenomena are encountered. As detailed later, this precludes unadjusted comparisons of independent test variables and results between a

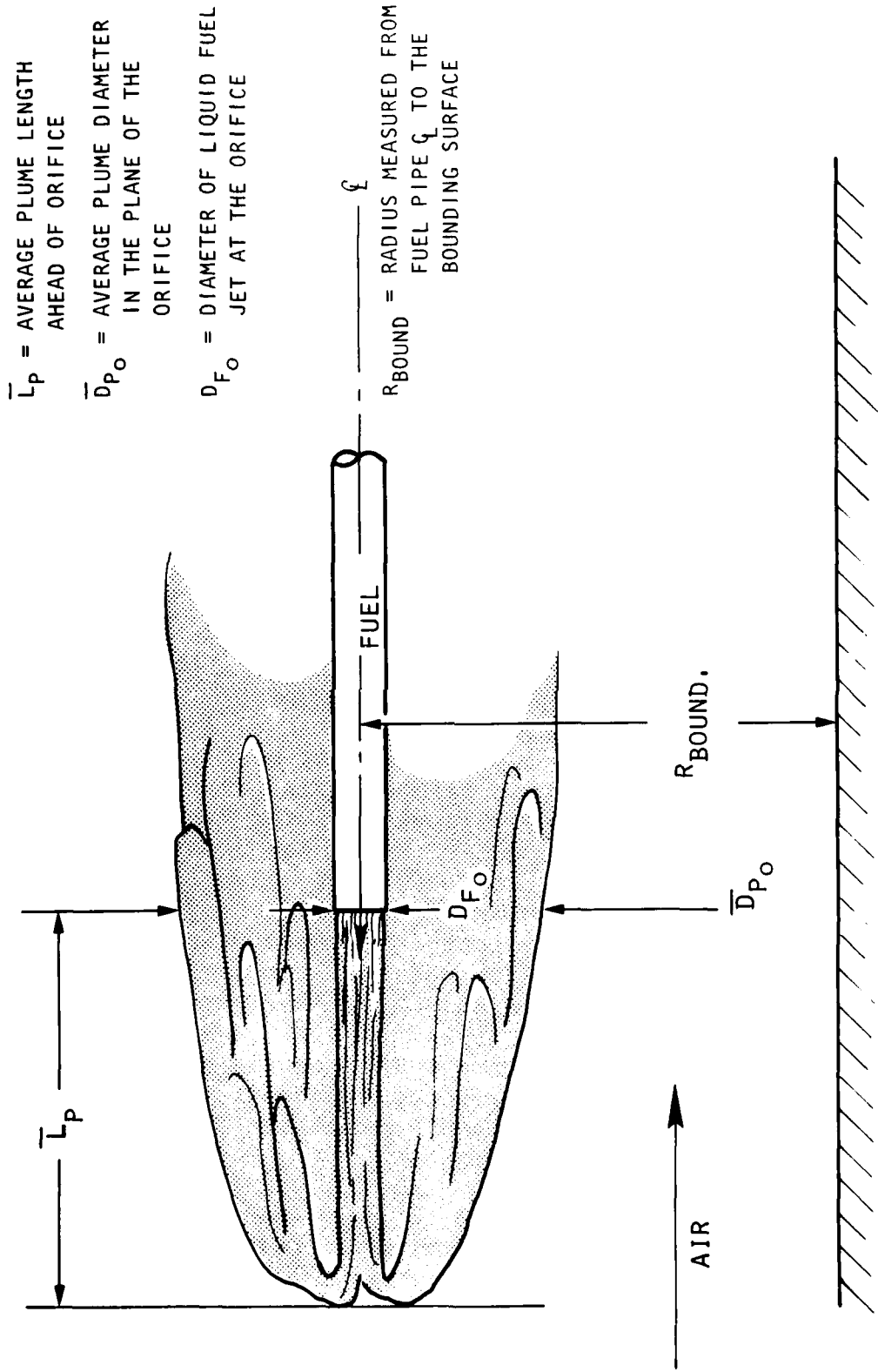


FIGURE II-4. OPPOSED FUEL AND AIR JETS

large diameter fuel jet (e.g., on the order of tens of centimeters) and a small one (e.g., one centimeter or less).

Figure II-5 displays the diameter ranges for some common substances/configurations, and for hydrocarbons of interest to AMF studies. Note that for the three hydrocarbons with viscoelastic additives, the smallest droplets are about 80 microns in diameter. Although droplet size data are lacking for most AMF flammability tests, observed flame propagation indicates that the droplet sizes for neat Jet A fuel can have a lower size bound approaching or less than 10 microns in diameter, depending on relative fuel/air velocity and other parameters.

Figure II-6 illustrates the droplet size distribution for a 0.57 mass median diameter (MMD) population of a hydrocarbon with viscoelastic additive shown in the previous figure. Data of this type are highly desirable in the analysis of AMF flammability tests.

#### DROPLET DISPERSION.

Given the products of liquid breakup just discussed, their subsequent transport and dispersion are crucial to the flammability of the fuel plume or cloud. For example, dispersion can convert a flammable fuel droplet population to one which will not propagate flame--by reducing the number of droplets (or mass of fuel) per unit volume of air below the Lean Flammability Limit (LFL). This was amply demonstrated during development of the Minitrack test apparatus by the RAE.<sup>26</sup> In the course of development of this apparatus, they found unrealistically high effectiveness of an AMF at very low additive concentrations--compared to large-scale Rocket Sled Test results. They postulated that dispersion was too rapid, so that the mist concentration was below the lower ignition limit by the time ignition sources were encountered. The solution was to add a nozzle 1/2-inch (12.7 mm) long to the 5/16 inch (7.9 mm) diameter orifice. This nozzle evidently narrowed the dispersion field and produced the desired comparability of results between the Minitrack and Rocket Test Sled devices.

For thorough AMF flammability test analysis, the fuel droplet size data previously discussed must be supplemented with droplet concentration data. A convenient method is to subdivide the droplet spectra into groups of approximately monodisperse droplets (e.g., mass median diameter); and specify the droplet number density (number of droplets per unit volume) for each group.

Considering the flow fields illustrated by Figures II-2, II-3, and II-4, it is evident that the droplet number density may be expected to vary significantly at different positions within a

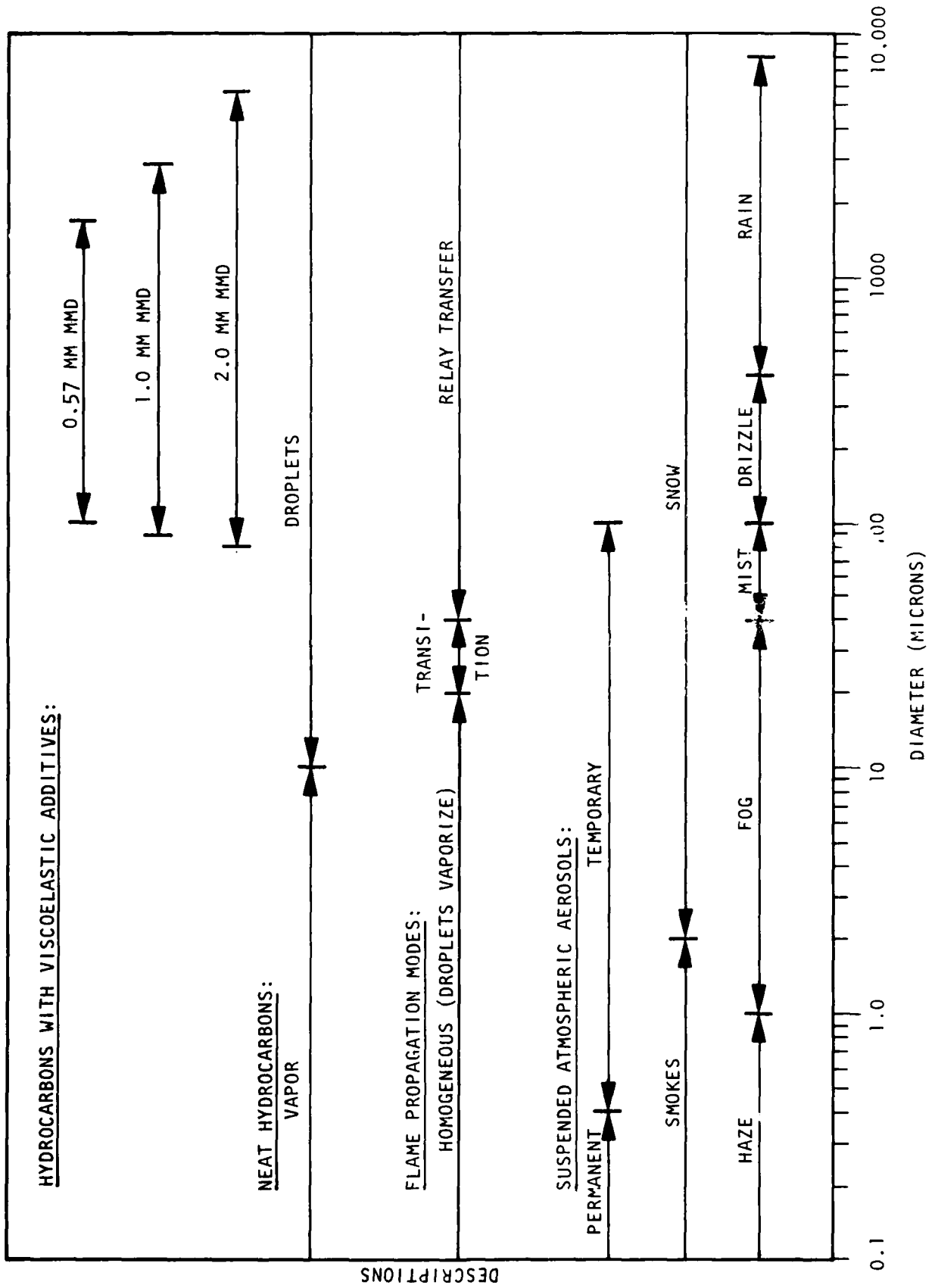


FIGURE II-5. TYPICAL DIAMETER RANGES FOR VARIOUS SUBSTANCES

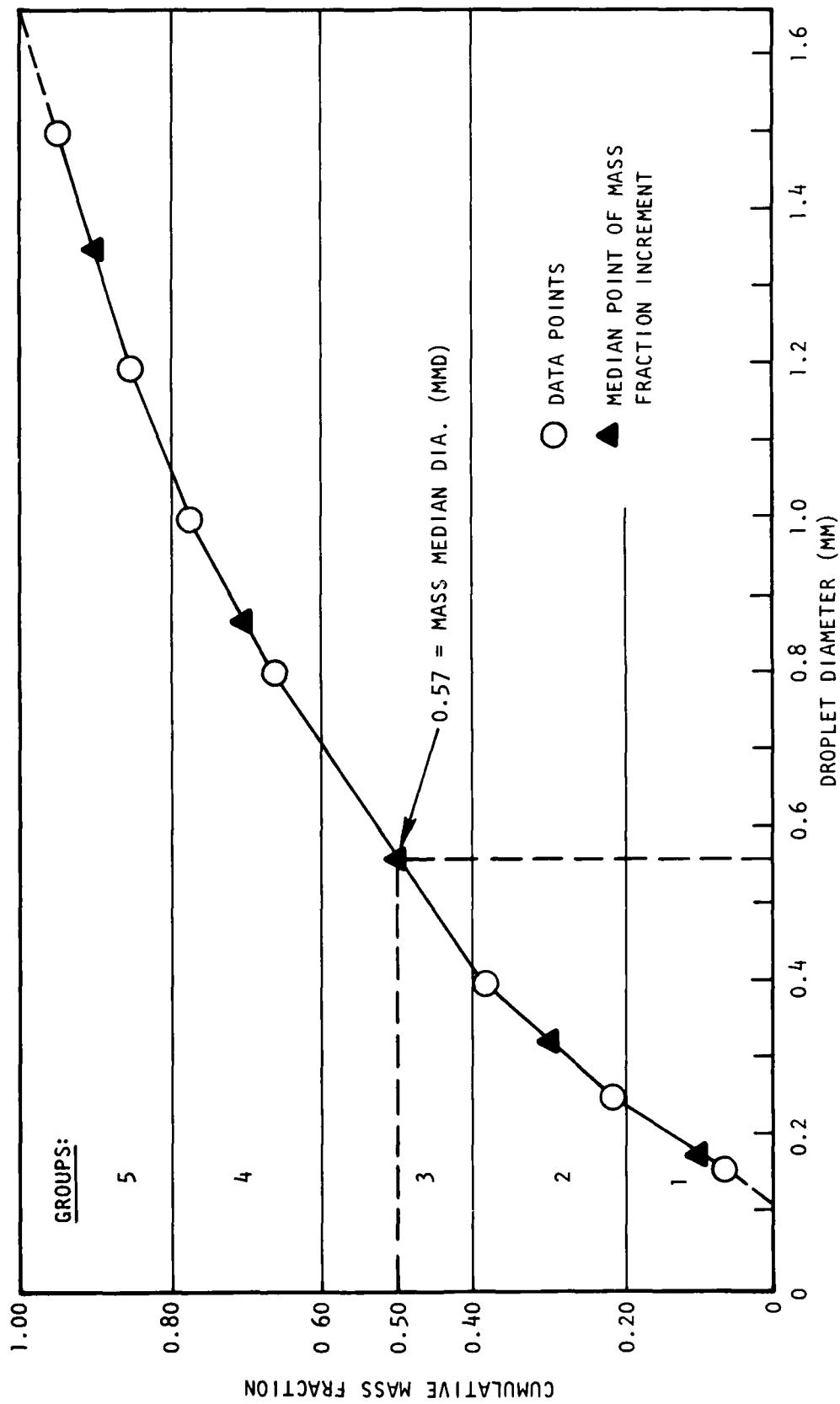


FIGURE II-6. TYPICAL MASS FRACTION VERSUS DROPLET DIAMETER FOR A HYDROCARBON WITH VISCOELASTIC ADDITIVE

given fuel mist cloud or plume. Locations of particular concern are (1) the liquid breakup region, (2) regions of hot surfaces and/or ignition sources, (3) transient flame regions, and (4) fireball and sustained fire regions.

At high relative fuel/air velocities, droplet drag is the dominant propulsive force--which varies with droplet shape and size. The direction and magnitude of this force is dependent upon the flow configuration of the proximate air mass. At near-zero local air velocities, gravity emerges as the propulsive force, opposed by droplet drag (i.e., settling). Both of these modes of transport are highly relevant to the AMF flammability tests analyzed.

Turbulence in the flow fields must be considered. Turbulence effects are evident in the full-scale aircraft crash tests--particularly the wing tip vortices and wakes.

#### HEATING AND IGNITION.

Heating of the fuel mist must be considered separately from ignition, since we are dealing with a turbine fuel, i.e. Jet A, which is typically at temperatures well below its flash point (about 100°F) under operational conditions. Hence, localized heating within a mist plume or cloud can result in increased evaporation and flammability. Likewise, extremes of bulk fuel and ambient air temperatures, coupled with high aircraft and ground surface temperatures, give a "worst case" environmental scenario.

Simulated ignition sources in full-scale crash and large-scale AMF flammability tests typically provide many orders of magnitude more than the few millijoules of energy that are the minimum necessary to ignite a flammable mist in air. The minimum ignition energy for a vapor/air mixture is even less, on the order of a tenth of a millijoule.

It is quite evident from photographic coverage of the large AMF tests that the shrouded rockets, liquid hydrocarbon-fueled torches, running turbojet engines, fuel pool fires, etc. provide extensive heating effects--involving temperatures well above the fuel's flash point, but below the minimum necessary for ignition. "Marginal" test conditions, involving lower concentrations of antimisting additive and/or higher relative fuel/air speeds in the breakup region, often provide a clear differentiation between progressive heating effects and localized ignition.

The clearest demonstration is provided by the wake flame in the flow field downstream from a hydrocarbon gas-fueled torch. Even with mist clouds of low flammability, a lengthening of the wake

flame is evident. This is due to direct mixing of fuel droplets in the plume with the torch's flame. With a more flammable air/mist flow past the torch, the wake flame lengthens and thickens. The enhanced flame is both radiating more heat and involving more of the flowing cloud in the convective "heating" and "combustion" envelopes. With a progressively more flammable flowing medium, the wake turbulence limits the maximum continuous length of the wake flame--with large excursions of non-burning mixture across the axis of the flame. Discrete burning regions join the general flow of the plume, with one of two possible consequences: (1) heat loss is greater than heat generated by interior burning, and the discrete region shrinks and self-extinguishes; or (2) heat loss is less than heat generated, and the fireball grows.

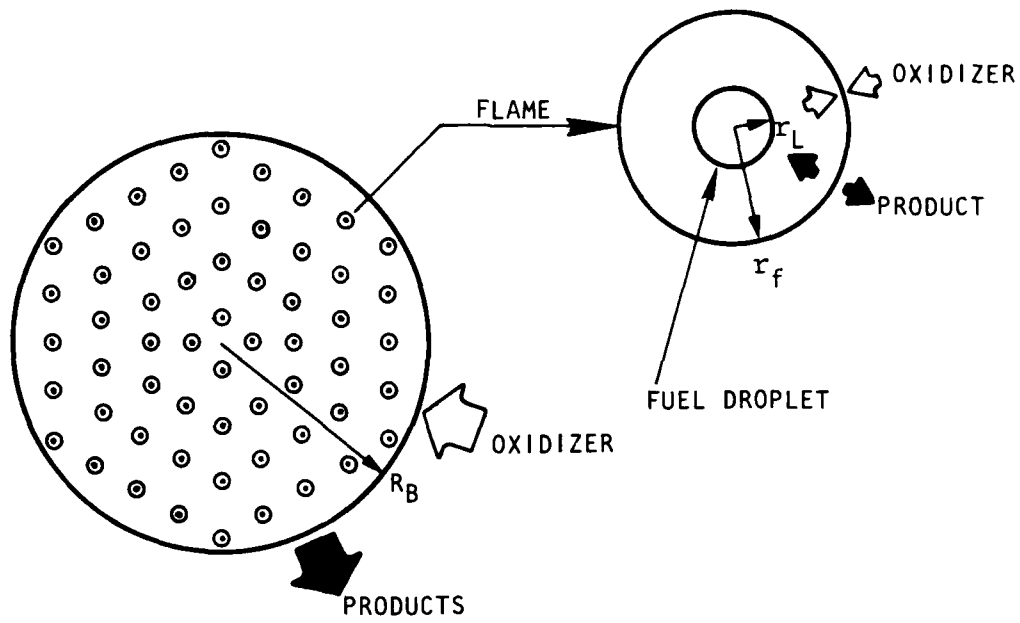
The important point is that the large-scale "ignition sources" provide widely varying combinations of high-temperature, low volume ignition sources in conjunction with relatively high-volume mist cloud heating/evaporation effects. It is evident that the preheating and evaporation effects of the large ignition sources are often crucial to the ignition of a plume containing AMF droplets.

In the small-scale tests, the mix of ignition and cloud heating effects also varies widely. From these observations, it is evident that in comparing the results of AMF flammability tests, the varying characteristics of the ignition sources may become highly significant.

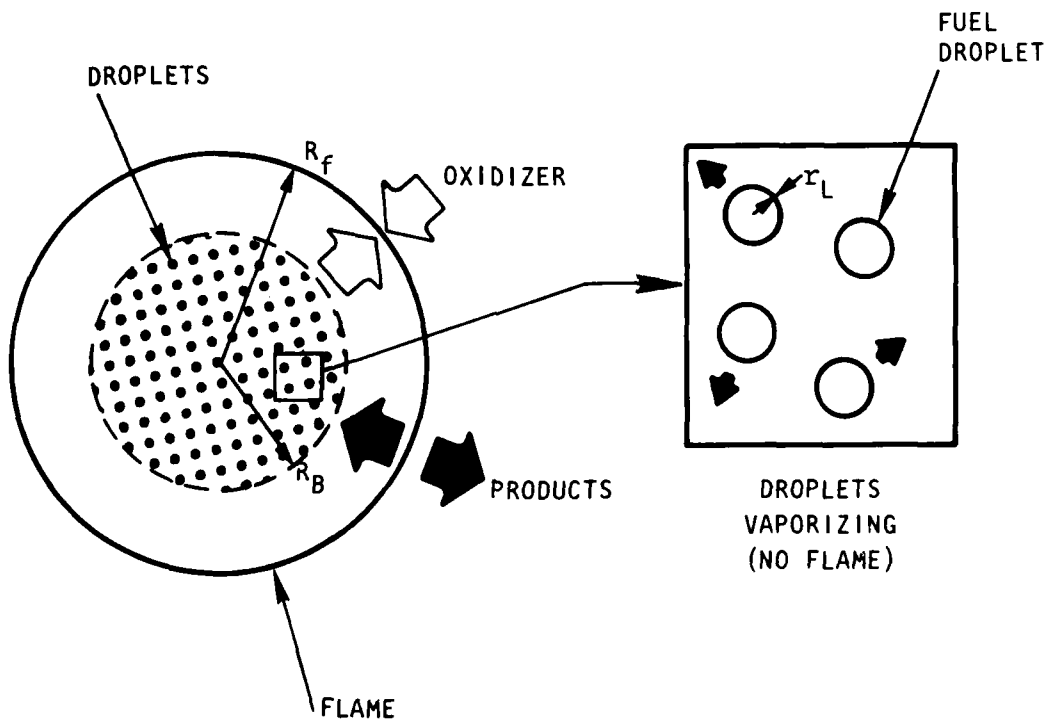
#### PROPAGATION.

The known flammability properties of monodisperse hydrocarbon droplets (including neat Jet A and AMF) are significant for illustration. Referring again to Figure II-5, below a droplet diameter of 10 microns, flame propagation causes immediate vaporization. Hence, droplets below 10 microns may be considered flammable vapor, provided that their concentration (e.g., number density--number of droplets per unit volume) is above the Lean Flammability Limit. Homogeneous flame propagation occurs over this range and up to a droplet size of 20 microns. Above 40 microns, flame propagation is droplet-to-droplet. An unexpected experimental result is that, for one hydrocarbon tested, the minimum ignition energy in the range of ten to a hundred microns was less than for a near-stoichiometric fuel vapor/air mixture under identical conditions.

The degree of dispersion affects droplet burning as well. Figure II-7 depicts conventional individual droplet burning as "Internal



A. INTERNAL GROUP COMBUSTION



B. EXTERNAL GROUP COMBUSTION

FIGURE II-7. DROPLET COMBUSTION MODES

Group Combustion"<sup>27, 28</sup>. This mode applies provided that the spray is sufficiently dilute in air, or that droplet dispersion is high enough in the preignition phase to avoid combustion inhibition due to fuel evaporation and vapor diffusion. With "External Group Combustion", by comparison, individual droplet burning does not occur due to the higher droplet number density and slower dispersion. Such variations in burning rate could significantly influence the combustion observed, and an AMF's resulting flammability (pass/fail) rating.

Of course, polydisperse droplet populations must be considered for the AMF flammability tests. Semi-empirical computer models have been developed<sup>29</sup> which address the transport, evaporation, ignition and combustion of polydisperse hydrocarbon droplet populations in flowing air. A typical finding is that a very small fraction of the mass of a polydisperse fuel droplet cloud, at the small end of the droplet size spectrum, can make the entire cloud flammable. This indicates the importance of evaluating AMF's at maximum relative fuel/air velocities to develop conservatively small droplets and potentially flammable conditions.

Figure II-8 provides the results of the model previously discussed, and illustrates interdependency of three important variables with time. A monodisperse hydrocarbon droplet population is exposed to an initial temperature of about 39°C. The fuel mass fraction increases as evaporation occurs over time, while the droplet radius diminishes. The heat absorbed by evaporation drops the air temperature about 21°C. The fuel mass fraction very closely approaches the Lean Flammability Limit.

In the full-scale crash tests with neat Jet A, liquid breakup and dispersion yield a totally flammable vapor/spray cloud. The flame propagates throughout the cloud and even to the very tips of the forward fuel plumes--located several feet ahead of the leading edges of the wings of the SP-2H. Similar engulfment was observed with the wing fuel spillage rigs testing neat Jet A.

We have noted in the observation of movies of flame propagation within a fuel mist cloud from various test facilities that definite spatial limits to the fireball sometimes occur. In some cases, these limits may be due to a low concentration of droplets which, if closer together, would propagate flame fronts and burn. This seems particularly likely where the fire propagates freely through a portion of the cloud formed at lower velocity, and does not propagate through a visible portion of the cloud formed at near-maximum relative fuel/air velocity.

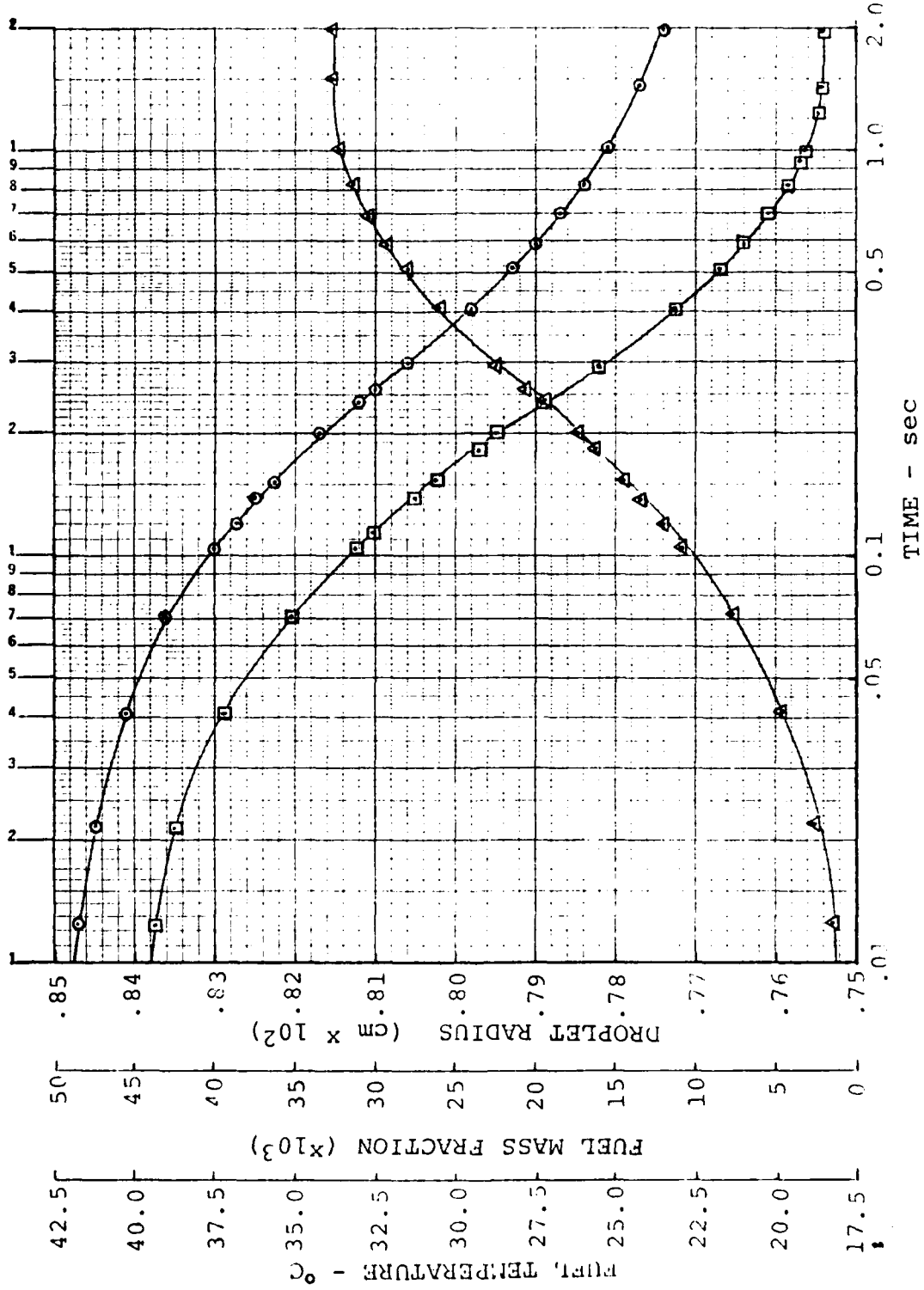


FIGURE II-8. VARIATIONS OF FUEL TEMPERATURE, MASS FRACTION, AND DROPLET RADIUS WITH TIME FOR A MONODISPERSE HYDROCARBON SPRAY

□— FUEL TEMPERATURE  
 △— FUEL MASS FRACTION  
 ○— DROPLET RADIUS

PASS/FAIL CRITERIA.

It is entirely logical and appropriate that the criteria for flammability performance of an antimisting fuel be based on characteristics related to flame propagation under simulated crash conditions. For all scales of flammability testing, the maximum size growth rate and/or radiated flux experienced in a given test are related to established criteria.

At large scale, the work of Salmon et al.<sup>5,6,7,8</sup> is of particular significance. From movies of fireball growth during the FAATC Wing Fuel Spillage Tests, a nominal or "effective" linear fireball dimension (e.g., radius) was plotted as a function of time. The slope of a linear fit to plots of fireball radius versus time yields a single value of slope, which is effectively the nominal flame speed in distance per unit time (e.g., feet per second). Based on extensive experience with a variety of AMF's, criteria were developed as follows:

Pass	0-10 fps
Marginal	10-20 fps
Fail	>20 fps

Fireball growth data have been developed from full-scale crash test data on the SP-2H by Salmon, and were found to compare well with the FAA Wing Fuel Spillage data.

It is particularly advantageous that fireball growth is related to flame speed in the cloud--the latter being a fundamental parameter in applicable fire modeling. Furthermore, it is evident that fireball growth is being applied in the "terminal region" (see Figure II-2) of the FAA Wing Fuel Spillage facility's free air jet. This is analogous to fireball maximum size and radiation measurements made as part of the tests with the FAA's Flammability Comparison Test Apparatus (FCTA). Wake flame criteria were involved in the NWC and JPL (small-scale) Wing Spillage tests. In the former testing, a "pass" was designated if there was no fire or if only self-extinguishing fireballs occurred, or if the torch flames did not propagate (e.g., detach). A "fail" involved igniting the pool of spilled fuel, and enveloping the airfoil in flames. A "marginal" condition consisted of igniting spilled fuel but not enveloping the airfoil in flames.

The JPL small-scale wing spillage tests involved a limit on the length of the wake flame during a test (typically, 1 meter). Measurements were also made of the greatest horizontal distance traveled by a fireball after detaching from the wake flame before

self-extinguishing or contacting a barrier. The length of the fireball at this maximum distance was also measured.

It is evident that in both these cases critical pass/fail criteria are being applied within the "established flow" region of Figure II-2, and may even extend forward into the "transition" region (from "potential core" to "established" flow).

It is apparent that the pass/fail criteria discussed so far can apply to one continuum--the free air jet as depicted in Figure II-2. Hence, with adequate aerodynamic characterization and heating/ignition/combustion modeling, the several criteria and phenomena of the various test rigs and facilities might be comprehensively and thoroughly related in quantified terms to adequate engineering accuracy.

In contrast, the SwRI Spinning Disc provides a rotational rather than translational environment. Progressive degrees of mist cloud flammability involve (1) supplementing the torch flame intersected by the radial fuel ejecta, (2) the development of a "fire ring", starting with acute angles and, with increasing flammability, developing into a stable, 360° ring of flame, and (3) propagating back to engulfment of the spinning disc itself.

#### SUSTAINED FUEL FIRE.

Sustained burning of the fuel mist cloud and ignition of spilled fuel pools is the ultimate post-crash fire hazard and failure mode for an antimisting fuel. Pool ignition has been included in some pass/fail test criteria, and extensive burning is encountered with severely failed AMF's (or neat Jet A) in all flammability test facilities.

Propagation in the mist cloud is a better basis for pass/fail criteria, since the allowable fireball sizes, growth rates, and/or heat fluxes are limited to provide a generous and desirable margin of safety.

## REFERENCES

1. Anonymous, Full Scale Aircraft Crash Tests of Anti-Misting Kerosene (Interim Report), Naval Air Engineering Center, Report No. NAEC-TR-183, 4 August 1980.
2. Klueg, E. P., Large-Scale Aircraft Crash Test of Antimisting Fuel, Federal Aviation Administration Conference Proceedings, "Aircraft Research and Technology for Antimisting Kerosene," February 18-19, 1981, Report No. FAA-CT-81-181, June 1981.
3. Webster, Harry, FM-9 Anti-Misting Fuel Large Scale Crash Test #3, Federal Aviation Administration, Summary of Presentation, 6th Meeting - US/UK Technical Committee on Anti-Misting Fuel, March 24, 1980.
4. Salmon, R. F., Wing Spillage Tests Using Antimisting Fuel, Federal Aviation Administration, Report No. FAA-CT-81-11, February 1981.
5. Salmon, R. F., Wing Spillage Test, Federal Aviation Administration Conference Proceedings, Report No. FAA-CT-81-181, June 1981.
6. Klueg, E.P., FM-9 Anti-Misting Fuel Wing Spillage Test Results, Federal Aviation Administration Summary of Presentation, 6th Meeting - US/UK Technical Committee on Anti-Misting Fuel, March 25, 1980.
7. Salmon, R. F., Flame Propagation Study of Jet A and FM-9 Anti-Misting Fuel in a Moving Airstream, Federal Aviation Administration Summary of Presentation, 6th Meeting - US/UK Technical Committee on Anti-Misting Fuel, March 24, 1980.
8. Salmon, R. F. and Klueg, E.P., Test Plan, FM-9 Antimisting Fuel Wing Spillage Tests, Federal Aviation Administration, February 15, 1979 (Revised July 12, 1979).
9. San Miguel, A., Williams, M.D., Antimisting Fuel Spillage/Air Shear Tests at Naval Weapons Center, Federal Aviation Administration, Report No. FAA-RD-78-50, March 1978.
10. Miller, R. E., Wilford, S. P., Simulated Crash Fire Tests As a Means of Rating Aircraft Safety Fuels, Royal Aircraft Establishment, Ministry of Defense (Aviation Supply), Technical Report Number 71130, May 1971.

11. Miller, R. D., Wilford, S.P., Fire Resistance of Antimisting Kerosine (AMK) Under Simulated Crash Conditions, Royal Aircraft Establishment, Ministry of Defence, 16 October 1978.
12. Anonymous, Ejection of Fuel From Tank on Rocket Sled, Appendix 1, Royal Aircraft Establishment, Ministry of Defence (Aviation Supply), Undated Draft.
13. Knight, J., Visit of the Technical Group on Safety Fuels to the UK, 28-30 June 1978, Royal Aircraft Establishment, Ministry of Defence, Materials Department, Farnborough, Hants, England, July 1978.
14. Makowski, T. D., Film Analysis of Jet Propulsion Laboratory Small Scale Wing Spillage Tests, Federal Aviation Administration, Technical Center, April 1980.
15. Sarohia, V., Fundamental Studies of Antimisting Fuels, Jet Propulsion Laboratory, California Institute of Technology, Pasadena, California, AIAA/SAE/ASME 17th Joint Propulsion Conference, Colorado Springs, Colorado, July 27-29, 1981.
16. Ferrara, A., Flammability Comparison Test Apparatus, Federal Aviation Administration Technical Center, Atlantic City, N.J. (Draft Report).
17. Ferrara, A., Cavage, W., Flammability Comparison Test Apparatus Operator's Manual, Federal Aviation Administration Technical Center, Atlantic City, N.J. (Draft Manual).
18. Eklund, T. I., Cox, J.C., Flame Propagation Through Sprays of Antimisting Fuels, Federal Aviation Administration, NAFEC Technical Letter Report NA-78-66-LR, November 1978.
19. Eklund, T. I., Neese, W. E., Design of an Apparatus for Testing the Flammability of Fuel Sprays, Federal Aviation Administration, Systems Research and Development Service, Report No. FAA-RD-78-54, May 1978.
20. Eklund, T. I., Experimental Scaling of Modified Fuel Breakup, Federal Aviation Administration, Systems Research and Development Service, Report No. FAA-RD-77-114, August 1977.
21. Zinn, S. V. Jr., Eklund, T. I., Neese, W. E., Photographic Investigation of Modified Fuel Breakup and Ignition, Federal Aviation Administration, Systems Research and Development Service, Report No. FAA-RD-76-109, September 1976.

22. Mannheimer, R. J., Degradation and Characterization of Antimisting Kerosene (AMK), Federal Aviation Administration Report No. FAA-CT-81-153, Southwest Research Institute, San Antonio, Texas, Interim Report, June 1981.
23. Mannheimer, R.J., Influence of Surfactants on the Fuel Handling and Fire Safety Properties of Antimisting Kerosene (AMK). Federal Aviation Administration Report No. FAA-RD-79-62, Southwest Research Institute, San Antonio, Texas, Final Report (Draft Copy), February 1979.
24. Davies, J.T., Turbulence Phenomena, Department of Chemical Engineering, University of Birmingham, Birmingham, England, Academic Press, New York and London, 1972.
25. Sforza, P.M., and Herbst, G., A Study of Three-Dimensional, Incompressible, Turbulent Wall Jets, Polytechnic Institute of Brooklyn, Farmingdale, N.Y., AIAA Journal, Vol. 8, No. 2, April 1969.
26. Miller, R.E., Wilford, S.P., The Design and Development of the Minitrack Test for Safety Fuel Assessment, Royal Aircraft Establishment, Ministry of Defence, Technical Report No. 71222, November 1971.
27. Suzuki, T., Chiu, H. H., Multi-Droplet Combustion of Liquid Propellants, Department of Aeronautics and Astronautics, New York University, Bronx, N.Y.
28. Chiu, H.H., Liu, T. M., Group Combustion of Liquid Droplets, Combustion Science and Technology, Vol. 17, pp 127-142, 1977.
29. Mahood, L., External Fire Model for Fuel System Vulnerability Assessment, Air Force Aero Propulsion Laboratory Report AFAPL-TR-79-2053, Falcon R&D, Denver, Co., July 1980.

### III. ANALYSIS OF FLAMMABILITY TESTS

#### GENERAL.

This section consists of analyses of the antimisting fuel (AMF) flammability tests, data correlations and uncertainties, and methods for enhancing data correlations.

#### FULL-SCALE CRASH TESTS.

The full-scale crash tests performed by the Naval Air Engineering Center, Lakehurst, N. J., have provided highly credible data on the performance of neat Jet A and AMF under "real-world" survivable crash conditions. The credibility is achieved primarily because:

1. An actual aircraft is employed with very plausible fuel tank damage mechanisms.
2. A variety of conservatively severe ignition sources are used.
3. Each test involves high initial speeds and deceleration of the aircraft over a carefully prepared impact course.
4. Good diagnostics on aircraft dynamics allow analysis and comparison of the tests.

The obvious limitation is the cost and time involved to test each candidate AMF.

Results of two crash tests (Nos. 1 and 2) of the SP-2H are presented in reference 1. In addition, we have analyzed data from test number 4.<sup>2</sup> Data comparisons are presented later in this section in conjunction with data from other tests. The reader is referred to the referenced reports if details of the testing are desired. The remainder of this analysis will focus on specific test aspects, relating the test conditions and parameters to (1) the phenomenology discussed in the previous section, and (2) to similar parameters of other AMF flammability tests.

FUEL AND AIR FLOW. Since the test aircraft were moving in relation to essentially quiescent atmosphere, the velocity of the aircraft relative to the ground suffices for an absolute value of relative air velocity. In reference 1, graphs of aircraft velocity versus position are provided for Tests 1 and 2 (involving,

respectively, neat Jet A and Jet A with 0.28% and 0.3% FM-9 anti-misting additive).

For our analysis, we obtained oscillograph traces of acceleration versus time for these same tests. We developed and applied a computer program which accepted data points manually extracted from the oscillograph traces and computed and/or plotted (1) distance from an initial point (aircraft runout position "0" in feet), (2) longitudinal velocity in feet per second, and (3) longitudinal acceleration in feet per second per second--all as a function of time. Figure III-1 presents these graphs to the same time scale for SP-2H Test Number 1, which involved neat Jet A fuel. Figure III-2 presents data on SP-2H Crash Test Number 2 (Jet A with 0.28% and 0.3% FM-9 antimisting additive) in the same format.

We have been informed that NAEAC has demonstrated the feasibility of processing their raw data tapes to provide such data on subsequent tests without the manual effort we had to expend in picking off the data points.

The utility of the data in this format is high. First, it is generally accepted that the maximum relative fuel/air velocity places the greatest stress on candidate AMF's. Data for computing the maximum relative fuel/air velocity in a given test are available from this format. Air velocity vs. time is readily available, and can be related back to position on the crash site by reference to the distance/time graph.

Velocities must be considered in conjunction with the deceleration forces acting on the fuel in the wing tanks. The latter determine the instantaneous force acting on the fuel being expelled through 6-inch high by 9-inch wide openings punched in the forward walls of the twelve wing fuel tanks.

The procedure given in reference 1 using instantaneous acceleration was applied in computing a velocity of neat Jet A relative to the aircraft. Table III-1 presents average and peak deceleration magnitudes and time duration needed for computing forward fuel expulsion velocities. Also included are the aircraft speeds for the corresponding times, and aircraft position data. Table III-2 presents the fuel expulsion velocities and total relative fuel-to-air velocities for five selected time increments. The increments were selected (1) as the relatively higher values of peak acceleration at high velocity, and (2) representative sustained deceleration at lower velocity later in the crash runout.

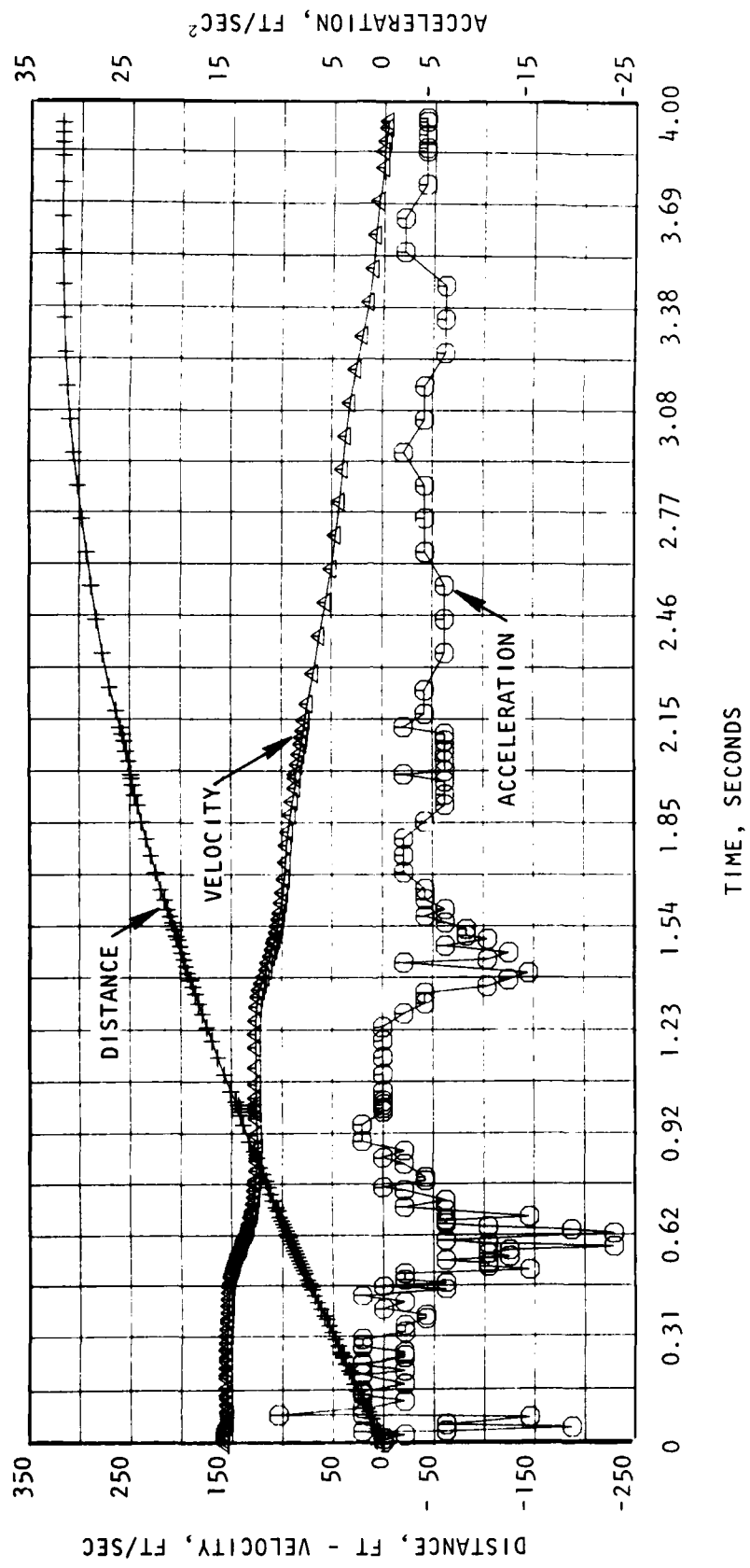


FIGURE III-1. DISTANCE, VELOCITY, AND ACCELERATION VERSUS TIME, SP-2H CRASH TEST NO. 1.

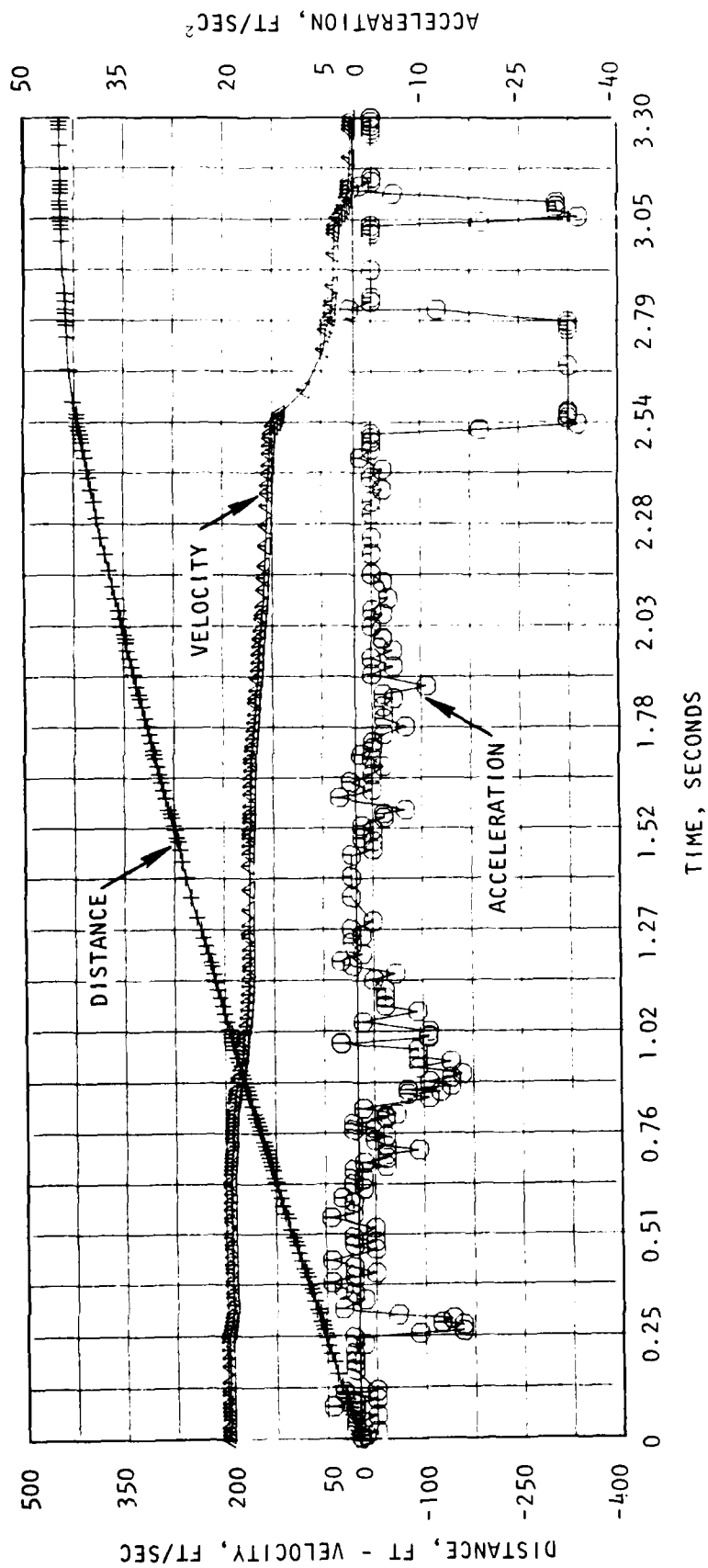


FIGURE III-2. DISTANCE, VELOCITY, AND ACCELERATION VERSUS TIME, SP-2H CRASH TEST NO. 2.

TABLE III-1. Selected Data from SP-2H Crash Test No. 1  
(Neat Jet A Fuel)

Time Increment No.	Duration		$\Delta T$ (sec.)	Deceleration		Aircraft Velocity (fps)	Aircraft Position	
	From (sec.)	To (sec.)		Peak (g's)	Avg. (g's)		From (ft.)	To (ft.)
1	0.028	0.078	0.050	5.2	2.6	154.0	4.5	12.2
2	0.078	0.113	0.035	(3.2)	(1.6)	154.5	12.2	22.0
3	0.113	0.310	0.197	0	0	154.7	22.0	34.0
4	0.310	0.390	0.080	1.3	0.9	153.8	34.0	62.2
5	0.390	0.760	0.370	4.7	2.3	150.1	62.2	113.7
6	0.760	0.850	0.090	1.6	1.1	125.3	113.7	125.0
7	0.850	0.885	0.035	0.65	0.31	124.2	125.0	130.6
8	0.885	1.000	0.115	(0.93)	(0.46)	125.5	130.6	142.2
9	1.000	1.240	0.240	0	0	125.7	142.2	174.2
10	1.240	1.660	0.420	4.5	2.0	111.2	174.2	220.9
11	1.660	3.000	1.340	1.5	1.5	94 to 36	220.9	307.1

TABLE III-2. SP-2F Crash Test No. 1, Liquid Breakup Model Input  
Velocities and Droplet Data Output

Time Increment No.	Velocities				Positions		Droplet Diameters			Breakup Time* (sec.)	Time Steps		
	Duration (sec.)	Average g's	A/C (ft/s)	Fuel (ft/s)	Fuel-to-Air (ft/s)	From (ft)	To (ft)	Primary D mm (cm)	Final D mm (cm)			10% Spray Mass < D (cm)	90% Spray Mass < D (cm)
1	.050	2.6	154	34	188	4.5	12.2	.182	.0369	.011	.076	1.0 E-3	17
5	.370	2.3	150	32	182	62.2	113.7	.190	.0382	.012	.080	1.1 E-3	14
6	.090	1.1	125	22	147	113.7	125.0	.252	.0480	.014	.11	3.0 E-3	26
10	.420	2.0	111	30	141	174.2	220.9	.267	.0503	.015	.12	3.3 E-3	27
11	1.340	1.5	94	26	120 to 62	220.9	307.1	.330	.0600	.018	.13	4.8 E-3	32
			to 36					.797	.125	.039	.27	23.7 E-3	51

\* Breakup time is total time for secondary breakup to occur; primary breakup time not included but is short (< 0.1 ms).

LIQUID BREAKUP. The major purpose of the analysis of the crash dynamic data was to establish compatibility between large-scale testing and liquid breakup analysis and modeling. Liquid breakup is discussed in detail in Section V. This is particularly important considering the general lack of droplet size and distribution data for large-scale tests.

Referring again to Table III-2, the input data were applied to the Falcon R&D Liquid Breakup Computer Model to obtain the droplet data presented. Applicable assumptions for this computation were:

Fuel: (Neat Jet A)

Density	$\rho_L = 0.807 \text{ g/cm}^3$
Surface Tension	$\sigma = 30 \text{ dynes/cm}$
Viscosity	$\eta_L = .015 \text{ poise}$

Air:

Density	$\rho_g = 1.293 \times 10^{-3} \text{ g/cm}^3$
Viscosity	$\eta_g = 1.722 \times 10^{-4} \text{ poise}$

Temperature (Fuel & Air)  $T = 0^\circ\text{C}$

Orifice Diameter (Avg.)  $D_o = 7.2 \text{ inch} = 18.3 \text{ cm}$

It is important to note that the model is limited in this application by the necessary assumption of a circular orifice, and by its current omission of the effects of Taylor-modified breakup-- which is evidently applicable in these tests. Droplet evaporation is also neglected in this example. Table III-2 summarizes the data for primary and final droplet mass median diameters, and the 10% and 90% diameters for the six time increments selected. Figures III-3 through III-8 present the droplet diameters versus cumulative mass percent as computed and graphed by the computer program for six time increments.

In all cases, the upper (solid) curve is the "primary" droplet size spectrum, terminating with the symbol "M." The "final" droplet spectrum is a lower dotted line, terminating in a number which represents the time steps taken in secondary breakup before reaching the "final" distribution. For these runs, steps 1 through 20 were each increments of 0.06 milliseconds; steps 21 through 40, 0.30 milliseconds, and steps 41 through 60, 1.50 milliseconds.

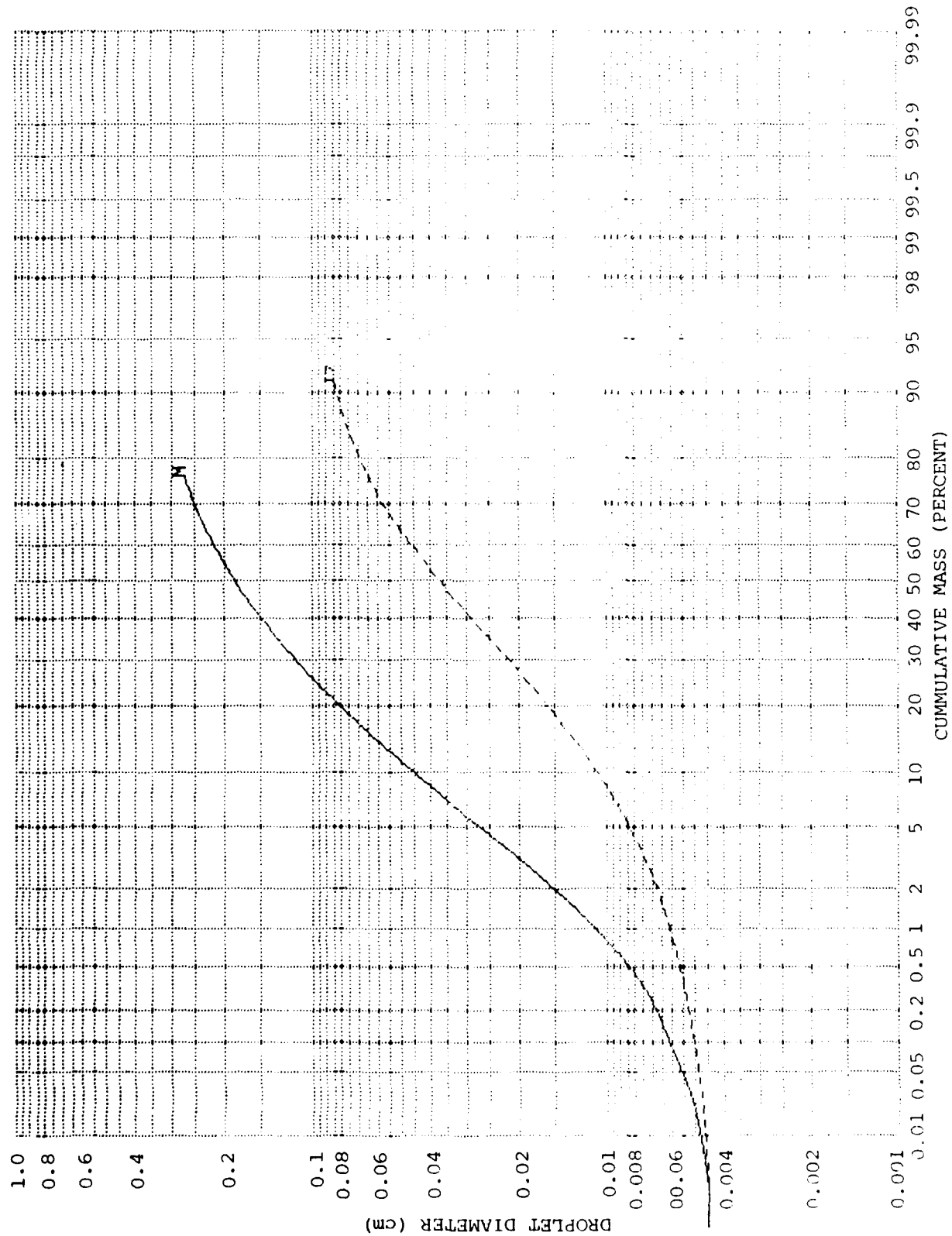


FIGURE III-3. DROPLET DIAMETER VERSUS CUMULATIVE MASS PERCENT - TIME INCREMENT NO. 1

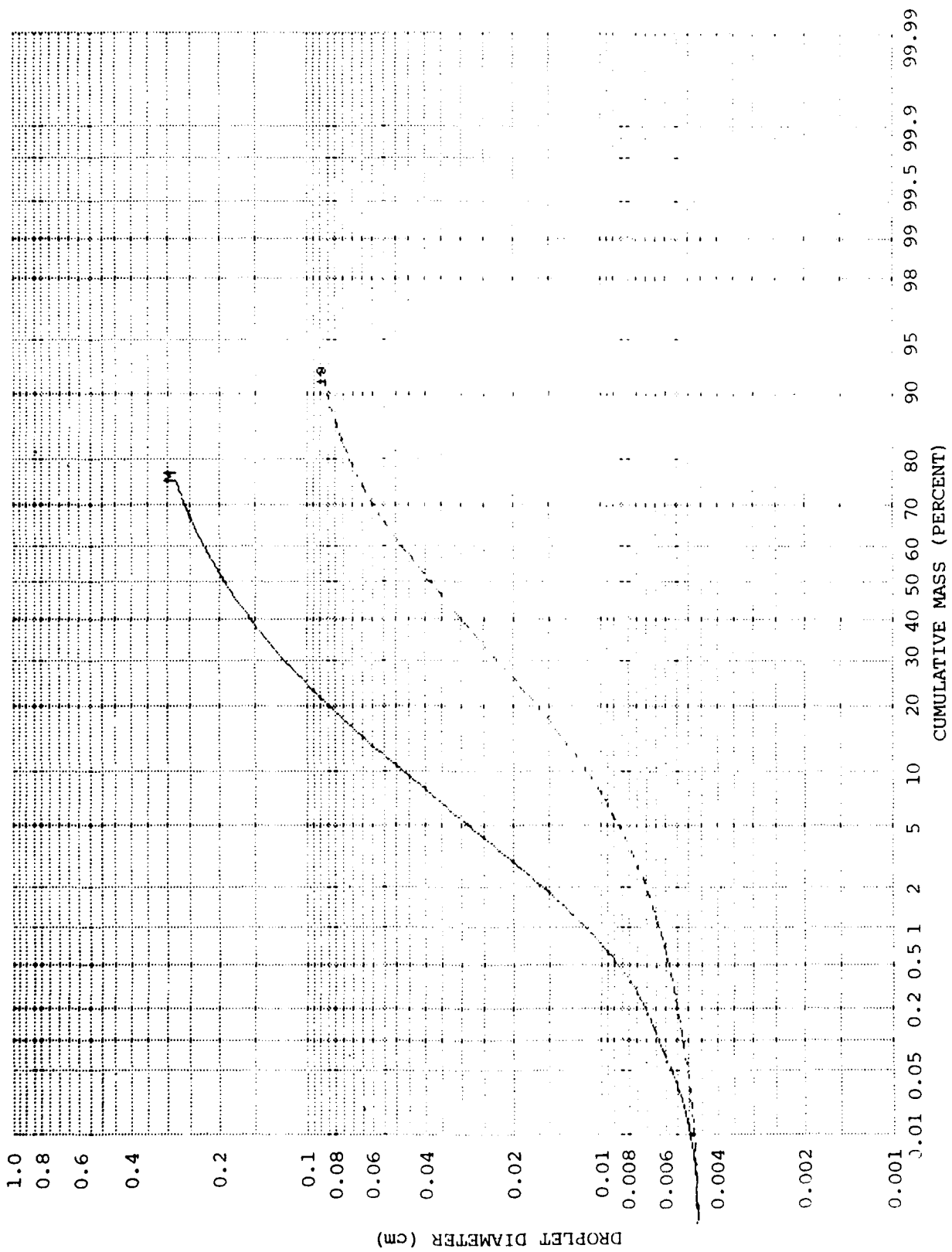


FIGURE III-4. DROPLET DIAMETER VERSUS CUMULATIVE MASS PERCENT - TIME INCREMENT NO. 5

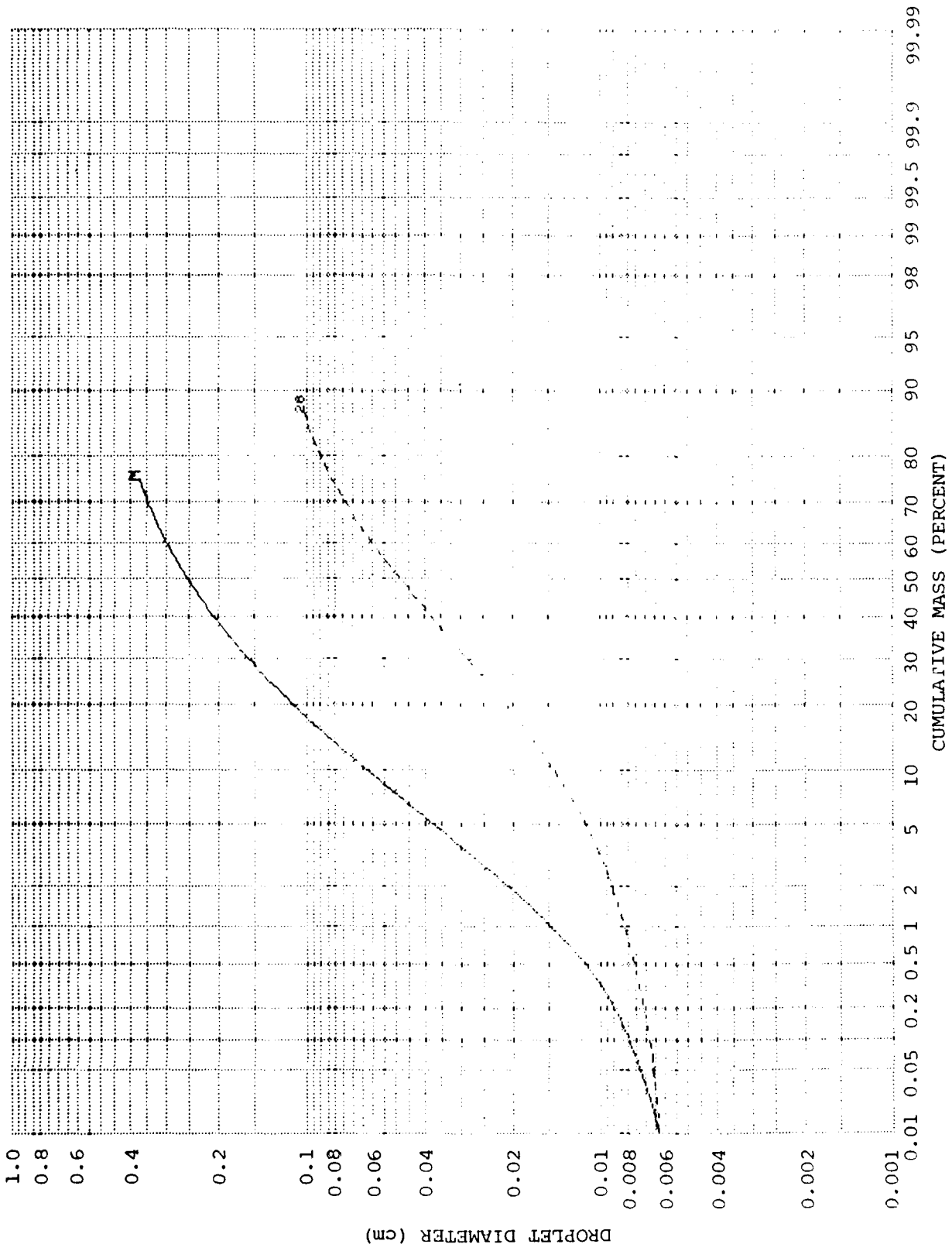


FIGURE III-5. DROPLET DIAMETER VERSUS CUMULATIVE MASS PERCENT - TIME INCREMENT NO. 6

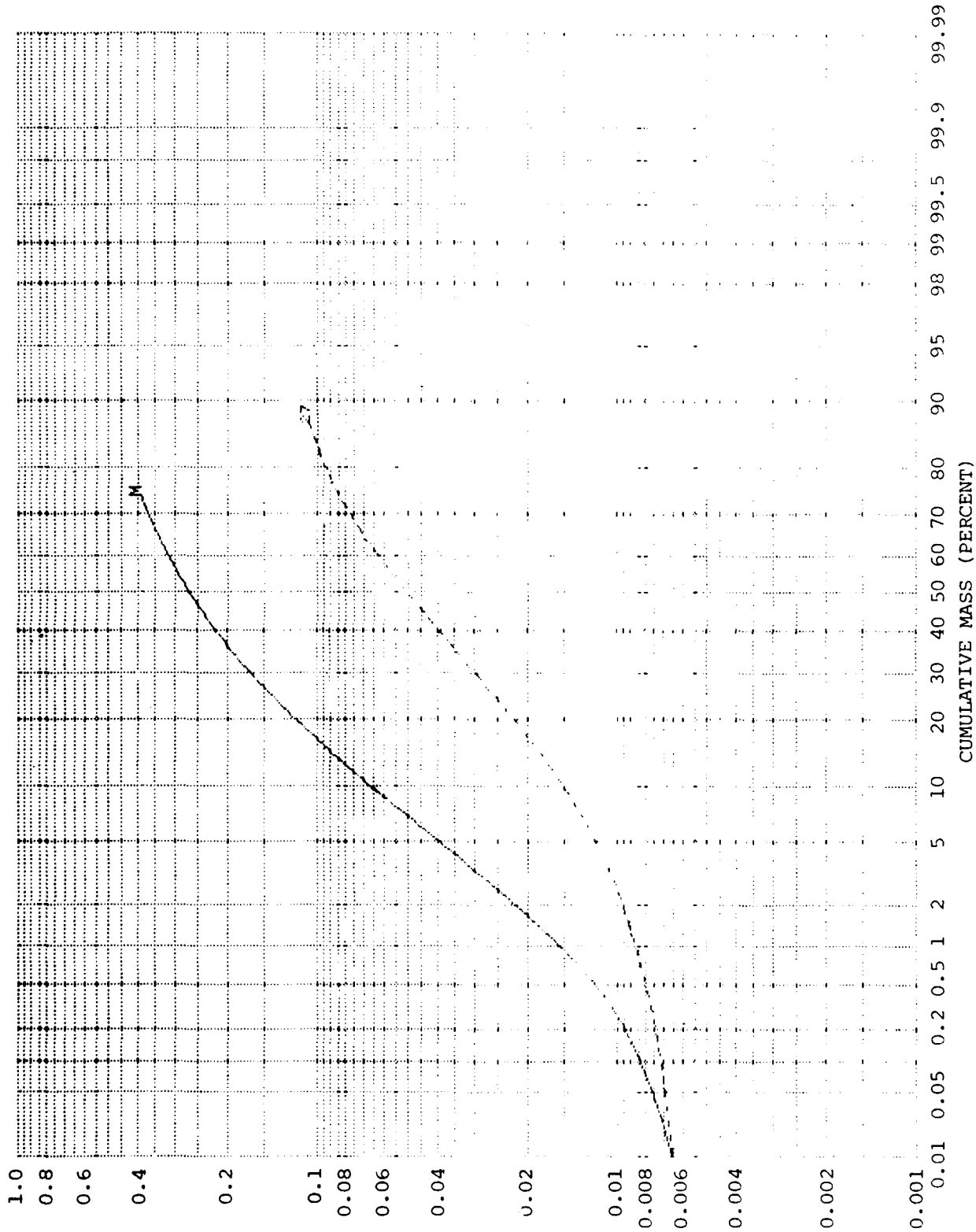


FIGURE III-6. DROPLET DIAMETER VERSUS CUMULATIVE MASS PERCENT - TIME INCREMENT NO. 10

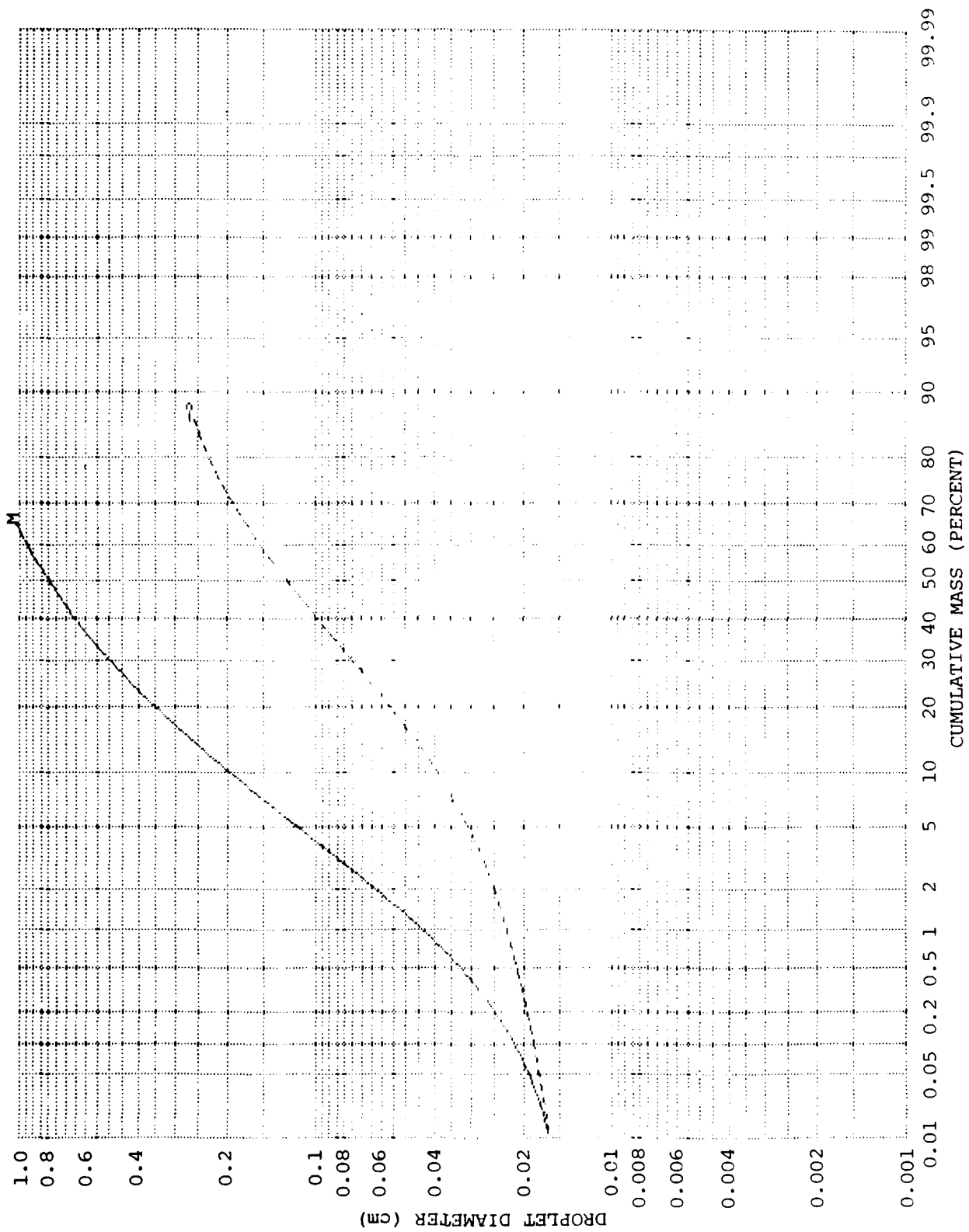


FIGURE III-7. DROPLET DIAMETER VERSUS CUMULATIVE MASS PERCENT -  
 TIME INCREMENT NO. 11, HIGH VELOCITY

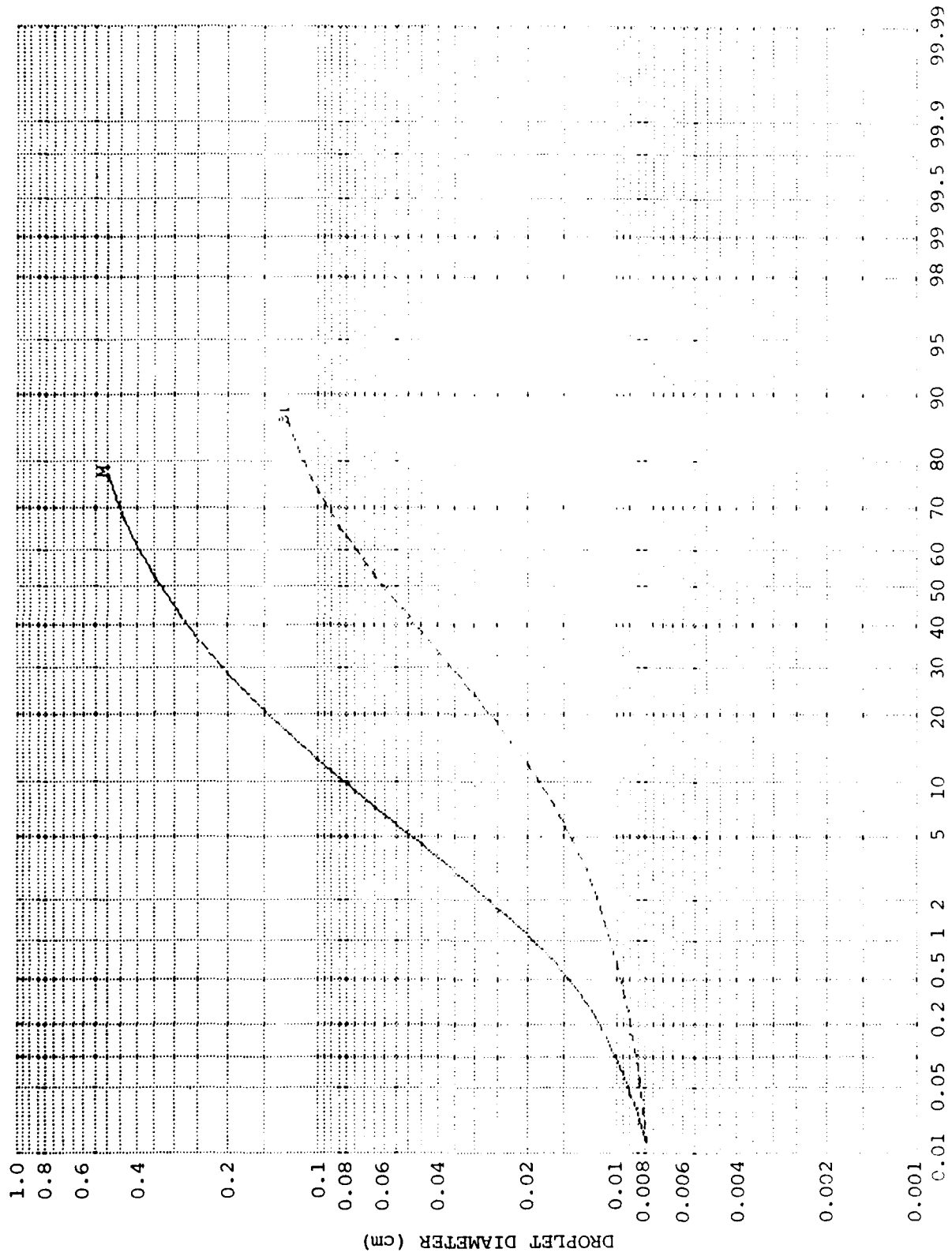


FIGURE III-8. DROPLET DIAMETER VERSUS CUMULATIVE MASS PERCENT - TIME INCREMENT NO. 11, LOW VELOCITY

Review of Table III-2 and the six related graphs reveals a consistent trend towards larger droplets with diminishing relative fuel-to-air velocity. Corresponding aircraft position data indicate the locations along the "runout" to which these elevated fuel-to-air velocities apply. The earlier time increments represent both the higher velocity and deceleration conditions along the entire crash runout. Hence, they represent the most stressful conditions for the spilled fuel. These position data indicate the sequences of minimum-sized droplet populations that are being deployed in the mist cloud along the crash "runout." The time data can be applied to fuel discharge data to obtain the quantity of fuel for each increment.

Of course, it is evident that all the droplet populations produced during this crash with neat Jet A fuel were readily flammable--the port wing is engulfed in flames from early in the crash sequence (per the photos in reference 1). However, for AMF testing, the application of the liquid breakup model could be an invaluable supplement to data analysis, as follows:

1. The model could be used to establish optimum locations along the crash runout to array fuel mist cloud (droplet) diagnostics.

2. Discrete droplet data from a crash test could be used in conjunction with the more comprehensive model predictions to define subdivided mist clouds with characteristic droplet populations.

3. Any regions of an AMF mist cloud in which ignition or propagation are observed in films could be compared with corresponding droplet population data. This feature would be invaluable when "marginal" conditions are encountered in crash tests, as are encountered in other flammability tests.

A similar analysis cannot be performed on Test Nos. 2 and 4 since the breakup model does not currently account for Taylor breakup, and a data base of antimisting fuel droplet spectra is not available for model alignment. However, it is quite feasible to extend the model to AMF's with further development.

Quantitative mist cloud analysis applied to full-scale crash tests is highly desirable for direct comparison to both large- and small-scale AMF flammability testing. If scaled rigs show that critical droplet populations are developed under similar (or scaled) test conditions, credibility is vastly enhanced. Indeed, a consistent set of critical droplet populations between various

AMF flammability tests would enable unprecedented correlation and credibility.

#### WING FUEL SPILLAGE TESTS.

Table III-3 compares the five wing fuel spillage facilities studied in terms of scale and dynamics. They are discussed in the following paragraphs.

#### FAA WING FUEL SPILLAGE FACILITY.

This facility represents a mature stage of AMF flammability testing. The facility employs a 69-inch square free air jet driven by a turbofan engine. This is sufficient for full-scale representation of a large breach in a wing tank, and high fuel spillage rates. An invaluable advantage is the fixed test article, which allows for fixed diagnostics, ignition sources, etc. Steady-state spillage, ignition, and propagation conditions can be studied, in addition to variable air and fuel flow conditions simulating various stages in a crash. Controllability of test variables and conditions is greater than for aircraft crash testing. The generally non-destructive nature and more rapid turnaround time compared to the crash tests make it an invaluable tool for studying at full scale the sensitivity of variables such as: AMF additive type and concentration, relative and absolute fuel and air velocities, fuel orifice size and shape, variable (reducing) air speed and fuel discharge, angle-of-attack, proximity of the ground plane, sensitivity to various temperatures, and type, location(s), and time variations of ignition sources. As discussed in the previous section, pass/fail criteria have evolved to a measurement of fireball growth rate, which has been correlated to the full-scale SP-2H crash tests.

A similar opportunity exists for correlation with the full-scale crash tests in terms of liquid breakup. For example, the six time increments of Table III-2 represent SP-2H crash conditions averaged over various time durations. Each such increment could be simulated under steady-state conditions with this wing spillage facility. "Cold" tests could be performed at these conditions, allowing deployment of droplet diagnostics without the complication of fire. Comparing droplet size and number density data from full-scale crash tests and FAA wing spillage facility could provide a wealth of "hard" data for full correlation and, if necessary, adjustments in independent test variables, such as air velocity, fuel velocity, etc.

TABLE III-3. Wing Fuel Spillage Facilities

Description	Scale	Airflow	Tank	Fuel Expulsion
FAA Wing Fuel Spillage Facility	Full	Free Air Jet	Static	Pressure Head
NWC Wing Spillage Facility	Large	Free Air Jet	Static	Gravity Head
RAE Rocket Sled Test Facility	Large	Static	Moving	Deceleration
RAE Minitrack Test Facility	Small	Static	Moving	Deceleration
JPL Mini-Wing Shear Facility	Small	Free Air Jet	Static	Pressure Head

The droplet data so developed would be equally as important as a basis for evaluating droplet data from small-scale AMF flammability test rigs for a like comparison.

#### NWC WING SPILLAGE FACILITY.

This facility is smaller in size than the FAA wing spillage facility, and may be considered a stage in the development of the latter. It is more limited in the number and range of independent test variables that can be simulated. It is not considered a good candidate for further characterization in terms of liquid breakup or flame ignition and propagation.

#### RAE ROCKET SLED TEST FACILITY.

As with the full-scale crash tests, no airflow simulation is needed since, in the "standard" test, the wing tank is first accelerated and then simultaneously opens its forward-facing slit-type orifice and is controllably decelerated. The fuel is expelled into a pre-deployed ignition array--as many as 36 one-pint kerosene containers with burning wicks. Alternately for the 'run on" tests, the orifice plug is released upon sled acceleration. After rocket motor burnout, friction provides low deceleration (e.g., 0.5 to 1.0 g) and fuel exits the open slit at very low velocity relative to the tank. Suspended burners ahead of the sled arrestor cable are provided as ignition sources for fuel released in this manner.

Reference 3 provides the basis for various deceleration rates, and compares deceleration pulses achieved with 1- and 2-rocket test runs versus 50th and 90th percentile crashes.

The deceleration pulses vary greatly in time history, with the following peaks:

95th Percentile Accident	=	26g
50th Percentile Accident	=	14g
1-Rocket Test	=	5g
2-Rocket Test	=	12g

Fuel ejection velocities versus time are also compared between the 1- and 2-rocket "standard" tests and for the 95th percentile accident for tanks of three different longitudinal dimensions (1.52, 3.05, and 6.1 meters; i.e. 9, 10, and 20 feet). Table III-4 presents representative values. It can be noted that both sled tests start with their maximum fuel ejection velocity, and gradually diminish by about 20 to 25 percent. In contrast, the crash pulses start at about 40 meters per second at time zero, peak at

TABLE III-4. Fuel Ejection Velocity in Meters/Sec.  
(From Reference 3)

95th Percentile Accident	Time: 0 ms.	75 ms.	150 ms.	160 ms.
Tank Length:	Velocities (in Meters Per Second):			
20 ft	39	81	15	N.D.*
10 ft	38	65	15	N.D.
5 ft	38	53	15	N.D.
2-Rocket Sled Test	68	55	52	51
1-Rocket Sled Test	43	35	36	35

\* N. D. - No Data

about 75 milliseconds, and decay to about 15 meters per second at 150 milliseconds.

The sensitivity of the differences between the magnitudes of fuel ejection velocities between pulse-type crash conditions and the sustained expulsions of the sled testing is not quantitatively assessed. This is another case where droplet size spectra and number density data from selected sled test runs could be compared directly with data from similar runs (but with deceleration pulses) of the full-scale crash tests. Liquid breakup modeling could also be used to assess the variation in droplet populations with widely varying relative fuel/air velocities between the given theoretical and test conditions.

In relation to breakup, the range of heights of the slit type orifices in the leading edges of the large wing tank appears to transcend ranges of distinctly different phenomena. RAE reports that for the larger tank, the 30-inch (762-mm) wide slit can be varied in height from 1/8 inch (3.2 mm) to 1 inch (25.4 mm), whereas the smaller tank slit is 18 inches (457 mm) wide by 1/2 inch (12.7 mm) high. Our analysis indicates that for minimum orifice dimensions above and below about 1/2 inch, different breakup phenomena apply (see Section V, "Liquid Breakup"). This would indicate that some scaling may be necessary to correlate droplet data from slits as small as 1/8 inch versus 1-inch slits.

#### RAE MINITRACK TEST FACILITY.

The Minitrack test facility<sup>4</sup> was developed to provide in a small scale test an indication of the capability of a given candidate AMF to pass the "standard" (i.e., deceleration) sled test using one rocket for propulsion. Typically, this gives a sled velocity of 35 meters per second at arrestor contact, with a mean deceleration of about 5 g. For the Minitrack with a fuel volume limitation of 50 ml, and fuel longitudinal dimension of 3 inches (76.2 mm), the corresponding speed selected was 37 meters per second, with a mean deceleration of 30 g (six times greater). It is interesting to note that the orifice dimension of 5/16 inch (8 mm) implies that scaling is according to our liquid breakup-based limit of 1/2 inch. Comparing the results of five different candidate AMF's, the RAE found that it took 2.3 to 3.3 times as much additive concentration in the large-scale sled test fuel compared to the Minitrack to get comparable "passing" results.

The necessary modification to the Minitrack to evidently limit spray dispersion (i.e., increase droplet number density) has been previously discussed in Section II. This is another case where droplet size spectra data on large- and small-scale AMF

flammability facilities would be invaluable. It is conceivable that the Minitrack could be adjusted to provide representative mist clouds in quantitative terms. Droplet measurements on a screening test such as this might also indicate anomalous performance of an AMF with a different sensitivity to the Minitrack's particular dynamics.

#### JPL MINI-WING SHEAR FACILITY.

This facility utilizes a free air jet 8 inches in diameter at discharge, capable of a maximum speed of 80 meters/second. Approximately two diameters downstream, centered (elevation view) in the jet, is the mini-wing leading edge, incorporating a slit 0.5 cm (0.2 inches) high for fuel release upwind. Maximum fuel ejection speed is 15 meters/sec. Located approximately 3.6 air jet diameters downstream (centered in the jet) is an oxy-acetylene flame whose holder and mass flow can be altered to vary ignition source size and energy release rate.

Thermocouples at four locations downstream (from about 7 to 17 diameters from the free jet orifice) along the jet flow axis monitor wake flames.

Test parameters are air jet speed, fuel ejection speed and mass flow, fuel temperature, and AMF concentration.

This facility must be considered in the broader context of a multifaceted program by JPL to advance AMF technology. This includes fundamental study of AMF behavior during breakup (e.g., pendant droplet testing), development of a somewhat larger small-scale wing shear apparatus, and application of advanced imaging techniques to quantitatively evaluate AMF mists.

The advanced imaging techniques have already been applied to the JPL Mini-wing testing. Reference 5 provides preliminary data and images on fuel mists for Jet A neat and with FM-9 AMF in concentrations of 0.1, 0.2, and 0.3% by weight. This work is particularly relevant to correlations of AMF flammability test rigs, since combustion-based correlations may be supplemented by quantitative droplet data correlations.

The data presented in reference 5 are promising, but need the following features to allow direct correlation with liquid breakup models and/or less sophisticated diagnostics being recommended for other AMF flammability tests:

1. The droplet mist should be characterized in the region of the ignition source. As illustrated by the example model

output, Figures III-3 through III-8, breakup may still be progressing--particularly in the evident wake of air and fuel off the trailing edge of the wing.

2. Data in the form of cumulative mass fraction versus droplet diameter (Figure II-6) are also highly desirable for the region of the ignition source.

3. Droplet number density data by droplet size range (e.g., increment of cumulative mass fraction, Figure II-6) in the region of the ignition source are also highly desirable.

The above may represent the practical and economic limit of data that may be obtained at other AMF flammability test facilities.

It is also desirable that a generous data base be established which directly relates droplet characterizations to flammability results over a wide range of independent test variables, including air and fuel ejection speed, fuel mass flow and temperature, AMF additive concentration, flameholder configuration, and flame mixture flow rate. To facilitate comparisons, the values of these parameters are needed, in addition to any scaling schemes.

Pass/fail criteria related to the JPL Mini-wing have been previously discussed--based on wake flame measurements by Makowski of the FAA. Another Pass/Fail method is defined by V. Sarohia (reference 5). The aforementioned thermocouples in the wake flame have registered a large difference in "reduced temperature," as much as an order of magnitude, depending on whether the ratio of fuel-to-air mass flow rates was above or below about 0.1. For example, increasing the mass flow ratio from 0.08 to 0.11 increases the "reduced temperature" at one thermocouple location (about 11 diameters from the air jet's orifice) from about 0.02 to about 0.21. This was for 0.1% FM-9 by weight in Jet A. Associated with these flammability test results are corresponding images of the two mist clouds. According to Sarohia, this large change in recorded temperature may be used to define "pass" and "fail" mist configurations.

No data have been located characterizing the free air jet utilized, other than the single velocity in the "potential core," and related air mass flow rates and temperatures. Characterization of extreme and mean velocities and turbulence intensities are desirable in the region(s) of liquid breakup, ignition/heating, and propagation.

## FAA FLAMMABILITY COMPARISON TEST APPARATUS.

The FCTA has been developed to provide a common apparatus for evaluating the flammability of AMF's at various facilities. Five units have been shipped to various test facilities, with a sixth retained at the FAA Technical Center. The FCTA provides a portable, self-contained, semi-automatic test system which requires minimal test fuel and can be operated indoors with adequate space and proper precautions. AMF's can be evaluated at various fuel flow rates and air speeds. The units have been calibrated and come with an operating manual. The FCTA is invaluable for screening the candidate AMF's and for monitoring the flammability performance of various batches of AMF at different points in their storage life.

Details on the FCTA are presented in reference 6. Flammability criteria have been discussed in Section II. Briefly, air from a pressurized tank is introduced into a 1-inch I.D. mixing pipe in a velocity range of 40 to 80 meters/sec. Test fuel is expelled from a cylinder by a motor-driven piston into a 0.25" thin wall stainless steel tube. This tube penetrates the air pipe and extends along its centerline 4.5 inches before expelling the fuel upstream into the air flow, typically at rates from 8 to 18 ml/sec.

The two-phase mixture proceeds downstream where it is expelled through a 16-inch diffuser whose large end is 4 3/16-inches in internal diameter. The diffuser protrudes through the right-hand side of the FCTA's cabinet. A bucket catches liquid from the diffuser's outlet, and a 4-foot by 8-foot steel pan collects air-carried ejecta. A propane torch is mounted along the axis of the diffuser, pointed downstream, with the flame holder tip about five inches from the exit plane of the diffuser. Any resulting combustion is recorded photographically against a background grid, and by a radiometer looking orthogonal to the axis of flow--20 inches to the side and 9 inches away from the right-hand wall of FCTA's cabinet. Runs are typically performed at various combinations of fuel flow rate and air speed to obtain sequentially more severe test conditions and combustion responses. The FCTA is the culmination of development work as given by references 7, 8, 9, and 10.

ANALYSIS. The FCTA differs from the wing spillage rigs in that (1) no replica wing is provided for fuel/spray impingement and possible reintroduction into the air flow, and (2) the air supply, liquid jet, plume, and diffuser regions are enclosed. Referring back to Section II, Figure II-4, when the diameter of

the fuel plume exceeds the diameter of the bounding pipe, impingement of the entire periphery of the plume occurs. This peripheral impingement is obviously fundamentally different from impingement upon an airfoil traversing approximately the horizontal diameter of the plume. Considering the mechanics of liquid breakup in the airstream, it is reasonable that the smallest and most rapidly subdivided fuel particles would be selectively recombined by impacting the inner wall of the 1-inch I.D. pipe of the FCTA; whereas tests with an airfoil give impingement across a small horizontal "slice" through the plume--involving only a small proportion of the outer plume droplets. In such a case, the peripheral impingement of the FCTA might provide coarser droplets and, hence, less flammable mixtures than with the same conditions but without peripheral impingement.

It is not evident whether the range of fuel and air flows of the FCTA will yield conditions of substantial peripheral impingement in some cases, and very low or minimal impingement in others. In some operations of the FCTA, a substantial proportion of the test fuel load, 20% or greater, has been observed to flow as a liquid from the diffuser after a test run. This would indicate, barring some malfunction of the FCTA, that very substantial impingement is occurring.

If FCTA operations do cross over from low to high impingement, the test results may be significantly shifted--since droplets stripped from liquid fuel in contact with the inner surface of the pipe are formed in a very complex boundary layer, whose characteristic velocity profiles and turbulence intensities may vary radically from the nominal air flow conditions calibrated and measured in the main flow stream. This is further complicated by the fact that fuel mixing is occurring before turbulent air flow has been fully established after passing through the sonic "choke" orifice.

It might be argued that the impingement and reformation of much of the liquid in a given FCTA test might represent the close proximity of a ground plane to a wing--e.g. with a low-wing aircraft crash scenario. Although it is true that large quantities of spray will be intercepted by the ground plane, the fact remains that as much as 180° of the outer plume would not impinge on the ground plane, whereas 360° of the plume impinges with the peripheral confinement of the FCTA.

Regardless of the mechanism whereby droplets are formed, an objective criterion can be based on liquid breakup analysis and modeling with appropriate droplet size and distribution data. The

FCTA appears ideally suited for droplet characterization in the region of ignition and fireball propagation. The already existing flammability data base could be rapidly supplemented by "cold" tests (e.g., no ignition source) involving relatively simple, portable droplet diagnostics. By comparing independent test variables of the FCTA (e.g., fuel and air velocity, AMF concentration) with droplet populations and flammability results, and by comparing similar data from large scale facilities such as the FAA Wing Spillage Facility, very firm and credible results should ensue. The postulated differences in breakup mechanisms discussed above become moot if relative fuel/air velocities can be found for the FCTA which give droplet populations which correspond (with scaling) to those of a large-scale facility.

#### SWRI SPINNING DISC.

The Southwest Research Institute Spinning Disc facility is unique in that it utilizes rotation to accelerate liquid AMF into the atmosphere past an ignition source. A disc about 2.5 inches in diameter is mounted horizontally on a high speed (variable) motor's shaft. A cup is centered in the disc, into which the test fuel flows from a static tube overhead. The cup connects with four radial flow channels in angular increments of 90° measured in the plane of the disc--each 2 mm in diameter and 10 mm long. The channels terminate at ports in the edge of the disc. About 3.9 inches (10 cm) from the disc's edge is an ignition flame. The disc apparatus has the interesting property that the liquid flow rate through it does not vary appreciably with RPM. Hence, for a typical test a suitable flow rate is established at low RPM, and then rotational speed is increased to a maximum of the order of 30,000 RPM. Very discrete and repeatable flammability phenomena can ensue. The first stage involves increasing growth of the flame envelope about the ignition source. At higher RPM, a remarkably stable planar semi-circle of flame develops about the torch. At still higher RPM, a full (360°), stable ring of flame typically develops. At a "worst case" condition, the flame propagates inward and engulfs the spinning disc.

ANALYSIS. Of particular concern was the physical comparability of liquid breakup by opposed air and fuel jets in longitudinal translation, versus the rotational scheme of the spinning disc. The relative fuel-to-air velocity for the spinning disc is reported as the tangential velocity of the disc; that is, the product of the disc's angular speed and its radius. Table III-5 presents tangential velocities for various rotational speeds.

TABLE III-5. Spinning Disc Dynamics

Rotational Speed (RPM)	Tangential Velocity (m/s)	Radial Acceleration (g)
6,000	19.8	1,260
12,000	39.6	5,070
18,000	79.2	11,400
24,000	158.4	20,300
30,000	316.8	31,700

This table also presents values of radial acceleration acting at each exit orifice in the disc's edge, based on:

$$A_R = r\omega^2$$

where  $A_R$  is the radial acceleration,  $r$  is the disc's radius, and  $\omega$  is the rotational speed.

Considering the high radial forces acting on the liquid at the ejection ports, and the fact that the liquid has been acted on by a radial force which has increased proportionately with distance from the disc's axis, it appears that a significant radial velocity should be vectorially added to the tangential velocity to obtain a more realistic value for the initial fuel-to-air velocity. It is also evident that the liquid is being acted upon within the flow channel by lateral Coriolis forces. These are typically expressed as the product of twice the angular velocity and the localized translational velocity vector. In this case of simple rotational motion, the translational velocity is related to the applied radial force as previously defined. This indicates that the liquid in the flow channels is being subjected to complex and extremely high forces. It seems plausible that at such high forces, unrealistic responses may be expected from viscoelastic test fuels in particular. It is possible that for one candidate AMF, the "gelling" experienced with high flow through filters may occur within this the disc's flow channels.

In addition, there is no evident mechanism except fluid drag to damp out the high rotational rates imparted to the liquid up to ejection. This could significantly influence the shapes of AMF droplets, in contrast to relatively negligible rotational effects in full- and large-scale spillage tests.

It is particularly important to directly compare droplet populations formed by the spinning disc with droplet data from large-scale tests. In this way, it is likely that an empirically derived relative fuel/air velocity (related to disc RPM) will prove more relevant than tangential velocity of the disc.

#### CORRELATION OF FLAMMABILITY TESTS.

The various AMF flammability test facilities were consistent in differentiating between fuels severely deficient in post-crash fireball reduction, and relatively successful ones. Table III-6 provides data on the characterizations of the flammability performance of neat Jet A and AMF for each of the facilities, versus appropriate independent test variables. For ease of comparison,

TABLE III-6. AMF Flammability Test Data Summary

Description (Facility/Apparatus)	Fuel		Temps.		Maximum Speeds		Orifice Config. (in.)	Fuel Flow (Gal/Sec)	No. of Tests	Flammability Results (Description/Quantity)	P M F a a i s r i s g l
	Type	Conc. (wt. %)	Fuel (°F)	Air (°F)	Air (Ft/Sec)	Fuel (Ft/Sec)					
NAEC SP-2H Crash Tests:	Jet A	0.00	68	70	203	34	237	58	1	Fire engulfed aircraft (12 orifices)	x
	FM-9	0.26	70	42	174	32	206	55	1	Limited, self-exting. fires	x
	FM-9	0.28	70	42	174	32	206	55	1	Limited, self-exting. fires	x
	FM-9	0.27	75	35	200	36	236	62	1	Avgas contam.-low spec. AMF	x
	FM-9	0.30	75	35	200	36	236	62	1	Low spec. AMF	x
FAATC Wing Spillage Tests:	Jet A	0.00	75	Amb.	220	27	247	20	Gp. 1	48 fps flame speed	x
	Jet A	0.00	75	Amb.	220	81	301	60	Gp. 1	80 fps flame speed	x
	FM-9	0.30	80	Amb.	<211	27	<238	20	Gp. 2	<10 fps flame speed	x
	FM-9	0.30	80	Amb.	211 to 228	27	238 to 255	20	Gp. 2	10 to 20 fps flame speed	x
	FM-9	0.30	80	Amb.	>228	27	>255	20	Gp. 2	>20 fps flame speed	x
	FM-9	0.30	80	Amb.	211 to 228	27	238 to 255	20	Gp. 3	10 to 20 fps flame speed	x
	FM-9	0.30	80	Amb.	216 to 233	54	270 to 287	40	Gp. 3	10 to 20 fps flame speed	x
	FM-9	0.30	80	Amb.	220 to 235	81	301 to 316	60	Gp. 3	10 to 20 fps flame speed	x
	FM-9	0.30	47	Amb.	225 to 236	27	252 to 263	20	Gp. 4	10 to 20 fps flame speed	x
	FM-9	0.30	62	Amb.	218 to 233	27	245 to 260	20	Gp. 4	10 to 20 fps flame speed	x
	FM-9	0.30	67	Amb.	215 to 230	27	242 to 257	20	Gp. 4	10 to 20 fps flame speed	x
	FM-9	0.30	81	Amb.	211 to 228	27	238 to 255	20	Gp. 4	10 to 20 fps flame speed	x
	FM-9	0.30	96	Amb.	208 to 221	27	235 to 248	20	Gp. 4	10 to 20 fps flame speed	x
	FM-9	0.30	110	Amb.	194 to 208	27	221 to 235	20	Gp. 4	10 to 20 fps flame speed	x
	FM-9	0.20	80	Amb.	166 to 191	27	193 to 218	20	Gp. 5	10 to 20 fps flame speed	x
FM-9	0.25	80	Amb.	174 to 199	27	201 to 226	20	Gp. 5	10 to 20 fps flame speed	x	
FM-9	0.30	80	Amb.	211 to 228	27	238 to 255	20	Gp. 5	10 to 20 fps flame speed	x	
FM-9	0.35	80	Amb.	238 to 250	27	265 to 277	20	Gp. 5	10 to 20 fps flame speed	x	
FM-9	0.40	80	Amb.	296 to 306	27	323 to 333	20	Gp. 5	10 to 20 fps flame speed	x	

TABLE III-6. AMF Flammability Test Data Summary (Continued)

Description (Facility/Apparatus)	Fuel		Temps.		Maximum Speeds			Orifice Config. (in.)	Fuel Flow (Gal/Sec)	No. of Tests	Flammability Results (Description/Quantity)	P M F a a S F i S G l
	Type	Conc. (wt. %)	Fuel (°F)	Air (°F)	Air (Ft/Sec)	Fuel (Ft/Sec)	Total (Ft/Sec)					
(5.5 ft. to ground)	FM-9	0.30	80	Amb.	211 to 228	27	238 to 255	4.25 dia.	20	Gp. 6	10 to 20 fps flame speed	x
(7.0 ft. to ground)	FM-9	0.30	80	Amb.	211 to 228	27	238 to 255	4.25 dia.	20	Gp. 6	10 to 20 fps flame speed	x
(11.5 ft. to ground)	FM-9	0.30	80	Amb.	211 to 228	27	238 to 255	4.25 dia.	20	Gp. 6	10 to 20 fps flame speed	x
	FM-9	0.30	80	Amb.	211 to 228	27	238 to 255	4.25 dia. flat	20	Gp. 7	10 to 20 fps flame speed	x
	FM-9	0.30	80	Amb.	211 to 228	27	238 to 255	4.25 dia.	20	Gp. 7	10 to 20 fps flame speed	x
	FM-9	0.30	80	Amb.	211 to 228	27	238 to 255	1 1/2 x 3 3/4, 3	20	Gp. 7	10 to 20 fps flame speed	x
NWC Fuel Spillage/ Air Shear Tests:	Jet A	0.00	88	81 to 100	248	11	259	6 dia.	10.3	1	40-ft. fireball	x
	FM-9	0.30	81	81 to 100	167	16,	190	6 dia.	14.5,	2	Failed ignition pulse, wing not engulfed	x
	FM-9	0.30	81	81 to 100	186	22,	208	6 dia.	20.9,	2	Pool fire or wing engulfed	x
	FM-9	0.35	80	81 to 100	186	17	208	6 dia.	19.5,	1	Self-extinguishing or no fire	x
	FM-9	0.35	80	81 to 100	206	22	228	6 dia.	15.3	1		x
	FM-9	0.40	81	81 to 100	203	18,	225	6 dia.	20.3	2		x
	FM-9	0.40	80	81 to 100	218	21	239	6 dia.	15.8,	1		x
	FM-9	0.40	82	81 to 100	240	21	261	6 dia.	19.8	1		x
	FM-9	0.45	80	81 to 100	269	17	286	6 dia.	19.0	1		x
	FM-9	0.45	84	81 to 100	285	16	301	6 dia.	18.5	1		x
	FM-9	0.50	77,	81 to 82	223, 270	16,	279	6 dia.	14.8	1		x
	FM-9	0.50	82	100	270	9			14.3	1		x
	FM-9	0.50	82	100	270	9			14.0, 7.9	3		x

TABLE III-6. AMF Flammability Test Data Summary (Continued)

Description (Facility/Apparatus)	Fuel		Temps.		Maximum Speeds			Orifice Config. (in.)	Fuel Flow (Gal/Sec)	No. of Tests	Flammability Results (Description/Quantity)	P M F a a a s r i s g l	
	Type	Conc. (wt. %)	Fuel (°F)	Air (°F)	Air (Ft/Sec)	Fuel (Ft/Sec)	Total (Ft/Sec)						
UK/RAE Rocket (2 Rockets)  Sled Tests:	Avtur	0.00	65	Amb.	220	26	246	0.5 x 18	16	1	Large fire	x	
	Diesel	0.00	51	Amb.	220	26	246	0.5 x 18	16	1	Large fire	x	
	FM-9	0.20	32	Amb.	220	26	246	0.5 x 18	16	1	Large fire	x	
	FM-9	0.30	-33 to -4	Amb.	220	26	246	0.5 x 18	16	3	No fire or flare	x	
	FM-9	0.30	34	Amb.	220	26	246	0.5 x 18	16	1	Borderline pass	x	
	FM-9	0.30	43 to 50	Amb.	220	26	246	0.5 x 18	16	8	No fire or flare	x	
	FM-9	0.30	50	Amb.	220	26	246	0.5 x 18	16	1	Borderline pass, flare	x	
	FM-9	0.30	52 to 84	Amb.	220	26	246	0.5 x 18	16	17	No fire or flare	x	
	FM-9	0.30	86	Amb.	220	26	246	0.5 x 18	16	1	Flare	x	
	FM-9	0.30	88	Amb.	220	26	246	0.5 x 18	16	1	Borderline pass	x	
	FM-9	0.30	88	Amb.	220	26	246	0.5 x 18	16	1	Borderline fail	x	
	FM-9	0.30	97	Amb.	220	26	246	0.5 x 18	16	1	Flare	x	
	FM-9	0.40	97	Amb.	220	26	246	0.5 x 18	16	2	Flare	x	
	FM-9	0.30	45	Amb.	289	33	322	0.5 x 18	17	1	Borderline pass	x	
	FM-9	0.30	59 to 78	Amb.	289	33	322	0.5 x 18	17	3	No fire or flare	x	
	JPL Mini-Wing Spillage Tests:	FM-9	0.30	73	Amb.	289	33	322	0.5 x 18	17	1	Borderline pass	x
		FM-9	0.30	77 to 86	Amb.	289	33	322	0.5 x 18	17	3	Flare (2), mist ign. (1)	x
FM-9		0.40	79 to 86	Amb.	289	33	322	0.5 x 18	17	2	Borderline pass	x	
FM-9		0.50	93	Amb.	289	33	322	0.5 x 18	17	1	No fire or flare	x	
FM-9		0.50	95	Amb.	289	33	322	0.5 x 18	17	1	Borderline pass	x	
FM-9		0.30	70	Amb.	190	28	218	0.2 x w	N.D.	1	.3 to 2.8 ft. wake flame	x	
FM-9		0.30	70	Amb.	210	18	228	0.2 x w	N.D.	1	.9 to 3.1 ft. wake flame	x	
FM-9		0.30	70	Amb.	210	28	238	0.2 x w	N.D.	1	.6 to 3.1 ft. wake flame	x	
FM-9		0.30	70	Amb.	210	37	247	0.2 x w	N.D.	1	1.2 to 2.8 ft. wake flame	x	
FM-9		0.30	70	Amb.	256	28	284	0.2 x w	N.D.	1	.4 to 2.2 ft. wake flame	x	
FM-9 & Glycol		0.30	70	Amb.	190	28	218	0.2 x w	N.D.	1	1.9 to 8.8 ft. wake flame	x	
FM-9 & Glycol		0.30	70	Amb.	210	18	228	0.2 x w	N.D.	1	.6 to 5.6 ft. wake flame	x	
FM-9 & Glycol		0.30	70	Amb.	210	28	238	0.2 x w	N.D.	1	1.6 to 3.8 ft. wake flame	x	
FM-9 & Glycol		0.30	70	Amb.	210	37	247	0.2 x w	N.D.	1	1.6 to 5.0 ft. wake flame	x	
FM-9 & Glycol		0.30	70	Amb.	256	28	284	0.2 x w	N.D.	1	1.6 to 3.1 ft. wake flame	x	

TABLE III-6. AMF Flammability Test Data Summary (Continued)

Description (Facility/Apparatus)	Fuel		Temps.		Maximum Speeds			Orifice Config. (in.)	Fuel Flow (Gal/Sec)	No. of Tests	Flammability Results (Description/Quantity)	P M F	
	Type	Conc. (wt. %)	Fuel (°F)	Air (°F)	Air (Ft/Sec)	Fuel (Ft/Sec)	Total (Ft/Sec)						
FAATC Flammability Comparison Test Apparatus:	Jet A	0.00	64	Room	131 to 164	6.4	170	0.09 dia.	.0021		Wake flame, <0.4 BTU/ft <sup>2</sup> -sec	x	
	Jet A	0.00	64	Room	164 to 197	6.4	203	0.09 dia.	.0021		Fwd. flame, 0.4 BTU/ft <sup>2</sup> -sec	x	
	Jet A	0.00	64	Room	197 to 246	6.4	252	0.09 dia.	.0021			x	
	Jet A	0.00	64	Room	131 to 164	7.9	172	0.09 dia.	.0026		Propagation into nozzle, 0.6 BTU/ft <sup>2</sup> -sec	x	
	Jet A	0.00	64	Room	164 to 230	7.9	238	0.09 dia.	0.026			x	
	Jet A	0.00	64	Room	246	7.9	254	0.09 dia.	.0026			x	
	Jet A	0.00	64	Room	131 to 246	12.7	259	0.09 dia.	.0032 to .0042				x
	FM-9	0.30	64	Room	148 to 246	11.2	257	0.09 dia.	.0021 to .0037				x
	FM-9	0.30	64	Room	148 to 246	12.7	259	0.09 dia.	.0042				x
	FM-9	0.30	64	Room	230	12.7	243	0.09 dia.	.0042				x
	FM-9	0.30	64	Room	148, 164	14.5	178	0.09 dia.	.0048				x
	FM-9	0.30	64	Room	181 to 246	14.5	260	0.09 dia.	.0048				x
	Jet A	0.00	77	Room	0	49 to 246	49 to 246	.079 dia.	.0022	7	Flame radiation increase (4 orifices)	x	
	Jet A	0.00	N.D.	Room	0	33	33	.079 dia.	.0022	6	Flame radiation increase	x	
FM-9	0.30	68	Room	0	227	227	.079 dia.	.0021	5	Flame radiation increase	x		
FM-9	0.30	73	Room	0	204	204	.079 dia.	.0021	5	Flame radiation increase	x		
FM-9	0.30	79	Room	0	200	200	.079 dia.	.0021	5	Flame radiation increase	x		
FM-9	0.30	93	Room	0	204	204	.079 dia.	.0021	5	Flame radiation increase	x		
FM-9	0.30	109	Room	0	200	200	.079 dia.	.0021	4	Flame radiation increase	x		
FM-9	0.20	70-	Room	0	152	152	.079 dia.	.0021	1	Flame radiation increase	x		
FM-9	0.30	80	Room	0	225	225	.079 dia.	.0021	1	Flame radiation increase	x		
FM-9	0.30	70-	Room	0	227	227	.079 dia.	.0021	7	Flame radiation increase	x		
FM-9 & Gyl-amine	0.30	N.D.	Room	0	282	282	.079 dia.	.0021	2	Flame radiation increase	x		
FM-9 & Gylcol	0.30	N.D.	Room	0	286	286	.079 dia.	.0021	2	Flame radiation increase	x		
FM-9 & SO-A	0.30	N.D.	Room	0	286	286	.079 dia.	.0021	2	Flame radiation increase	x		

SWRI Spinning Disc  
Tests:

a uniform set of units was employed in the matrix for all sources of test data. The most important independent test variables are grouped in the left-hand columns of the matrix, and the flammability results are provided at the extreme right. Implicit in our matrix is the working hypothesis that the relative fuel-to-air velocity is fundamental to liquid breakup. Since both temporal and spatial conditions are non-uniform for many of the tests, we sought to define maximum relative speeds for each of the tests. Unfortunately, the maximum absolute velocity of ejection of the liquid fuel was not explicit in much of the data, and analytical methods were reported in others. The fuel velocity data presented in Table III-6 typically represent conservatively low peak fuel ejection velocities in the absence of data to the contrary.

In the first case, the NAEC SP-2H Crash Tests, the analytical methods of reference 1 were applied. This particularly involves using the assumed coefficients of velocity and contraction, 0.985 and 0.62, respectively. This provides a relatively high fuel ejection velocity, since a sharp-edged orifice is assumed. It is noted that with a rounded-edge orifice, the contraction coefficient increases to 1.0--which yields no contraction from the 6" x 9" rectangular orifice--and hence a minimum fuel ejection velocity for the same conditions.

In the case of the FAATC Wing Fuel Spillage Tests, a coefficient of 1.0 was assumed in the absence of data on fuel stream contraction. Effort is underway to characterize the liquid fuel jet at this facility which may resolve this question. For the NWC Wing Spillage Tests, a sharp-edged orifice was utilized--so a contraction coefficient of 0.61 was applied to the 6-inch round fuel orifice.

In the remainder of the tests of Table III-6, coefficients of 1.0 were applied in the absence of other data. It is important to note, however, that in the case of the Southwest Research Institute (SwRI) tests, the tangential speed of the spinning disc at its outer edge is utilized for fuel ejection velocity--i.e., the radial component of fuel ejection velocity is ignored. This is consistent with SwRI's method, and computing the radial component with viscoelastic fluids was not feasible.

The orifice shape effects are considered significant to breakup. The column provided gives the configuration of a single, typical orifice. Where multiple orifices were used, the number is given in the same column, or under "results."

The fuel flow rate in the next column applies to the orifice defined in the prior column. This fuel flow column may seem redundant, since liquid ejection velocity and orifice configuration are given. However, it was noted in several of the tests that flammability results differed significantly with higher versus lower "loadings" of the airstream by ejected fuel--under otherwise similar conditions.

Table III-7 provides the most comprehensive data for comparing flammability results at nominal fuel temperatures of seven facilities--involving FM-9 AMF, particularly at 0.30 weight percent concentration. The fuel-to-air velocities for the "pass" condition for the SP-2H crash tests and the FAA Wing Spillage Tests are remarkably close. The progressively increasing speeds for a "pass" condition with increasing concentration are self-consistent and reasonable. This consistency is shared by the NWC Wing Spillage Tests, but with a very significant shift upwards in level of FM-9 concentration for a similarly acceptable limit of flammability performance. The 0.40% concentration in the NWC test has a "pass limit" velocity 16 ft/sec less than the corresponding limit on the FAA Wing Spillage facility for 0.30% concentration. At the same 0.40% concentration, the "fail limit" is 57 ft/sec higher on the FAA facility than for the NWC's smaller-scale Wing Spillage facility. The two most likely possibilities are that the NWC test is more severe (as with a scale effect), or that the difficulties with AMF sample quality, mixing, and/or handling gave an effectively inferior performance at the NWC facility. The FAA's Flammability Comparison Test Apparatus is intended to preclude the latter ambiguity in the future.

The UK/RAE 2-rocket sled tests give a "pass-to-fail" threshold velocity for the 0.30% FM-9 concentration (246 ft/sec) that corresponds to the median speed of the FAATC's Wing Spillage Tests for the "marginal" condition and the same FM-9 concentration. The problem is that the "fail" condition for the "2-rocket" testing is at a fuel temperature only 6°F greater than the nominal 81°F tested at FAA which gave a "pass" condition. Furthermore, testing at the FAA to 96°F gave a "pass limit" of 235 ft/sec, a drop of only 3 ft/sec. This discrepancy is aggravated at higher concentration--0.40% FM-9 fails in the UK/RAE 2-rocket test at 246 ft/sec and 97°F, whereas the same concentration passes at the FAA Wing Spillage Facility at 322 ft/sec, a difference of 76 ft/sec (31%) for a 17°F differential.

The UK/RAE 3-rocket sled tests show a "marginal" condition at 322 ft/sec down to 79°F fuel temperature, whereas the FAATC Wing Spillage tests show a "pass" condition at 322 ft/sec--both for

TABLE III-7. Fuel-to-Air Speeds in ft/sec by Facility, FM-9 Concentration, and Flammability.

		FM-9 Concentration (Weight %) in Jet A							
		0.20	0.25	0.30	0.35	0.40	0.45	0.50	
NAEC SP-SH Crash Tests	Pass								
	Marginal		236 (.27%)	236					
	Fail								
FAATC Wing Fuel Spillage Tests	Pass	<193	<201	<238	<265	<323			
	Marginal (Median)	206	214	246	271	328			
	Fail	>218	>226	>255	>277	>333			
NWC Wing Spillage/ Air Shear Tests	Pass				208	225			279
	Marginal			190	228	239	286		
	Fail			208		261	301		
UK/RAE Rocket Sled Tests-2 Rockets	Pass			246 (thru 84°F)					
	Marginal								
	Fail	246		246 (>86°F)		246 (97°F)			
UK/RAE Rocket Sled Tests-3 Rockets	Pass			322 (<68°F)					322 (93°F)
	Marginal			322 (73°F)		322 (79 - 86°F)			322 (95°F)
	Fail			322 (>77°F)					

TABLE III-7. Fuel-to-Air Speeds in ft/sec by Facility, FM-9 Concentration, and Flammability (Cont'd).

		FM-9 Concentration (Weight %) in Jet A						
		0.20	0.25	0.30	0.35	0.40	0.45	0.50
JPL Mini-Wing Spillage Tests	Pass			218 to 284				
	Marginal							
	Fail							
FAATC Flammability Comparison Test Apparatus-Nominal Fuel Flow (.0021 thru .0042 gal/sec)	Pass			257				
	Marginal			259				
	Fail			243				
FAATC Flammability Comparison Test Apparatus-High Fuel Flow (.0048 gal/sec)	Pass			163				
	Marginal			178				
	Fail			195				
SwRI Spinning Disc Tests	Pass	<152		<200 to 227 (to 109°F)				
	Marginal							
	Fail	>152		>200 to 227				

the same 0.40% FM-9 concentration. Relevant temperature versus velocity curves are provided by Figure III-9.

It is interesting to note that the temperature sensitivity shown by the UK/RAE testing works in the other direction, as well. An FM-9 concentration of 0.30 is sufficient for a "pass" result at 322 ft/sec at 68°F per the UK/RAE 3-rocket sled tests, whereas chilling the same concentration fuel to 47°F at the FAA Wing Spillage facility gives a "pass limit" speed of 225 ft/sec--a discrepancy of nearly 100 ft/sec (43%). In fact, chilling the 0.30% fuel from 81°F to 47°F at the FAA facility only increased the "pass limit" speed by 15 ft/sec. Comparing slopes in Figure III-9, a 3.3°F fuel temperature rise in the UK tests and a 35°F rise in the FAA tests both give a "pass limit" velocity reduction of 20 ft/sec.

It is apparent that the FAA Wing Spillage and UK/RAE 2-rocket sled tests agree at 0.30% FM-9 concentration and about 80°F fuel temperature--but diverge very significantly as test fuel temperature either increases or decreases. It is possible that the very different natures of the heating and ignition sources of the two facilities may account for much of the discrepancy. The UK/RAE facility applies much more heating to a mist configuration which rapidly decelerates in the region of the ignition sources, whereas the FAATC Wing Spillage Facility provides transient heating by a wake flame in a relatively high velocity flow field involving a small portion of the total fuel/air plume.

For the JPL Mini-Wing Spillage Tests, data usable for this comparison were available from an FAA report (reference 11). JPL test data were presented (reference 5) in a scaled format which did not provide all the necessary parameters of Table III-7. The maximum speed presented, 284 ft/sec, is not necessarily a "pass limit", since no failure velocities were available. However, the reported maximum wake flame length of 3.1 ft. is near a limit cited elsewhere<sup>12</sup> of 1 meter (3.28 ft). Comparing the highest speed, 284 ft/sec, to the FAATC Wing Spillage Facility's "pass limit" of 238 ft/sec gives an apparent overstatement of 46 ft/sec (19%), using the latter as a standard. This difference may increase, depending upon how much additional velocity is necessary with the JPL Mini-Wing to get a 3.3 ft long wake flame. Scale effects may account for much of this discrepancy.

The FAATC's Flammability Comparison Test apparatus (FCTA) utilizes maximum heat output as measured by a radiometer--compared with the flame size/speed evaluation schemes of the other facilities. As detailed in reference 13, "pass," "marginal," and

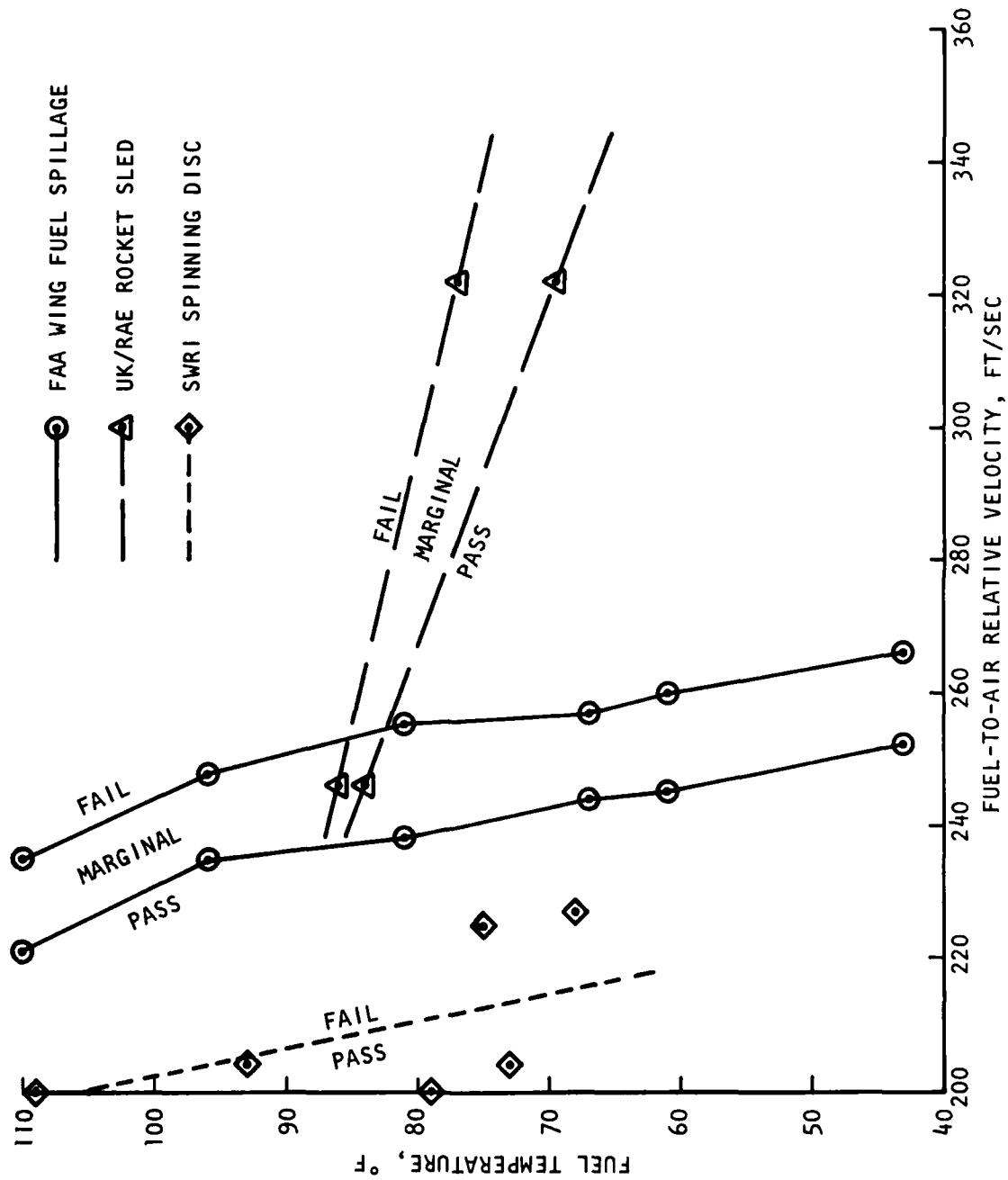


FIGURE III-9. FUEL TEMPERATURE VERSUS FUEL-TO-AIR RELATIVE VELOCITY

"fail" limits have been defined in terms of heat output--separated by values of 0.6 and 1.0 BTU/ft<sup>2</sup>sec. The 0.6 "pass" to "marginal" threshold corresponds to propagation upstream and into the FCTA's nozzle as observed with a particular batch ("A") of AMF.

Examination of the three sets of curves provided shows that within the range of velocities tested, about 150 to 250 ft/sec, each fuel typically reaches a peak value of heat output at a given flow rate and then diminishes with increasing velocity. This is particularly significant where, for a given fuel flow rate, heat output achieves "marginal" and even "fail" values, then falls back at increasing air velocity to "pass" values of heat output.

It is then possible to interpret very high values of absolute air velocity (and relative fuel-to-air velocity) as acceptable conditions. The entries in Tables III-6 and III-7 for the FCTA illustrate the problem. A "fail" velocity of 243 ft/sec was encountered at .0042 gal/sec (16 ml/sec) flow, whereas a "marginal" speed of 259 ft/sec was found for the same fuel flow rate. A "pass" velocity at this same flow rate was established at 148 ft/sec.

Examination of Table III-7 shows that the relative fuel-to-air velocities for the "pass" condition vary significantly with flow rate. For the same fuel, 0.30% FM-9 (Batch A), the "pass limit" velocity at lower flow is 257 ft/sec, whereas at somewhat higher flow it is 163 ft/sec--a difference of 94 ft/sec (58%) based on the higher flow.

In comparison with the FAATC Wing Spillage Facility, the lower flow range's results are much more desirable--the "pass limit" exceeds that of the Wing Spillage Facility's by only 19 ft/sec.

It seems quite reasonable that the heat output criterion of the FCTA can be related to the criteria of other AMF flammability test facilities--particularly the FAA's Wing Spillage Facility. For example, the drop in heat output for speeds past the failure limit may be reasonably attributed to the geometry of the flame, nozzle shielding of the flame from the radiometer, and/or the limited field of view of the radiometer. Past the failure point ("propagation into nozzle"), it is likely that a relatively stable flame front forms within the diffuser at the location where the flame speed equals the flow stream's velocity. Increasing the air velocity may increase the intensity of burning within the flame front. With more complete combustion inside the diffuser, less radiation would be sensed outside by the

radiometer. This may explain why the heat flux diminishes with increasing air velocity (at the same fuel flow) after the "fail" condition is reached. Droplet characterization may show that the higher fuel/air velocities give a more finely divided fuel, eliminating any ambiguity that "pass" conditions are encountered at higher velocities than "fail" conditions.

Finally, the quantity of fuel that exits the FCTA's diffuser as flowing liquid after the run may require measurement and appropriate corrections--since variations in that parameter mean differences in fuel spray available to burn, and may affect total heat output in an otherwise unknown way.

The SwRI Spinning Disc is physically the most different from the idealized contra-stream flows of fuel and air. However, the upper range of its pass/fail threshold is only 10 ft/sec less than the corresponding value for the FAA Wing Spillage Tests. Figure III-9 shows liquid fuel temperature sensitivity, in comparison with other facilities. Note that the slope of the Spinning Disc curve is quite similar to that of the FAA Wing Spillage facility. The lower velocity values of the Spinning Disc (about 40 ft/sec) compared to the Wing Spillage data should be due in part to the fact that the radial velocity of fuel ejection from the disc is not accounted for.

The literature (references 11 and 13) documents a discrepancy between flammability results of the SwRI Spinning Disc and the JPL Mini-Wing Facility. The Spinning Disc testing indicates that amine is not necessary in the carrier fluid, whereas the JPL tests indicate the opposite. We could not resolve the difference using existing data, but characterizations of test facility conditions and droplet spectra should do much to resolve such differences.

#### ENHANCING CORRELATIONS.

Considering AMF flammability tests as a group, there are uncertainties associated with both independent test variables (e.g., relative fuel-to-air velocity) and the flammability-related results (dependent test variables). Particularly for small-scale tests, some scaling of fuel-to-air relative velocity may be essential to properly replicate full-scale crash conditions. This is difficult considering the number, complexity, and interdependence of aerodynamic, liquid-breakup, heating, ignition, and flame propagation phenomena. The varying pass/fail characterizations of the combustion phenomena of the several test facilities do not always lend themselves to direct, quantitative comparisons.

It is essential that another set of quantitative dependent variables be determined for those AMF flammability test facilities which are to be utilized in the future. The additional characterizations should consist of fuel droplet size spectra and number densities where ignition and flame propagation occur. For engineering analysis, compact droplets may be assumed spherical, with appropriate empirical corrections for higher surface area-to-volume ratios.

Such droplet characterizations would provide hard data with which to correlate the results of liquid breakup models, and provide essential input to ignition and combustion models.

Of course, the JPL Mini-Wing Shear tests are incorporating highly advanced methods to perform fundamental studies of all stages of liquid breakup. Much more rudimentary "off-the-shelf" droplet diagnostics are available which could provide the minimum set of droplet data necessary for directly comparing two or more AMF flammability facilities. The two most evidently compatible candidates are the FAA's large-scale Wing Fuel Spillage facility and their Flammability Comparison Test Apparatus (FCTA). Both have established a significant data base on neat Jet A and certain AMF's. The FCTA has the additional advantage of standardization and deployment to several R&D organizations. They are readily amenable to "cold" tests (i.e., without ignition sources) which can be in other respects identical to flammability tests already conducted or to tests specially performed to confirm repeatability.

The JPL's fundamental research should provide, as a subset of its data output, droplet size spectra and number density data fully compatible with data from the aforementioned facilities. The RAE and SwRI test rigs are also amenable to droplet characterizations and subsequent across-the-board comparisons. "Cold" tests (i.e., no ignition) do not appear feasible for the NAEC full-scale SP-2H Crash Tests. However, the similarity in scale and flammability correlations with the FAATC Wing Fuel Spillage facility previously discussed relax the need for droplet data from the NAEC crash tests.

As an essential complement to the droplet data acquired at facilities of interest, the semi-empirical liquid breakup model should be extended to include (1) Taylor breakup effects with large jets, and (2) additional AMF fuels. Such a model, given adequate alignment and verification with AMF tests' independent variables and droplet spectra, would allow uniquely confident interpolation and extrapolation of data, regardless of the source facility. The cost of such an effort should be more than compensated for by

reducing the need for repeated testing (particularly at large scale), and vastly increasing understanding and confidence in AMF performance.

AERODYNAMICS. Further aerodynamic characterization appears particularly appropriate for the various Wing Fuel Spillage rigs that employ free air jets. It is evident that the pass/fail criteria of the several air jet facilities apply to various jet regions. Velocity and turbulence intensity data are desirable in the regions of the ignition source(s) and typical propagation. Anemometers with this capability are commonly available. Such data are important for assessing liquid breakup and flammability of the resulting mist.

FUEL JETS. Determinations of the contraction coefficients related to the jets of ejected fuel should be made for all AMF flammability test facilities utilized in the future.

DROPLET DIAGNOSTICS.

Recent emphasis on atmospheric studies has led to the development of particle measuring diagnostics which may prove far more cost-effective than the older, more rudimentary and labor-intensive techniques. The most attractive systems use lasers for direct imaging, or a particle sizing interferometric method for the off-axis detection of scattered light (Particle Measuring Systems, Boulder, Colorado; and Spectron Development Laboratories, Inc, Costa Mesa, California, respectively). The latter method provides droplet velocity and turbulence intensity data in addition to droplet sizes and number densities--a desirable but not indispensable capability. Diagnostic systems can be purchased which greatly facilitate data reduction, at large potential savings in manpower. Equipment can be purchased outright, leased, or provided for a specific time period fully manned with an experienced crew. The latter may be particularly attractive for "one-shot" droplet characterizations of a given AMF flammability test facility.

Laser light detection and ranging (LIDAR) methods of the Computer Genetics Corporation (CGC) were also evaluated for application to aircraft crash tests and large-scale AMF flammability tests. CGC has applied Brillouin, Rayleigh, Mie, fluorescent and Raman scattering techniques to atmospheric, hydrographic, and pollutant parameter measurements. A typical use is to remotely monitor municipal power plant stack emissions.

Based on our specific inquiries, acquiring droplet size distribution data, particularly in the densities encountered with AMF testing, is not fully developed and operational with LIDAR systems at the present time.

## REFERENCES

1. Anonymous, Full Scale Aircraft Crash Tests of Anti-Misting Kerosene (Interim Report), Naval Air Engineering Center, Report No. NAEC-TR-183, 4 August 1980.
2. Klueg, E. P., Large-Scale Aircraft Crash Test of Antimisting Fuel, Federal Aviation Administration Conference Proceedings, "Aircraft Research and Technology for Antimisting Kerosene", February 18-19, 1981, Report No. FAA-CT-81-181, June 1981.
3. Miller, R. E., Wilford, S. P., Simulated Crash Fire Tests As a Means of Rating Aircraft Safety Fuels, Royal Aircraft Establishment, Ministry of Defence (Aviation Supply), Technical Report Number 71130, May 1971.
4. Miller, R. E., Wilford, S. P., The Design and Development of the Minitrack Test for Safety Fuel Assessment, Royal Aircraft Establishment, Ministry of Defence, Technical Report No. 71222, November 1971.
5. Sarohia, V., Fundamental Studies of Antimisting Fuels, Jet Propulsion Laboratory, California Institute of Technology, Pasadena, California, AIAA/SAE/ASME 17th Joint Propulsion Conference, Colorado Springs, Colorado, July 27-29, 1981.
6. Ferrara, A., Cavage, W., Flammability Comparison Test Apparatus Operator's Manual, Federal Aviation Administration Technical Center, Atlantic City, N.J. (Draft Manual).
7. Eklund, T. I., Cox, J. C., Flame Propagation Through Sprays of Antimisting Fuels, Federal Aviation Administration, NAFEC Technical Letter Report NA-78-66-LR, November 1978.
8. Eklund, T. I., Neese, W. E., Design of An Apparatus for Testing the Flammability of Fuel Sprays, Federal Aviation Administration, Systems Research and Development Service, Report No. FAA-RD-78-54, May 1978.
9. Eklund, T. I., Experimental Scaling of Modified Fuel Breakup, Federal Aviation Administration, Systems Research and Development Service, Report No. FAA-RD-77-114, August 1977.
10. Finn, S. V. Jr., Eklund, T. I., Neese, W. E., Photographic Investigation of Modified Fuel Breakup and Ignition, Federal Aviation Administration, Systems Research and Development Service, Report No. FAA-RD-76-109, September 1976.

11. Webster, Harry, FM-9 Anti-Misting Fuel Large Scale Crash Test #3, Federal Aviation Administration, Summary of Presentation, 6th Meeting - US/UK Technical Committee on Anti-Misting Fuel, March 24, 1980.
12. Mannheimer, R. J., Degradation and Characterization of Anti-misting Kerosene (AMK), Federal Aviation Administration Report No. FAA-CT-81-153 , Southwest Research Institute, San Antonio, Texas, Interim Report (Draft), September 1980.
13. Ferrara, A., Flammability Comparison Test Apparatus, Federal Aviation Administration Technical Center, Atlantic City, N.J. (Draft Report)..

#### IV. ANTIMISTING FUELS RHEOLOGY

The broad objectives in examining the rheological characteristics of antimisting fuels under this program are to assess existing techniques and characterizations of fluid properties relative to\*

- flow (through fuel lines, from crash formed orifices, etc.), and
- breakup associated with crash release.

These features, of course, are in support of an overall program objective of correlating rheological and flammability test data.

In reviewing existing work on fuel rheology, particular attention was given to what is measured versus what is needed to characterize fluid behavior in the indicated situations. These features were explored with full recognition that no known single measurement technique is apt to be appropriate to yield all the rheological parameters of interest, and that it is not practical to specify a set of parameters appropriate to achieve full generality across the undefined range of rheological behavior of possible antimisting fuels. It was considered advantageous, therefore, to concentrate on those rheological features which have been observed for current or past candidate fuels, and on features indicated as potentially important to liquid breakup.

Accordingly, our rationale for technique examination has involved two considerations--near term and long term. For near term, more detailed fluid properties are desirable to better quantify flow and breakup process performance. For the long term, selected fluid properties are desired which correlate with overall antimisting fuel performance and therefore can be used for quality control of the fuel.

The general types of liquid properties which appear to be appropriate for near term needs include: the shear and elongation (tensile) stress-strain rate flow curves, the corresponding viscosities, discontinuities or regions of rapid change of slope in the flow curves, appropriate measures of fluid elasticity, time dependent effects

---

\*An original intent was to explore the findings in connection with unintentional degradation, as well as the flow and breakup features. While some qualitative remarks relative to unintentional degradation were gleaned, so very little is apparently known about this topic that meaningful discussion of it here is not possible.

(such as thixotropy), gelation-like effects, strain-rate relaxation times, and surface tension.

Parameters suitable for the long term quality control type needs are not well known, in general, but can likely be established for specific modified fuels which represent viable candidates. For example, an FM-9 fuel might be rheologically characterized by simple tests which confirm that the additive concentrations are within certain prescribed limits, the lower and upper critical shear rate values fall within suitable ranges, the shear and tensile viscosities are suitable to give simple breakup and flow performances within selected limits, and the intentional degradation can be achieved with a selected system by applying an amount of mechanical power in a given range.

In view of the rheological uncertainties involved in the flow and breakup of generic types of antimisting fuels, a pragmatic approach to their rheological characterization is to emphasize techniques which actually involve selected features of fuel flow and breakup under conditions similar to those expected to be encountered in various flammability tests. This will permit key behavioral features to be observed and accounted for, if not fully analyzed.

For flow, the techniques which involve the following are believed to be the most relevant:

- rotational rheometers
- capillary rheometers (flow-through tubes)
- filter/screen/porous bed-type schemes
- open siphon/pendant drop-type schemes.

A number of rotational type instruments, including some which are commercially available, have been reviewed by Van Wazer, et. al.,<sup>1</sup> Walters,<sup>2</sup> and Gaskins and Philippoff.<sup>3</sup>

Of this group the rotating disc type unit represented by the Brookfield Model LV Synchro-Lectric Viscometer with LV adapter represents a convenient device for low-shear viscosities. This relatively inexpensive unit, indicated as a constant temperature viscosity scheme to be examined under this program, is a commonly used and viable instrument for determining low shear viscosities of antimisting fuels. Despite its usefulness in this role, the overall utility of the Brookfield unit is somewhat limited in its ability to obtain a wide range of shear rates for a narrow viscosity range.

The group of rotating cone and plate rheometers, such as the Weissenberg Rheogoniometer,<sup>1</sup> the Mechanical Spectrometer (Rheometrics) and the Rotary Rheometer (Instron)<sup>2</sup>, have been used to characterize

non-Newtonian liquids with varying degrees of success. These units are reported to suffer from problems with secondary flow and ejection of material from the wedge region for certain antimisting fuels (especially FM-9 fuel). As a result, these units have somewhat limited ability to characterize the shear behavior of antimisting fuels, but do represent viable candidates for this purpose in low shear rate regions where such effects are unimportant.

The third group of rotating viscometers is represented by the coaxial cylinder units such as the Rotovisco (Haake).<sup>1</sup> While this unit has less inherent capability for assessing viscometric normal stress effects, it has been used with a certain amount of success in characterizing viscoelastic antimisting fuels.<sup>4</sup> It has also been used previously<sup>5</sup> with other viscoelastic materials and, together with an ELZ Visco-Elastic Attachment (Haake),<sup>3</sup> has been used for measuring the elastic recoverable shear strain.\* The procedures for reducing these couette flow measurements have been given in some detail by Krieger and Associates.<sup>6-8</sup>

The capillary viscometers have also been reviewed by Van Wazer, et al.,<sup>1</sup> Walters, and Gaskins and Philippoff.<sup>3</sup> A number of instruments of this type are available commercially for gravity or low pressure induced flow. The high pressure units which have been developed in certain laboratories are essentially one-of-a-kind units.<sup>3, 21</sup> The operation of this type of instrument is based on flow through tubes and a derivation of the associated fluid analysis and instrumental parameters is given in the literature.<sup>1, 2, 8, 12</sup> Three primary rheological parameters can be determined with this type of instrument:

---

\*The use of finite elastic strain concepts to describe fluid response was proposed in several early theories,<sup>9-15</sup> following Reiner and Freudenthal's<sup>16</sup> development of a dynamical theory of strength based on a maximum stored distortional energy. Their approach depends on the idea that the energy used in deforming a viscoelastic liquid is in part stored (as elastic or recoverable strain energy) and in part dissipated (in viscous flow). This scheme introduces a rate dependence, since if energy is input so slowly that it can all be dissipated, there can be no accumulation of energy to cause rupture. Although it is recognized that such an approach has sometimes been viewed as antiquated, Truesdell<sup>17</sup> has related it to second order fluids, and Petric<sup>18</sup> notes a revival of interest in the idea. The recent experimental results from Vinegradov and co-workers<sup>19, 20</sup> show that the state of affairs is not so simple, but the Reiner idea offers a useful first approximation. It is conjectured that the approach may merit some further consideration as a semi-empirical scheme for use with antimisting fuels, because of its relative simplicity and physical appeal. Such activity should take into account recoverable elongational strain as well as recoverable shear strain.

shear stress, shear rate, and recoverable shear strain. The high pressure capillary viscometers have been successfully used to characterize a number of viscoelastic materials at high shear rates (in the range of  $10^4$  to  $10^6$  sec<sup>-1</sup>),<sup>5</sup> but such units have apparently been sparingly used with antimisting fuels. In part this has stemmed from the dilatant/gelling behavior of FM-9 fuel which tends to plug the capillary tubes.\*

A Cannon-Ubbelohde four bulb shear dilution viscometer has been used successfully by Peng<sup>22</sup> to obtain zero shear viscosities.

The filter, screen and porous bed-type measurement schemes have been advanced as simple, field-type rheological tests, largely in connection with intentional fuel degradation work. Much of this work originated at the Royal Aircraft Establishment (RAE) and included studies using filters made of stainless steel meshes, Millipore PTFE membranes and cured aircraft filter papers.<sup>4</sup> The aim of this RAE work was to characterize as far as possible the filtration behavior of FM-9 fuel over a range of levels of degradation. They found, as U.S. workers have subsequently, that in many of the experiments a build-up of gel (from FM-9 fuel) occurred on the downstream side of the filter, and this caused variations of flow rate for passage of successive batches of fuel. Intermittent dislodgement of the gel also resulted in erratic filtration rates. For single, short-duration runs with a new or cleaned filter, the results are apparently rather consistent. Porous bed tests have been pursued by Mannheimer.<sup>23, 24</sup>

Although there is some attractiveness of such simple tests in their possible future role in quality control of antimisting fuels, there is little justification for extending their results to other situations or configurations where the rheological behavior may have little relationship to flow through a filter, screen or porous bed. From a more fundamental point of view, these types of schemes yield results which represent a confounding of both shear and elongational flow phenomena. As long as the results desired pertain to flow through such a filter or bed, the results actually achieved may be directly interpretable. However, accounting for the results in

\*This shear-induced gelation phenomenon observed with FM-9 fuel is noted in the discussion of liquid breakup elsewhere in this report. When gelation is induced in the flow stream away from boundaries and not severely degraded by extensive mechanical action, the phenomenon is essentially reversible, i.e., upon cessation of straining the gel relaxes and regains its low viscosity nature. Near material boundaries, however, there has been some indication that an additional additive or solvent may be needed to avert gel buildup.

terms of separate shear and elongational flow features represents a questionable procedure at best, and some alternate technique or configuration that could give separately interpretable results is generally preferred.

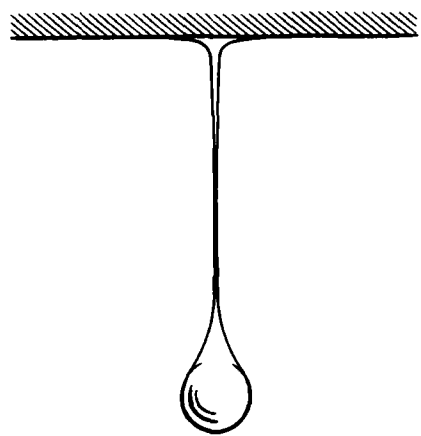
In this connection another simple test noted as the cup viscosity test, was also indicated as a scheme to be examined under this program. The cup-type viscometers, of which there are several types including the Demmler, Ford, Zahn and Gardner one-shot cups, are a number of classes of short-tube or orifice viscometers. The comments by Van Wazer, et. al.<sup>1</sup> relative to these devices are most appropriate.

"The original design concept of these viscometers were derived from the Hagen-Poiseuille law which states that the efflux time of a fixed volume through a capillary is proportional to the viscosity of the fluid. Unfortunately, the viscometers that were developed consisted of short capillaries or orifices. Flow in these viscometers does not obey the Hagen-Poiseuille law and efflux times are not in any simple relation to the viscosities...

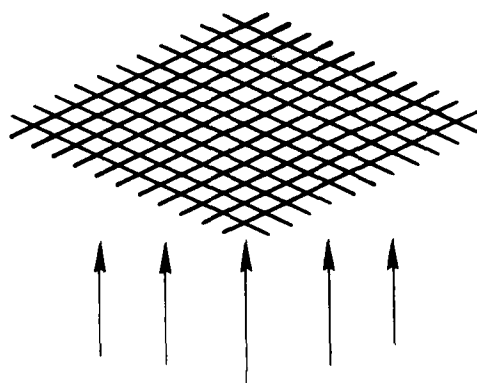
This type of viscometer, however, is widely used. The popularity is due to simplicity and inexpensive operation. In some industrial fields, this type of measurement has been applied to correlate a sample property in terms of the results obtained. However, this is true only when variation of the fluid property from sample to sample is small. For a highly non-Newtonian fluid, these viscometers will definitely fail."

The open siphon and pendant drop type schemes noted as flow measurement techniques were employed by Peng and Landel,<sup>25</sup> and Sarohia and Landel<sup>26</sup> in connection with evaluating the elongational viscosities of antimisting fuels. The basic geometrical configuration for these schemes (as well as for filtration) are shown schematically in Figure IV-1. These two test techniques are somewhat unique as schemes for direct evaluation of tensile viscosities, although a third scheme based on converging flow (also noted in Figure IV-1) has also been used by Metzner and Metzner.<sup>27</sup> The latter is not known to have been used for antimisting fuels. Each of these have limitations: all give non-steady state results, tend to be laboratory-type schemes, and require some degree of fastidiousness to obtain useful results. On the other hand, they probably represent the best techniques available at present for tensile viscosity determinations of antimisting fuels.

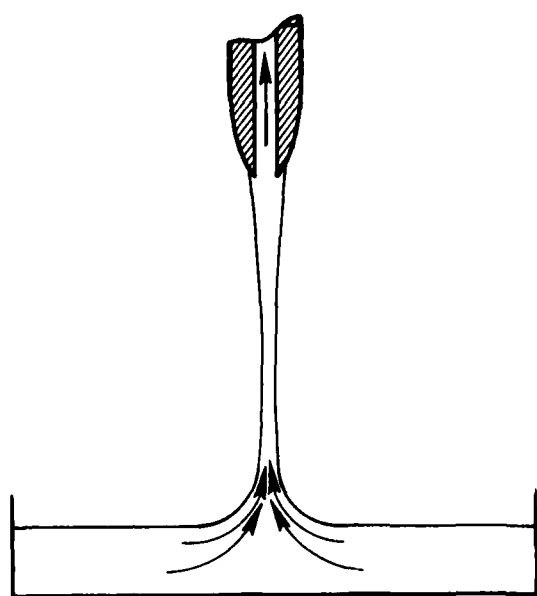
Attention will now be turned briefly to rheological techniques and measurements which are more closely associated with fuel breakup. As might be expected, information in this area is rather sparse. The reasons, of course, are obvious since breakup represents a



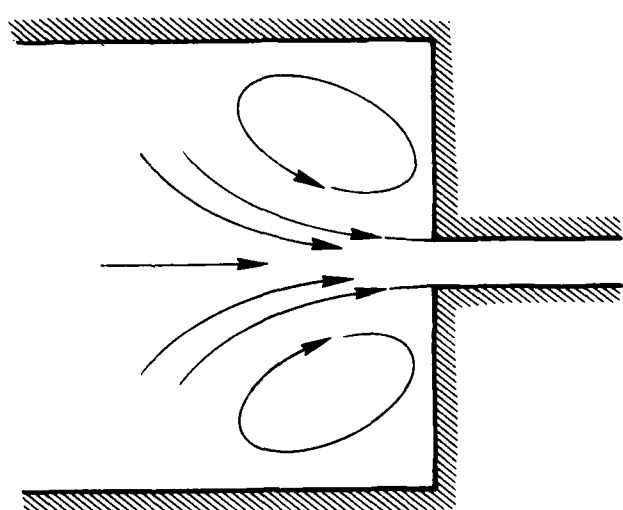
PENDANT DROP



FILTRATION/SCREEN/  
POROUS SOLID



OPEN-SIPHON  
(FANO FLOW)



CONVERGING FLOW

FIGURE IV-1. VISCOMETER/RHEOMETER SCHEMES (ELONGATIONAL FLOW)

discontinuity in flow, and the fluid measurements and techniques noted apply basically to flow prior to (or during various intermediate stages of) breakup. Correlations of fluid properties with breakup are about the best that can be expected at present, and this topic has been discussed at length throughout the liquid breakup section of this report. It is perhaps useful to highlight some of the results indicated, suggested or implied from that section.

The current investigation of antimisting fuels breakup has given some indication of the rheological features apt to be important in the breakup process. The tensile viscosity and/or elasticity associated with an elongational strain rate is of special import in the formation and breakup (or not) of liquid filaments and threads. Shear viscosity plays a minor role in this action, unless this viscosity is quite large.

On the other hand, shear viscosity appears to play a dominant role in instability (wave) growth and ligament shedding. The contribution of tensile viscosity in this case is believed to be minor.

The formation of gel-like material for particular strain rates, such as with FM-9 fuel, may have a profound influence on breakup. The reversibility of this gel-like nature may be of far greater import to the flow through pipes, pumps and fuel filters than to liquid breakup, since the fluid is not expected to relax before breakup occurs.

These observations seem to suggest that in liquid breakup, a principle which may be loosely described as a "principle of least resistance," seems to govern what happens in response to a given driving force. This view also seems to be correlated to some extent with the rheological properties of the antimisting fuel. In particular, whichever viscosity--shear or tensile--is the lesser will determine what happens at that stage of the breakup process, provided the configuration permits (or causes) a flow governed principally by that parameter to occur.

The closely related situation which may be envisioned as occurring frequently in liquid breakup consists of simultaneous shear and elongational flow. The governing parameters in this case are not well known. This type of motion borders on the hypothesized actions of drag reducing fluids in suppressing turbulence in a liquid. A laminar counterpart to this turbulent flow action involves combined longitudinal flow and secondary flow in curved tubes. The effects of polymer additives in this combined flow case have been examined by Tsang and James.<sup>28</sup>

Measurement techniques specifically configured to characterize the fluid properties relevant to breakup do not currently exist, and from a fundamental standpoint may be unnecessary. For purposes of quality control, however, it is probable that one or more simplified type field tests which emphasize the breakup features of antimisting fuels should be devised.

One relevant technique which appears to be a test to measure the onset of shear induced dilatancy (or gelation in FM-9 fuel) is the so-called "Inertial Rheometer" devised by Gustavino and co-workers.<sup>29,30</sup> This scheme has rather surprising sensitivity, but needs further characterization in terms of particular experimental variables, pump pressures and flow parameters. It may be that the secondary flow phenomena explored by Tsang and James<sup>28</sup> may cause some elongational flow effects when coiled tubes are employed, but the bulk of the phenomena are believed to be induced by shear flow.

Another type scheme which is merely suggested at this point, as it has not been explored experimentally under the present effort, is a scheme based on breakup, but intended to serve as a routine check (or characterization) of elongational (and perhaps dilational) flow. This technique is basically a pendant drop type configuration, with supplementary laminar airflow to cause drop separation and filament rupture (or not), if necessary. The point is to explore the diameter changes of droplets, or droplets on the threads which are produced for a variation of elongational viscosity. If the droplet diameter change is sufficiently sensitive to changes in elongational viscosity, then with proper calibration, a measurement of droplet size can be used to indicate elongational viscosity of the fuel. Calibration of this scheme may involve measurements similar to those made earlier by Sarohia and Landel.<sup>26</sup>

Finally, it should be noted that one or more particular rheometric techniques cannot be recommended to the exclusion of others, since each may have a range over which the values it indicates are perfectly valid. However, it does appear that the potential capabilities of rheometers such as the Rotovisco (with elastic recoil attachment) and the high pressure capillary units have not been fully exploited in antimisting fuels evaluations.

## REFERENCES

1. J. R. Van Wazer, J. W. Lyons, K. Y. Kim, and R. E. Colwell, Viscosity and Flow Measurement, Interscience, New York (1963).
2. K. Walters, Rheometry, Chapman and Hall, London (1975).
3. F. H. Gaskins and W. Philippoff, "Instrumentation for the Rheological Investigation of Viscoelastic Materials," J. Appl. Polymer Sci., 2(5), Pages 143-154 (1959).
4. J. K. Knight, R. E. Miller, and S. P. Wilford, Rheology of Antimisting Safety Fuels, RAE Memorandum (19 June 1978).
5. W. H. Andersen, N. A. Louis, and G. Ialongo, Investigation of the Aerodynamic Breakup of Viscoelastic Liquids. Phase I-- Subsonic Dissemination, Contractor Report ARCSL-CR-77037 (August 1977).
6. I. M. Krieger and S. H. Maron, "Direct Determination of the Flow Curves of Non-Newtonian Fluids," J. Appl. Phys., 23(9), Pages 147-149 (1952).
7. I. M. Krieger and H. Elrod, "Direct Determination of the Flow Curves of Non-Newtonian Fluids. II. Shearing Rate in the Concentric Cylinder Viscometer," J. Appl. Phys., 24(2), Pages 134-136 (1953).
8. I. M. Krieger and S. H. Maron, "Direct Determination of the Flow Curves of Non-Newtonian Fluids. III. Standardized Treatment of Viscometric Data," J. Appl. Phys., 25(1), Pages 72-75 (1954).
9. M. Mooney, "Secondary Stresses in Viscoelastic Flow," J. Colloid Sci., 6, Pages 96-107 (1951).
10. M. Mooney, "A Test of the Theory of Secondary Viscoelastic Stress," J. Appl. Phys., 24(6), Pages 675-678 (1953).
11. W. Philippoff, F. H. Gaskins and J. G. Brodnyan, "Flow Birefringence and Stress. V. Correlation of Recoverable Shear Strains with Other Rheological Properties of Polymer Solutions," J. Appl. Phys., 28(10), Pages 1118-1123 (1957).
12. W. Philippoff and F. H. Gaskins, "The Capillary Experiment in Rheology," Trans Soc. Rheol., 2, Pages 263-284 (1958).

13. T. Kotaka, M. Kurata, and M. Tamura, "Normal Stress Effect in Polymer Solutions," J. Appl. Phys., 30(11), Pages 1705-1712 (1959).
14. A. S. Lodge, Elastic Liquids, Academic Press, New York (1964).
15. R. B. Bird, H. R. Warner, Jr., and D. C. Evans, "Kinetic Theory and Rheology of Dumbell Suspensions with Brownian Motion," Adv. Polymer Sci., 8, Pages 1-90 (1971).
16. M. Reiner and A. Freudenthal, "Failure of a Material Showing Creep (A Dynamical Theory of Strength)," Proc. 5th Int. Cong. Appl. Mech. Pages 228-233 (1938).
17. C. Truesdell, "Fluids of the Second Grade Regarded as Fluids of Convected Elasticity," Phys. Fluids, 8(11), Pages 1936-1938 (1965).
18. C. J. S. Petrie, Elongational Flows, Pittman, London (1979).
19. G. V. Vinogradov, A. Ya Malkin, and V. V. Volosevitch, "Some Fundamental Problems in Viscoelastic Behavior of Polymers in Shear and Extension," Appl. Polymer Symp., 27, Pages 47-59 (1977).
20. G. V. Vinogradov, "Ultimate Regimes of Deformation of Linear Flexible Chain Fluid Polymers," Polymer, 18, Pages 1275-1285 (1977).
21. F. H. Gaskins and W. Philippoff, "Instrumentation for the Rheological Investigation of Viscoelastic Materials," J. Appl. Polymer Sci., 2(5), Pages 143-154 (1959).
22. S. T. J. Peng, Rheological Behaviors of AMK, Jet Propulsion Laboratory, Presentation, March 24-26, 1980.
23. R. J. Mannheimer, Rheology Study of Antimist Fuels, Report No. FAA-RD-77-10, Southwest Research Institute for FAA Systems Research and Development Service (January 1977).
24. R. J. Mannheimer, Influence of Surfactants on the Fuel Handling and Fire Safety Properties of Antimisting Kerosene (AMK), Southwest Research Institute for FAA Systems Research and Development Service (February 1979). (FAA-RD-79-62)
25. S. T. J. Peng and R. F. Landel, "Preliminary Investigation of Elongational Flow of Dilute Polymer Solutions," J. Appl. Phys., 47(10), Pages 4255-4259 (1976); and Errata, J. Appl. Phys., 50(7), Page 5883 (1979).

26. V. Sarohia and R. F. Landel, Influence of Antimisting Polymer in Aviation Fuel Breakup, Jet Propulsion Laboratory, AIAA/SAE/ASME, 16th Joint Propulsion Conference, June 30-July 2, 1980.
27. A. B. Metzner, and A. P. Metzner, "Stress Levels in Rapid Extensional Flows of Polymeric Fluids," Rheologica Acta, 9(2), Pages 174-181 (1970).
28. H. Y. Tsang and D. F. James, "Reduction of Secondary Motion in Curved Tubes by Ploymer Additives," J. of Rheology, 24(5), Pages 589-601 (1980).
29. T. M. Gustavion, P. Cox and W. Cavage, A Status Report on the Investigation and Development of a Laboratory Test to Characterize Antimisting Behavior in Polymer Modified Jet A Fuel (AMK) Antimisting Kerosene, FAA Technical Center Memo to W. T. Westfield, May 18, 1980.
30. T. M. Gustavino, Measurements of the Rheology of Polymer Modified Aviation Kerosene, FAA Technical Center Memo, June 10, 1980

## V. LIQUID BREAKUP

### RATIONALE.

The introduction of antimisting fuel as a means of reducing fuel fires in aircraft crashes is in recognition of the fact that coarse droplet fuel sprays represent a smaller fire hazard than fine sprays.

The flow and deformation properties of a fuel are known to influence how the fuel breaks up and what the resultant sizes of spray droplets are in a crash environment as well as in an aircraft engine. Liquid breakup, however, is the process which actually determines the spray droplet sizes. The key concerns in considering fuel breakup in actual or simulated crash test configurations, therefore, are to:

- Establish the nature and final size distributions of drops (or other shapes) in relevant neat and antimisting fuel sprays.
- Identify mechanisms expected to be important to the breakup process over the range of small- to large-scale laboratory tests and in full-scale crash scenarios.
- Ascertain the expected dependence of candidate breakup mechanisms on the rheological characteristics of likely antimisting fuels.
- Determine techniques for incorporating breakup information to correlate flammability test data, including the extension of limited test data to other scenarios.

The expected process, mechanisms and results of breakup are of principal concern in this section.

The overall breakup process depends not only on the properties of the liquid fuel, but also on the frontal surface of liquid exposed to the airstream and on the magnitude of the relative air velocity. This process may change with scale both due to the size and shape of the liquid surface interacting with the airstream, and due to different breakup mechanisms being involved with these liquid surfaces of different sizes. These types of changes are likely to occur over the range of small- to large-scale configurations employed to date in flammability testing of antimisting fuels.

The breakup mechanisms of importance are expected to include oscillatory, stripping and Taylor breakup. Relevant findings reported in the general spray literature were used, together with limited results directly applicable to antimisting fuels, in identifying these key mechanisms and their likely role in jet and droplet breakup. Information stemming from previous FAA and related work on antimisting fuels was also taken into consideration.

The droplet size distributions and mass concentrations of sprays produced in various tests can, in principle, be determined experimentally. The exclusive use of experimental techniques to characterize droplet size information is very inefficient and is often not feasible. In our opinion a better approach is to incorporate additional liquid breakup mechanism information into a physical model of the breakup process and align the model with selected experimental findings. The model can then be used to extrapolate necessarily limited test data to a wide range of operating conditions and test scales, including the full-scale crash tests.

Physical models which account for complex liquid breakup phenomena are relatively rare. Under the present effort one existing model of this type, patterned after the early work of Mayer,<sup>1</sup> was located. This model treats the aerodynamic stripping breakup of liquid injected into a subsonic airstream, accounts for both primary and secondary breakup, and characterizes the complete resulting size distribution on a number and a mass basis. Although this model was the result of a major developmental effort for other applications, extensions of the model are necessary to make it fully applicable to antimisting fuel testing and analysis. The model is considered to be an excellent candidate for this type of modification in the future.

To enhance confidence in the utility of this breakup model we have, at company expense, put a computer coded form of it on-line and found excellent correlation with available data on Newtonian liquids under conditions of interest under this program. These results are included later in the discussion.

Information as to how the breakup process governs droplet sizes in different situations is important both to achieve an understanding of why the antimisting fuel works as it does, as well as to obtain insight on potential fuel and/or system modifications for improved fire resistance. Liquid breakup is recognized as an intermediate step in establishing the correlation of flammability test data and in conducting exploratory development tests of antimisting fuels. It is, especially significant in the correlation of flammability test data gathered from a range of small to large size test configurations because of its impact on results

3  
achieved in tests of different scale. Once data correlation is complete, it is probable that breakup considerations can be circumvented and the flammability results can be directly related to the rheological properties of the treated fuel. In particular, it is anticipated that a quality-control type of test on selected fuel properties would be adequate to ensure suitable antimisting fuel performance over a wide range of full-scale crash scenarios.

The preceding topics form the rationale for the subsequent discussion of liquid breakup as it applies to antimisting fuels.

#### LIQUID BREAKUP MECHANISMS.

A large number of past studies have been conducted to further the understanding of atomization phenomena and the mechanisms of liquid breakup. A few investigations which have emphasized the more fundamental aspects of aerodynamic breakup of liquids have succeeded in clarifying many features of the process. Several of these features are relevant to spray formation of antimisting fuels.

Until rather recently most of the investigations concentrated on the breakup of low viscosity Newtonian liquids with small lateral dimensions, such as jets, sheets and individual drops. The principles and controlling physical properties determined in these small scale cases also apply to larger scale jets, drops and globs of liquid for suitable ranges of governing parameters. Studies involving the breakup of highly viscous, non-Newtonian liquids are rather limited, and the corresponding mechanisms are less well quantified. Highlights of the relevant findings of these various studies are included in this section to indicate the nature of the breakup mechanisms and parameters that may be involved in producing antimisting fuel sprays. A more complete summary of the general atomization and spray formation literature can be found elsewhere.<sup>2-5</sup>

OSCILLATORY BREAKUP. The breakup of a small, low-speed liquid jet moving into still air was the first problem of this type to be treated analytically and this was done by Rayleigh.<sup>6</sup> While such a jet, per se, is of little direct concern here, the considerations of small liquid column or filament breakup which are intimately related to that of a small jet are quite relevant. This is because such filaments are often produced as intermediate elements in the rupture of large jets and drops. As such, the rupture behavior of these elements affects the final result of antimisting fuel disruption.

What Rayleigh actually analyzed were the oscillations of a cylinder of incompressible, inviscid fluid of circular cross section under the action of surface tension. In this case the column of liquid is inherently unstable. Small initial instabilities arising from unspecified sources are expected to grow exponentially as axially symmetric waves--which rupture the column when the largest wave amplitude equals the column radius. The lengths of the resulting liquid segments are determined by the wavelength,  $\lambda_{opt}$ , of the most rapidly growing disturbance. This wavelength,  $\lambda_{opt}$ , depends only on the diameter  $D_j$  of the column, is independent of the other physical properties of the liquid or surrounding air, and is given by

$$\lambda_{opt} = 4.508 D_j. \quad (1)$$

The corresponding diameter  $d$  of spherical drops formed by action of surface tension on each segment of the ruptured column is

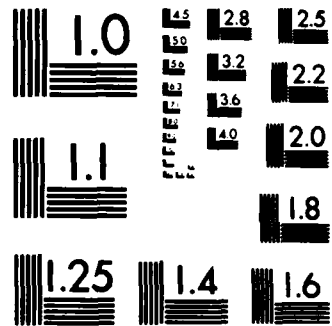
$$d = \left[ \frac{3}{2} D_j^2 \lambda_{opt} \right]^{1/3}. \quad (2)$$

While Rayleigh and many subsequent investigators have used this theory or its extensions to treat jets, Keller, Rubinou and Tu<sup>7</sup> have shown that the theory is not directly applicable to jets. The difficulty is not due to (slow) motion of the jet, but arises because the analysis assumes that the oscillation grows in amplitude everywhere along the jet, including the region near the nozzle where the jet originates. In reality, the oscillation is negligible near the nozzle and grows with increasing distance from the nozzle along the jet. The first case of oscillation over the entire length of the column represents an example of temporal instability, whereas wave growth with length along a jet represents spatial instability. The general topic of spatial instability analysis is treated by Betchov and Criminale.<sup>8</sup>

Keller and coworkers further showed that spatial growth rates of certain modes of instability of the jet are related to the temporal growth rates of corresponding modes of oscillation of the cylinder for low jet speeds. This explains why good agreement is observed between the results predicted for an oscillating liquid column and experiments on low speed jets.

As it turns out, the case of oscillating liquid columns which Rayleigh treated is the one chief interest here, rather than the case of jets. However, the connection between the two and the fact that part of the available experimental information applies to jets gives impetus for examining the results of other





MICROCOPY RESOLUTION TEST CHART  
NATIONAL BUREAU OF STANDARDS-1963-A

investigations carried out with small jets to estimate likely breakup behavior of columns or filaments.

Subsequent efforts of Rayleigh<sup>6</sup> and the later work of Weber<sup>9</sup> produced more refined estimates of  $\lambda_{opt}$  by taking into account properties of both the liquid and the surrounding air. With low speed jets, however, the air still only has a secondary influence on breakup.

Weber derived the following expression for the optimum wavelength

$$\lambda_{opt} = \sqrt{2} \pi D_j \left[ 1 + 3 \left( \frac{\eta^2}{\sigma \rho_l D_j} \right)^{1/2} \right]^{1/2} \quad (3)$$

where  $\eta$  is the shear viscosity,  $\sigma$  is the surface tension, and  $\rho_l$  is the density of the liquid. The average diameter  $d$  of spherical drops initially produced by breakup of the cylindrical column is still given by equation (2).

In recent years the stability of jets in stagnant air has been investigated further by Middleman and coworkers<sup>10-12</sup> to more fully evaluate the influence of the ambient medium, high speed laminar flow, turbulence in the nozzle, and the use of viscoelastic liquids. They found that the time to breakup  $t_b$  is given by a relationship

$$t_b = \frac{1}{\alpha^*} \ln \frac{D_j}{2\delta} \quad (4)$$

where:  $\alpha^*$  is the growth rate of the instability wave  
 $D_j$  is the jet diameter, and  
 $\delta^j$  is the initial radial dimension of the disturbance in the jet.

In these studies the instability was characterized by measurement of jet breakup length,  $L_b$ , which is related to jet velocity  $V_j$  and breakup time  $t_b$  by  $L_b = V_j \cdot t_b$ . Phinney's re-examination of these data<sup>13</sup> suggests that the initial disturbance at the jet exit may depend on jet velocity.

These findings further indicate that columns (i.e., jets, ligaments or filaments) of Newtonian liquids tend to disintegrate readily as a result of initial disturbances which grow as stationary waves, even at very low speeds relative to air. The drops resulting from the breakup of such a column depend mainly on the column diameter.

Additional investigations of the breakup of low speed jets of viscoelastic and viscoinelastic liquids were conducted by Goldin, et al.<sup>14</sup> and by Gordon and coworkers.<sup>15</sup> Their findings indicate the instability pattern of a jet of viscoelastic fluid may be dramatically different from that for a Newtonian fluid.

For 0.1% polymer,\* shear thinning, viscoelastic solutions, exponential wave growths were absent. Large isolated drops appeared at random intervals and the jet became a string of drops, irregularly spaced, connected by thin filaments of liquid. Some filaments subsequently broke, and individual drops were then released. The filaments generally showed significant longevity and did not always break.

Jets of liquids with lesser elastic properties (e.g., 0.05% solution as above) showed an initial region where a disturbance propagated as an exponentially growing wave of constant wavelength. Growth of this wave was stunted before breakup occurred, and a string of regularly spaced small droplets, joined by filaments of liquid, was again formed. With increasing distance from the nozzle, a breakup region existed where the connecting filaments developed secondary instabilities and ultimately broke. The filaments then either collapsed to form small satellite drops or were snapped into an adjacent primary drop.

With viscoinelastic liquids, filaments were also observed, but these filaments ruptured at the filament-droplet joints. The resulting free ligaments each disintegrated into several small satellite drops.

The unusual longevity of the filaments between droplets was characterized as due to stretching or elongational flow which increased the elongational (tensile) viscosity of the filament. While this flow might be induced by relative motion of the droplets to which the filaments were attached, Gordon, et al., employed jets perturbed by controlled disturbances. This resulted in negligible relative motion between droplets. Even in this case of uniform droplet spacing, the steady exponential decrease in filament diameter indicated that a low pressure region within each droplet was drawing liquid and creating a stretching motion in the filament joining the two drops. Extensional strain rates on the order of  $20 \text{ sec}^{-1}$  were observed.

---

\* One of the materials used was Separan AP-30 (Dow Chemical Co.), a partially hydrolyzed polyacrylamide of high molecular weight.

Further considerations in oscillatory-type breakup of jets, sheets and drops take into account the motion of the fluid and varying degrees of influence of the surrounding air. As the velocity of a jet is increased above the negligibly low value used previously, breakup of the jet into drops becomes partially influenced by interaction of the jet with air. The air velocity increases over the wave crests and decreases in the trough regions. Simultaneously, the pressure decreases over the crests and increases over the troughs, in accordance with Bernoulli's theorem.<sup>19</sup> This situation causes the wave amplitude to increase, as the reduced pressure tends to increase the height of the crests and the increased pressure tends to deepen the troughs. These motions are opposed by surface tension forces and tend to be damped by viscous forces. The first order interaction of air with the liquid is thus a force normal to the average velocity of the liquid jet; shear forces enter as smaller interactions of higher order.<sup>20</sup> The net result of this interaction arising from an increase in jet velocity is that the optimum wavelength for breakup decreases and the growth rate of the optimum wavelength disturbance increases. These effects lead to a decrease in breakup time, breakup distance, and drop size.

As the jet velocity is increased further, the wave motion on the jet changes from axially symmetric (varicose or dilational) to asymmetrical (sinuous)\* as a result of increased surface interactions with the air.

Oscillary type breakup of tangentially moving sheets and hollow cones of Newtonian liquids, such as may be produced by fan or swirl type hydraulic nozzles, has also been considered by several investigators.<sup>21-24</sup> This breakup occurs in a manner similar to that of a liquid column. Small disturbances in the sheet develop to form waves which rapidly grow until they reach a critical amplitude. Tears occur in the wave crests and troughs, and fragments of the sheet corresponding to a half wavelength (of sinuous waves) are broken off. These fragments contract by surface tension into unstable cylindrical ligaments. In addition, holes that often form in the sheet also result in the formation of ligaments. These ligaments ring the holes. Some of the ligaments move with their long axes in the direction of flow, but the majority of them move transversely. The ligaments, themselves, are unstable, exhibit growing oscillations and disintegrate into droplets.

---

\* For clarity it is noted that the diametrically opposed sides of a jet (or two surfaces of a sheet) oscillate in phase to produce sinuous waves, or they oscillate out of phase to produce dilational waves.

Two different maximum growth rate instability waves are involved in this process; one is of wavelength  $\lambda$  on the sheet, and another is of wavelength  $\lambda_{opt}$  on the cylindrical ligament. The latter is given approximately by the Raleigh criterion equation (1). A sheet of thickness  $h$  which breaks into a band of width  $\lambda$  (where  $\alpha$  is a constant in the range between 0 and 1) is expected to collapse into a cylindrical ligament of diameter

$$2 \left( \frac{h\alpha\lambda}{\pi} \right)^{1/2}.$$

The resultant droplet diameter  $d$  resulting from the ligament disruption is given by

$$d = 2.1 (h\alpha\lambda)^{1/2}. \quad (5)$$

It will be noted that the droplet diameter can be expressed directly in terms of the wavelength of disturbance on the sheet. Dombrowski and Johns<sup>24</sup> have refined this analysis and tested it experimentally. They express the drop diameter  $d$  in terms of the jet diameter  $D_j$  by

$$d = \left[ \frac{3}{\sqrt{2}} \right]^{1/3} \cdot \left[ 1 + \frac{3\eta}{(\rho_l \sigma D_j)^{1/2}} \right]^{1/6} D_j \quad (6)$$

with

$$D_j = 0.9614 \left[ \frac{K^2 \sigma^2}{\rho_g \rho_l V^4} \right]^{1/6} \cdot \left[ 1 + 2.60 \left( \frac{K^4 \rho V^7}{72 \rho_l^2 \sigma^5} \right)^{1/3} \right]^{1/5} \quad (7)$$

and where  $K$  is a constant to be determined empirically,\*  $V$  is the relative air-to-liquid velocity,  $\rho_g$  is the gas density, and  $\eta$ ,  $\sigma$ , and  $\rho_l$  are the viscosity, surface tension, and density of the liquid, respectively.

Sheet breakup of non-Newtonian liquids has been investigated experimentally by Dombrowski, et al.<sup>25</sup> using shear thinning aluminum soap petroleum "gels", and by Ford and Furmidge<sup>26</sup> using shear thinning water-in-oil emulsions. The former<sup>25</sup> shows an example in which a 1/2-inch diameter jet of petrol gel injected into still

\* The parameter  $K$  is related to the sheet thickness  $h$  at a distance  $x$  from the nozzle orifice by  $h = K/x$ .

air at about 150 ft/sec first develops surface irregularities, then surface waves--which increase in extent until they are formed into a large sheet. Such sheets are very thin and disintegrate when they become unstable. While sheets are formed under particular conditions, their formation from jets should be recognized as possible but not commonplace.

Thin sheets were produced in these investigations by forcing liquid through a fan nozzle where the liquid experienced a high shear rate. The shear-thinned viscoelastic sheets so formed all disintegrated into stable ligaments, but the nature of ligament breakup was found to depend on the consistency,\*  $\eta_c$ , of the liquid. At values of  $\eta_c \approx 1$  the sheet broke up almost spontaneously into droplets. Increased values of  $\eta_c \approx 2$  gave ligaments resistant to fracture and with beads formed on them. In the range of  $25 < \eta_c < 100$ , the ligaments remained unbroken. For values of  $\eta_c$  greater than about 100, the ligaments broke up into shreds, i.e., short cylindrical lengths. At high values of  $\eta_c$  (near 1600), the shreds were formed directly from the sheet. Fraser<sup>28</sup> further notes that sheets of dilatant (shear thickening) viscoelastic fluids,\*\* consisting of high particulate concentration slurries, break down close to the fan nozzle orifice through the formation of holes. The associated ligaments formed are larger, as are the resulting drops, than observed with Newtonian liquids because the sheet has not expanded so far.

The preceding studies indicate that the major effects of elongational flow and fluid elasticity in the breakup of viscoelastic filaments are to oppose their breakup and to increase the size of droplets or liquid fragments. Figure V-1 indicates the probable role of viscoelasticity in filament breakup when breakup does occur.

---

\* Consistency is a viscosity equal to the slope of the shear stress vs. shear rate curve for the liquid at any given point.<sup>27</sup> The values of  $\eta_c$  reported in Reference 25 were in Gardner units, since a Standard Gardner mobilometer was used. The values represent the number of grams corresponding to a rate of fall of 0.1 cm/sec of a plunger which moves down through the liquid in a close (but not tight) fitting cylinder. These values are approximately proportional to consistency in poise.

\*\* Two types of phenomena are known to occur with dilatant materials:<sup>29</sup> volumetric dilatancy, which denotes an increase in total volume under shear; and rheological dilatancy, which refers to an increase in apparent viscosity with increasing shear rate. This latter property is more commonly associated with dilatant fluids, and is the one of main interest here.

LIGAMENT BREAKUP

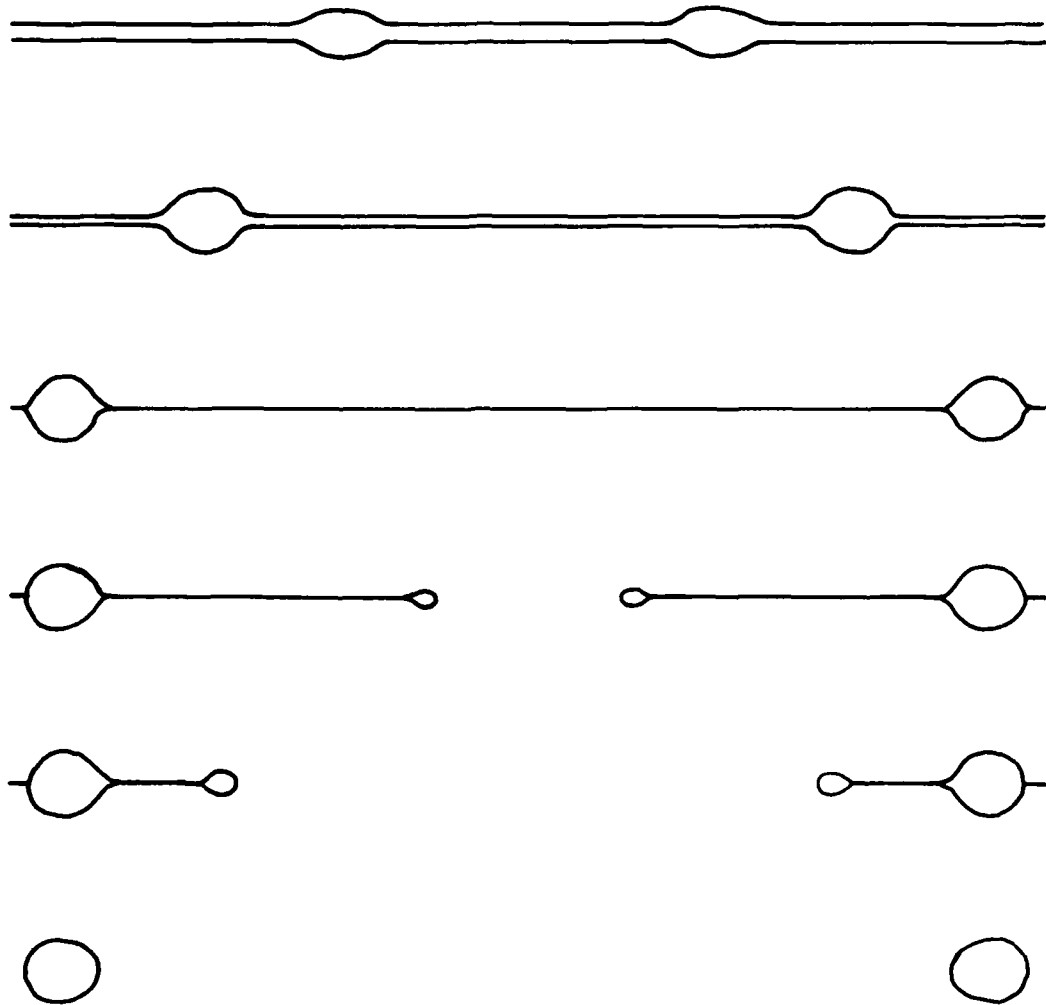


FIGURE V-1. PROBABLE ROLE OF VISCOELASTICITY IN BREAKUP

In closing this section on oscillatory breakup, it is noted that the oscillatory breakup of drops has also been treated both experimentally and theoretically.<sup>30-34</sup> However, this type breakup is of little interest for antimisting fuels. The scheme according to which the breakup of droplets is categorized, on the other hand, is of interest. It will also indicate why oscillatory breakup is essentially negligible in the present context.

A common assumption made in treating the breakup of liquids is that when the maximum aerodynamic force tending to disrupt the liquid exceeds the surface tension force that holds it together, the liquid will burst. This condition is quantified by equating these two forces, which for wind against a spherical surface of diameter  $D_0$  gives a relationship of the form

$$\frac{1}{2} C_D \rho_a (u - v)^2 = 4\sigma/D_0 \quad (8)$$

where  $C_D$  is the drag coefficient of the drop,  $u$  is the air velocity and  $v$  is the velocity of the liquid at breakup. By rearranging expression (8) the breakup criteria can be expressed in terms of a critical Weber number  $We_c$  by

$$We_c = \frac{\rho_a V^2 D_0}{\sigma} = \frac{8}{C_D} \quad (9)$$

for the relative air-to-liquid velocity  $V$ .

The assumption on which this condition is based is true only for small rates of stress loading and not at high (e.g., shock) loading rates, since breakup and associated flow of liquids are known experimentally to be a time-dependent process. Nevertheless, the condition has been useful in practice for indicating regions where certain types of droplet breakup occur. It should be recognized that large liquid viscosity or elasticity can also affect breakup behavior, so that classification based solely on Weber number is known to be incomplete.

Andersen and Wolfe<sup>34</sup> determined experimentally that a liquid drop can undergo five separate modes of breakup in an airstream, depending on the conditions:

1. Dumbell oscillation - This action is observed at low values of  $We$  ( $>8$ ), just above the critical value required for breakup. A droplet undergoing dumbell oscillation breaks into two smaller drops.

2. Bag breakup - For slightly higher values of  $We$ , a drop flattens and its center is then blown out in a concave manner to form a thin-walled hollow bag which breaks. With a relatively high viscosity, elastic fluid, the bag typically ruptures and deflates without producing small droplets.

3. Stamen breakup - This variation of bag breakup is characterized by a forward protruding stem, which is formed in the center of the bag prior to breakup.

4. Stripping breakup - At still higher values of  $We$  ( $>100$ ) the breakup of a flattened drop occurs by continual stripping (shear) of the liquid away into ligaments and droplets by the wind (gas stream). This is the dominant mechanism by which drops are broken up over a wide range of conditions, as well as by which jets and bulk liquids are broken up aerodynamically.

5. Taylor breakup - At very high values of  $We$  ( $\approx 10^4$ ) a drop suddenly accelerated by a high velocity air stream will flatten aerodynamically and its frontal surface will quickly become corrugated by Taylor instability growth. The corrugations rapidly deepen until the drops shatter into smaller fragments, which may then continue to undergo breakup by surface stripping. This type of breakup is important for bulk liquids and large jets which undergo significant deformation before fragmentation.

STRIPPING AND TAYLOR BREAKUP. As indicated in the previous drop breakup classification scheme, stripping and Taylor breakup occur at relative air-to-liquid velocities higher than those which cause oscillatory disintegration. These two forms of breakup are grouped together here because they compete with each other in the initial breakup of bulk (large scale) liquid. The conditions of liquid dimensions and relative velocity determine which mechanism is of dominant importance. The following discussion of these two mechanisms pertains most directly to Newtonian liquids, but the general features and results seem to correlate with experiments in the very few cases where non-Newtonian liquids have been investigated.

A slug of bulk liquid injected into a low aircraft-speed (60-150 knots) counterflowing external airstream undergoes simultaneous bulk deformation and stripping (surface erosion) at its free surfaces exposed to the air flow. The initial surface stripping of the liquid is slow due to low wind speed and relatively small exposed liquid surface area. As a result, deformation of the bulk liquid has time to occur. The deformation results in lateral spreading and geometrical thinning of the liquid. While the thickness of the deformed liquid in the direction of the relative air

flow decreases, Taylor instabilities (waves) grow on the liquid's windward surface. When the amplitude of these instabilities becomes equal to the thickness of the deformed liquid, the liquid fractures into a number of smaller pieces. This rapidly produces a large liquid surface area. In turn, this increase in area greatly enhances the overall stripping rate and the pieces continue to break up by surface stripping. In this situation, the Taylor breakup process dominates the initial disintegration of the liquid, while surface stripping completes the breakup into droplets.

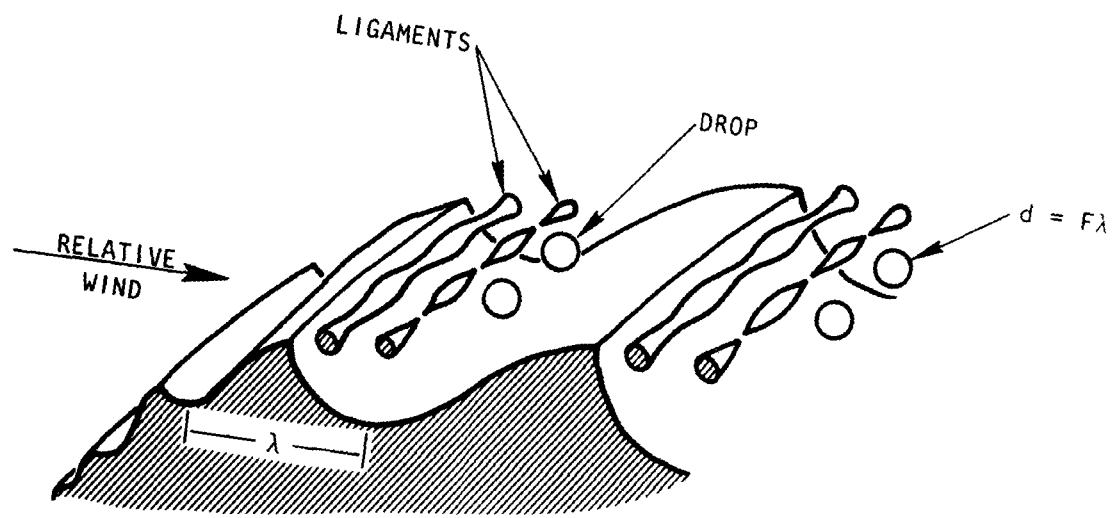
For the case of continuous flow from a large jet into a counter-flowing airstream, as above, a steady-state deformation condition is reached whereby the jet spreads laterally and its penetration against the airstream is halted at some distance from the orifice. In this terminal region, the liquid flow is nearly lateral (as it reverses direction relative to the air velocity) and the liquid forms a curved sheet convex to the wind with a thickness which decreases rapidly with distance from the jet axis. It is in this region where Taylor instabilities are expected to grow on the windward surface and break up the rather thick liquid sheet into small pieces. These pieces then continue to break up by surface stripping, as above.

If the jet is small rather than large, Taylor breakup is negligible, except perhaps at very high air velocities, and the dominant breakup mechanism is surface stripping.

The stripping and Taylor mechanisms are indicated in a somewhat idealized but illustrative manner in Figure V-2.

Stripping breakup occurs when liquid shear by wind is accompanied by growth of surface waves which form and shed ligaments. These ligaments separate from the main liquid mass, undergo growing oscillations due to instability of the column, and break up (or not) into drops--depending on conditions or liquid properties. If these drops formed by primary breakup are large and the relative velocity is still high enough, the drops may break again. This latter action is called secondary breakup.

As noted earlier, individual drop sizes are generally related to specific wavelengths of surface waves, so it is expected that the size spectrum of drops produced by stripping breakup is determined by the spectrum of wavelengths excited by the wind. Waves of very small wavelength do not develop because of viscous dissipation, and very long wavelengths develop slowly because of inertial effects. Between the very short and very long wavelengths, there exists a spectrum of wavelengths that can be excited to appreciable



STRIPPING BREAKUP (SURFACE EROSION)

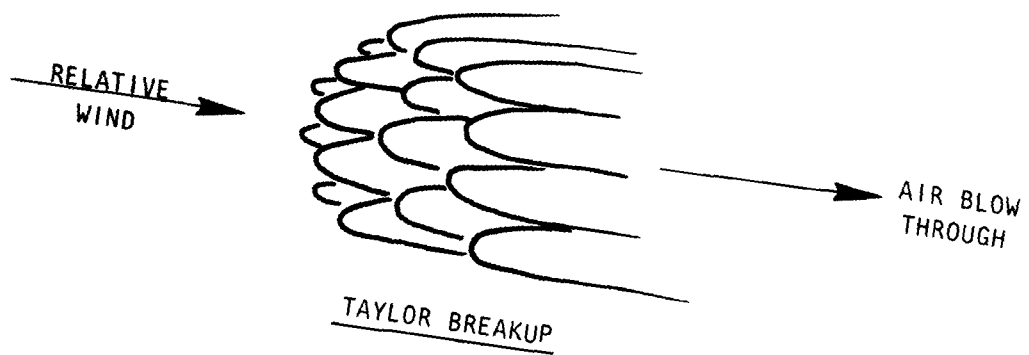


FIGURE V-2. BREAKUP MECHANISMS

amplitudes during the time of action of the high velocity gas flow. The waves actually generated show effects of capillarity and wind acceleration. Their growth rate is determined by the balance of wind energy causing their growth and viscoelastic energy dissipation in the wave.

The stripping breakup mechanism concept appears to stem from the early work of Castleman<sup>35</sup> on the disruption of a high velocity jet. Development of the concept, however, was carried out largely in connection with the aerodynamic breakup of single drops by several investigators; including Lane,<sup>36</sup> Hinze,<sup>31,32</sup> Gordon,<sup>37</sup> Hanson and coworkers,<sup>38</sup> Engel,<sup>39</sup> Andersen and Wolfe,<sup>34</sup> and Ranger and Nicholls.<sup>40</sup> Detailed investigations involving jets were carried out by Clarke<sup>41</sup> and Morrell,<sup>42,43</sup> Sherman and Shetz,<sup>44</sup> and Weiss and Worsham.<sup>45</sup>

The work of Sherman and Schetz<sup>44</sup> is of particular interest in that it confirms by high speed photography the formation of ligaments and ligament shedding under high-speed shear conditions.

The study of Weiss and Worsham<sup>45</sup> produced one of the best available sets of droplet data. They employed hot wax in a hot gas stream to avoid effects of evaporation and devised a scheme to obtain representative samples of droplet mass-size distributions. They correlated their data by means of the following equation for the mass-median diameter,  $d_{mmd}$ :

$$d_{mmd} = .60 \frac{[\rho_l D_j]^{1/6}}{V^{4/3}} \sigma^{5/12} \eta_l^{1/3} \left( \frac{1}{\rho_g} + \frac{10^3}{\rho_l} \right) (\eta_g V_j)^{1/12} \quad (10)$$

where  $V_j$  is the jet velocity and  $D_j$  is the jet diameter, and all quantities are in cgs units.

Andersen and coworkers<sup>46</sup> note that, based on a number of studies, the mass median droplet size produced by small jets is proportional to the quantity

$$\frac{\eta_l^a D_j^b}{V^c},$$

where the experimental index constants vary over the approximate ranges:  $a = 0.2 - 0.45$ ,  $b = 0 - 0.5$ , and  $c = 0.75 - 1.33$ . Values

of these indicies (especially b) are uncertain for jets with orifice diameters larger than about 0.5 inches. They also note that a large amount of experimental work shows that for a wide range of conditions the drop and jet breakup time  $t_b$  due to surface stripping are given by

$$t_b = k \left( \frac{D_j}{V} \right) \left( \frac{\rho_l}{\rho_g} \right)^{1/2} \quad (11)$$

The experimental constant  $k$  has been found to range from about 2 to 6, with a value near 3.5 often representing a "best" value.

Taylor breakup stems from growth of the instability of the free boundary surface of a liquid. This instability arises when the liquid is subjected to an acceleration normal to the surface, with the acceleration directed into the liquid. Acceleration in the opposite direction from the more dense liquid toward the less dense air acts to stabilize the interfacial boundary.\*

The classical case of interfacial stability of a semi-infinite liquid under constant acceleration was analyzed by Taylor<sup>48</sup> and was examined experimentally by Lewis.<sup>49</sup> They did not consider liquid sheet fragmentation specifically.

Keller and Kolodner<sup>50</sup> investigated the growth rate of the fastest growing Taylor instability induced by a wind impinging normally on the surface of a nonviscous liquid with finite surface tension. They obtained theoretical expressions for the approximate size of the liquid pieces formed by this mechanism, and the time required for this to occur.

Bellman and Pennington<sup>51</sup> also investigated the growth of the fastest growing Taylor instability for the cases of (1) a non-viscous liquid with surface tension, (2) a viscous liquid without surface tension, and (3) a viscous liquid with surface tension. Their results show that the presence of surface tension generally

---

\* Another type of phenomenon known as Helmholtz instability also exists. This type of instability develops in the surface of a liquid by a shearing wind stress. According to Reference 46 the wavelengths excited by the wind in the classical Helmholtz sense are much smaller than the observed breakup sizes, suggesting that this type of instability does not represent a primary breakup mechanism.

has a negligible effect on the wavelength of the fastest growing disturbance, and that this wavelength is viscosity dependent. The main effect of viscosity is to retard the growth rate of the disturbances and to increase the wavelength of the fastest growing disturbance. This, of course, would result in larger liquid pieces being produced by this breakup mechanism.

Much of what is known about Taylor breakup has resulted from studies of water droplet breakup conducted by several workers; including Reinecke and Waldman,<sup>52</sup> Simpkins and Bales,<sup>53</sup> and Harper, et al.<sup>54</sup> These investigations give additional confidence in the validity of this mechanism for breakup.

A full theoretical or experimental treatment of Taylor breakup of deformed liquid jets does not seem to be available in the literature, either for Newtonian or non-Newtonian liquids. This situation makes it difficult to know, without further investigation, the combination of conditions of jet size, relative velocity and liquid properties where Taylor breakup becomes important. Preliminary estimates from a brief examination of photographs of jet breakup in antimisting fuels test configurations under typical operating conditions suggests that in these situations Taylor breakup is unimportant for initial jet diameters less than about 0.5 inch, but may begin to become significant for diameters larger than about 1 inch. This is a topic which deserves further detailed attention in order to better quantify the change in breakup behavior with test scale.

#### ANTIMISTING FUELS BREAKUP.

The previous section has concentrated on general breakup mechanism information with relatively little input from antimisting fuels studies. In the present section the latter is emphasized. This separation has been made purposely in an attempt to clearly indicate how the rather sparse breakup information on antimisting fuels dovetails with (and is supported by) the general information. Several of the antimisting fuels that were one-time or current candidates are also noted since their breakup behavior is relevant--yet it is not expected to be the same for all such materials. Final droplet size information from sprays of antimisting fuels is not currently available, except for two tests, so direct correlations of this type among the several fuel candidates and test configurations are not generally possible at present. Droplet size distribution measurements of selected candidate fuels are planned in connection with investigations being conducted at the Jet Propulsion Laboratory.

Photographic investigations have provided most of the available information on breakup mechanisms specifically related to these fuels. Zinn, Eklund and Neese<sup>55</sup> examined the aerodynamic breakup of fuels injected through a 5/16-inch I.D. plain nozzle, costream into a 110-knot air flow. The nozzle was fed by a 58.6 foot-long fuel hose of 1/2-inch I.D. The fuels used included neat Jet A, and Jet A solutions of 0.2 mass percent Conoco AM-1, 0.4 mass percent Dow XD8132.01, and 0.7 mass percent Imperial Chemical Industries (ICI) FM-4.

While the Jet A fuel, itself, is a Newtonian liquid, the resulting fuels modified with AM-1 exhibit a shear thinning behavior,<sup>56</sup> and with FM-4 and XD8132.01 show a shear thickening or dilatant nature. The shear thickening behavior of FM-4 differs significantly from that of the Dow material. The former exhibits slight shear thinning, power law fluid behavior under laminar flow conditions for shear strain rates less than about 100 sec<sup>-1</sup>, and a mildly dilatant shear stress-shear strain rate (flow curve) nature for larger values.<sup>57</sup> The fuel with Dow additive is essentially Newtonian below a critical shear rate (about 800 sec<sup>-1</sup> for 0.7 weight percent XD8132.01 in Jet A), and tends to form a gel-like solid above this value. Preliminary results obtained by Mannheimer<sup>56</sup> indicate that a second critical point exists at high shear stress (and slightly higher shear rate) beyond which a near-Newtonian behavior is again observed.

The fuels with AM-1 and FM-4 additives are known to exhibit viscoelastic properties<sup>57,58</sup>, and each of the three modified fuels are known to exhibit high elongational viscosities.<sup>59</sup> The elongational viscosities at given strain rates increase with additive types in the sequence XD8132.01, FM-4, and AM-1 (for the respective mass concentrations in solution of 0.7%, 0.3% and 0.2%). The variations of shear and tensile viscosities with their corresponding strain rates are shown in Figure V-3 for a solution of 1.3 mass percent AM-1 in JP-8 fuel. The tensile viscosity curve in Figure V-3 is dashed to show approximate behavior over a range of strain rates, including the region where data (indicated by points) were taken.

The photographs taken by Zinn, et al. at various distances from the nozzle indicate that the rheological nature of the modified fuels has a significant influence on the final fuel particle configuration. The AM-1 fuel is characterized by small ligaments near the nozzle, which are drawn out into sheets and into thin droplet-containing threads by the moving air. The FM-4 fuel exhibited somewhat larger ligaments and fewer droplet-laden filaments. The XD8132.01 fuel broke up into relatively large,

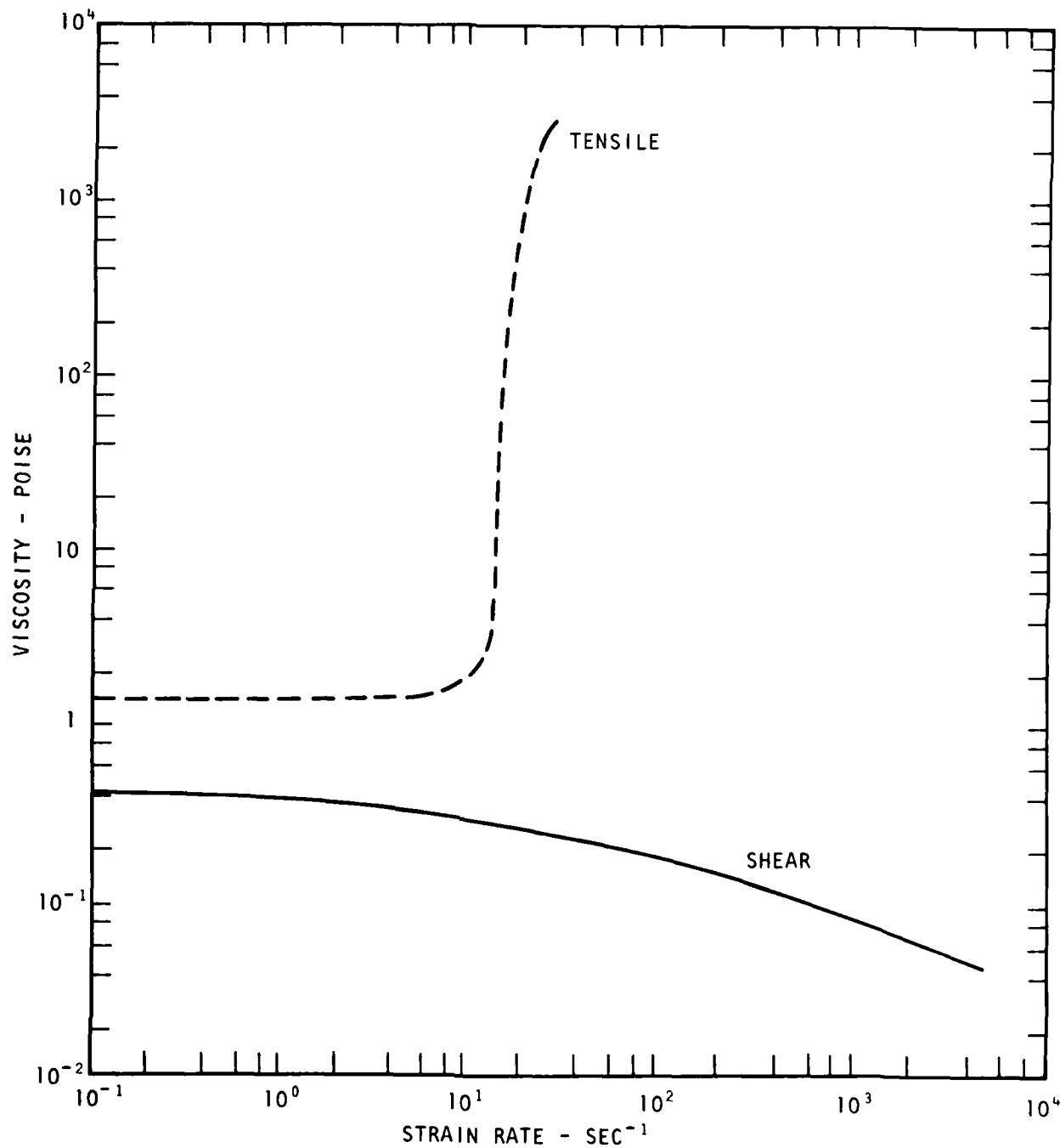


FIGURE V-3. APPROXIMATE SHEAR AND TENSILE VISCOSITIES FOR 1.3% AM-1 IN JP-8 FUEL (ADAPTED FROM REFERENCE 66)

irregularly shaped globules. The corresponding flammability tests were inconclusive because of uncertainties of fuel spreading and dilution.

The long fuel flow hose used on these tests ahead of the nozzle is expected to have preconditioned the fuel viscosities while achieving fully developed shear flow. The thread formation observed with AM-4 and FM-4 is consistent with direct ligament formation at the nozzle, followed by inhibited breakup and filament thinning, characteristic of viscoelastic liquids with high tensile viscosities, as noted earlier. The large globule formations observed for XD8132.01 appear to be the result of direct breakup of liquid ligaments, preconditioned by shear strain rates exceeding the first critical point and exhibiting a high tensile viscosity.

The subsequent investigations by Eklund<sup>60</sup> and Eklund and Neese<sup>61</sup>, in connection with developing a small-scale test apparatus to compare the flammability of modified fuel sprays, also included taking photographs of the breakup of antimisting fuels. In these cases additives were mixed with the neat fuel to form the following mass percentages in Jet A: 0.4% FM-4 and 0.2% AM-1. Also, 0.3% FM-9 in Avtur was tested.

The modified fuels nature indicated earlier is supplemented here by the shear thickening FM-9 fuel. The rheological properties of this fuel are similar to those of the XD8132.01 treated fuel, except that the FM-9 fuel is only slightly viscoelastic under particular flow conditions.<sup>62</sup> Further, FM-9 exhibits antithixotropy,\* show concentration-dependent lower and upper critical shear rate values,<sup>63</sup> and exhibits a tensile viscosity of somewhat uncertain values.<sup>64,65\*\*</sup> The lower critical shear strain rate at 75°F for 0.3 mass percent of FM-9 in Jet A is about 3100 sec<sup>-1</sup>.<sup>66</sup> The second critical shear strain rate for this material occurs at about 9100 sec<sup>-1</sup>.<sup>63</sup>

In these tests the sprays were again directed costream with the air flows, which in this case were 200 mi/h and 285 mi/h. The observed breakup of modified fuels was essentially as before,

---

\* Antithixotropy may be of particular importance in liquid breakup considerations since the shedding of individual fragments typically occurs in the millisecond time regime. Primary breakup would be expected to occur before aerodynamically induced strain on the liquid would cause significant tensile viscosity effects to become apparent.

\*\* The tensile or elongation viscosity of FM-9 fuels has been a measurement challenge and the results to date show significant disparities.

except the photographs showed a significantly greater filament formation tendency with AM-1 fuel than for FM-4 fuel. The FM-9 treated fuel showed even greater breakup into droplets and regular shaped fuel globs than was apparent earlier with the Dow material.

The breakup behavior observed in these tests for FM-9 is interpreted here as involving an antithixotropic fuel that is not preconditioned to exhibit high tensile viscosity at or near the time of breakup, such as might be expected for a fuel which has experienced large shear or elongational strain rates via flow through a long pipe or nozzle. The breakup is believed to occur primarily as a result of shear flow-governed instabilities which grow and break in a time interval that is short compared to the time it takes the liquid to develop high tensile viscosity under the flow conditions experienced during breakup. Further, the breakup is believed to occur primarily in the low shear viscosity region where the shear strain rate is well above the second critical point.

In this region, the range of wavelengths of wind induced instabilities which can grow is restricted, as are the resultant drop sizes that are produced when these disturbances break. These size restrictions arise from the combined effect of available wind driving force and the second critical shear strain rate. As the maximum shear strain rate which can be produced by the wind approaches the second critical point from above, the lower and upper drop size limits approach one another. The drop size which these limits approach is typically rather large. Breakup of this treated fuel for maximum shear strain rates below the second critical point occurs in a related manner, but the results are different. In this region the drop size range is expected to be rather wide, compared to that which can be generated above the second critical point.

These breakup results are not obvious, and have been determined using the breakup model (noted later) in an application involving FM-9 treated fuel.

The ignition and flame propagation features of these modified fuels clearly showed that the AM-1 fuel strands ignited rather easily, and sprays of this fuel possessed a burning tail. Both FM-4 and FM-9 fuels showed good resistance to ignition.

A significant breakup finding embedded in these flammability results is that the mere suppression of fuel droplet formation is not by itself adequate to indicate good resistance to ignition and burning of a fuel. These findings were confirmed by additional test work carried out by Eklund and Cox.<sup>67</sup> This feature was

apparently overlooked by Hoyt and coworkers<sup>68</sup> in their very recent effort to correlate fuel drag reduction properties with jet breakup.

On a strictly physical basis, the reasons seem apparent as to why a fuel which has formed droplet chains joined by filaments potentially represents poor resistance to ignition and flame propagation. Drawing on the earlier discussion of oscillatory breakup of viscoelastic jets and filaments, it will be recalled that the filaments between droplets tend to thin rather significantly, and may break due to aerodynamic forces. The filaments or threads often remain as filaments without disruption or significant retraction into globs or drops. When the surface area of an original filament is compared with the total area of a line of drops that would be formed if Rayleigh breakup were to occur, it is found that the two areas are nearly the same (with that of the filament being slightly greater). However, in the droplet chain form, as the filament thins the total surface area of the filament-droplet configuration will become appreciably greater than that of the separate drops. Further, the original filament size is contributory, in that shear thinning AM-1 fuel is expected to yield finer original filaments than would be expected for a shear thickening material, such as FM-4 fuel. The increased surface area of the thin and thinned filament structures are expected to exhibit enhanced evaporation, ignitability and, hence, flammability.

The investigation by Faul<sup>62</sup> of jet and droplet breakup is also relevant. He examined jets of neat Avtur and AM-1, and FM-9 in Avtur--as well as droplets of neat Avtur and FM-4 and FM-9 in Avtur. The mass concentrations of additives used in the fuels were 0.2%, 0.3% and 0.4% for AM-1, FM-9 and FM-4, respectively.

The jet results tend to be consistent with previous work and with explanations advanced earlier in this section. In particular, the suppression of turbulence in AM-1 fuel jets is a rather well documented action observed in connection with drag reducing viscoelastic fluids, a group to which AM-1 fuel belongs.<sup>68,69</sup> A considerably greater degree of turbulence was observed in FM-9 jets, implying that the viscoelastic effects in this case were far less than for AM-1 fuel.

For the droplet tests, the fuels were fed to the test region through a 0.4 mm inside diameter capillary, with length-to-diameter ratio of about 750. Using low flow rates, Avtur fuel injected into still air gave a very short jet followed by a stream of discrete spherical droplets formed by Rayleigh-type breakup. At the point of separation from the capillary jet, the droplets broke

away cleanly--showing no signs of filament formation. An increased viscosity fuel sample (presumably viscoelastic), prepared with 75 mass percent liquid paraffin and 25 mass percent Avtur, also showed no filament formation, but some occurrence of small droplets near larger ones. The latter were presumably caused by a small amount of necking between the larger drops, which subsequently broke away to form the satellite droplets.

In the case of FM-4 fuels, a continuous string of drops interconnected by fuel filaments was observed. This type structure is typical for a viscoelastic fluid as noted earlier.

With FM-9 fuel, droplets were produced which appeared similar to those of FM-4 fuel in that they were joined by filaments during the early part of their fall. As Faul noted,<sup>62</sup>

"On emergence from the capillary an elongated droplet formed which flowed into more discrete droplets as it moved downwards, eventually accelerating and forming a filament behind it. As the droplet fell away the filament stretched until it parted, exhibiting elastic behavior; the upper part of the broken filament recoiled into the next droplet forming above it. Sometimes the shock of the recoil would be enough to detach this next droplet from its string prematurely. ... This behavior suggests that FM-9 fuel also has viscoelastic properties, but unlike FM-4 fuel there is a sudden breaking of the filament followed by elastic recoil. This suggests that with FM-9 fuel there is some viscoelasticity where the fuel has formed a more rigid shear induced structure."

The flow of liquid through the long capillary prior to ejection would be expected to cause each fuel, but particularly FM-9, to experience an appreciable shear strain rate and thereby precondition the fuel issuing from the capillary tip. Subsequent shear and/or elongation of the liquid as it fell away from the tip could then readily force the liquid into the gel-like shear induced structure noted above.

This situation examined by Faul and another by Sarohia and Landel,<sup>64</sup> represent the only known cases where elastic effects of FM-9 fuel have been clearly observed.

Additional tests conducted by Faul consisted of atomizing Avtur and AM-1, FM-4 and FM-9 fuels with an airblast atomizer. The neat Avtur broke rapidly into small sized drops. The FM-4 fuel tested under the same conditions showed long strings of

fuel pulled out from the atomizer; these remained intact for about 25-50 mm, even under relatively high blast pressures. The AM-1 fuel behavior was analogous to that of FM-4, except the filament formation tendency was even more pronounced. The FM-9 fuel behavior was more like Avtur but with the resulting drops being larger and less spherical. Paul commented:<sup>62</sup>

"Examination of cine-film clearly shows that FM-9 fuel is firstly drawn out of the atomizer jet by the air flow and then torn apart to form lumps of fuel varying in size and shape, suggesting that under these conditions the fuel has a form of shear-induced structure. This behavior is also shown to a certain extent in the work on droplets where the FM-9 fuel droplets suddenly break from their associated filaments; but unlike the results from the droplet work there appears to be no elastic recoil or stringing with the airblast atomizer sprays. This suggests that the viscoelastic behavior of FM-9 fuel only becomes apparent under very specific flow conditions as encountered in droplet formation."

These observations further support the working hypothesis that FM-9 breakup depends significantly on its shear induced nature (but not to the exclusion of tensile effects).

The investigations of Sarohia and Landel<sup>64</sup> also included jet and drop breakup of neat Jet A, and solutions of AM-1 and FM-9 (with carrier fluid) in Jet A. These jets were injected into moving airstreams. Their results generally confirm the findings of Paul. They confirmed for jets that the most suitable (i.e., fastest growing) wavelength for neat Jet A and FM-9 fuels is approximately 4 to 5 times the jet diameter, as is expected from the Rayleigh criterion. Such wave growth was observed to be almost completely suppressed for AM-1 fuels. Both thread and sheets were observed to form from AM-1 fuel jets injected into a moving airstream with velocities of 27 m/s.

Sarohia and Landel also carried out pendant drop tests in which a large drop was allowed to fall under the action of gravity, while being attached by a filament of the liquid to a wetted capillary tip. The purpose of this test was to determine experimental values of the elongational viscosity of FM-9 fuel, which they did. In the process of making these measurements they also observed filament rupture and elastic recoil of the broken filament back to the adjacent droplets.

An interesting feature of this configuration was that the measurements were carried out under conditions which might be expected to

reasonably simulate those occurring in the actual breakup of filaments. Some consternation arises, however, in that filament formation seems to be a rare occurrence in the observed breakup of FM-9 fuel. Nonetheless, it appears that as a scheme for tensile viscosity measurement, this approach or some adaptation of it represents one of the few feasible techniques known.

The previous investigations essentially exhaust the available information on fundamental breakup studies of antimisting fuels. There are, however, two other qualitative breakup features which result from observations of the FAA Wing Fuel Spillage tests and the full-scale crash tests which should be noted.

In the case of the Wing Fuel Spillage test configuration located at the FAA Technical Center, liquid breakup of jets is expected to occur in a manner indicated schematically in Figure V-4. Especially note that Taylor breakup is expected to occur in the leading edge of the aerodynamically deformed fuel jet. Videotape records of individual tests conducted with this test rig show the cell-like structure expected for Taylor breakup and support the hypothesis that this breakup mechanism is operative in these tests.

Similarly, videotape/photographic records of the full-scale crash tests that have been conducted at Lakehurst, N.J. indicate an analogous cell-like structure. This indicates that Taylor breakup is operative in the dispersal of antimisting fuels in full-scale crashes.

In both of these cases where Taylor breakup cells are identified, it will be recognized that the cell structure is not a long-term steady-state type phenomenon, but rather tends to fluctuate with time during actual tests. These fluctuations are characteristic of the phenomenon, and some sort of average over their range (perhaps together with estimates of the extremes) represents a reasonable expectation in accounting for their role in antimisting fuels breakup. Accounting for these phenomena quantitatively represents a challenge for future endeavors.

It is relevant to note that of the various other test configurations which have been or are being used in connection with antimisting fuels spray and flammability evaluation, none are known to have been characterized in terms of the fuel breakup achieved. In view of the extreme sensitivity of ignition energy requirements to spray droplet sizes (discussed elsewhere in this report) which has been discovered recently, it appears that some degree of droplet size characterization deserves further attention. Particular attention to this feature is recommended for the full-scale

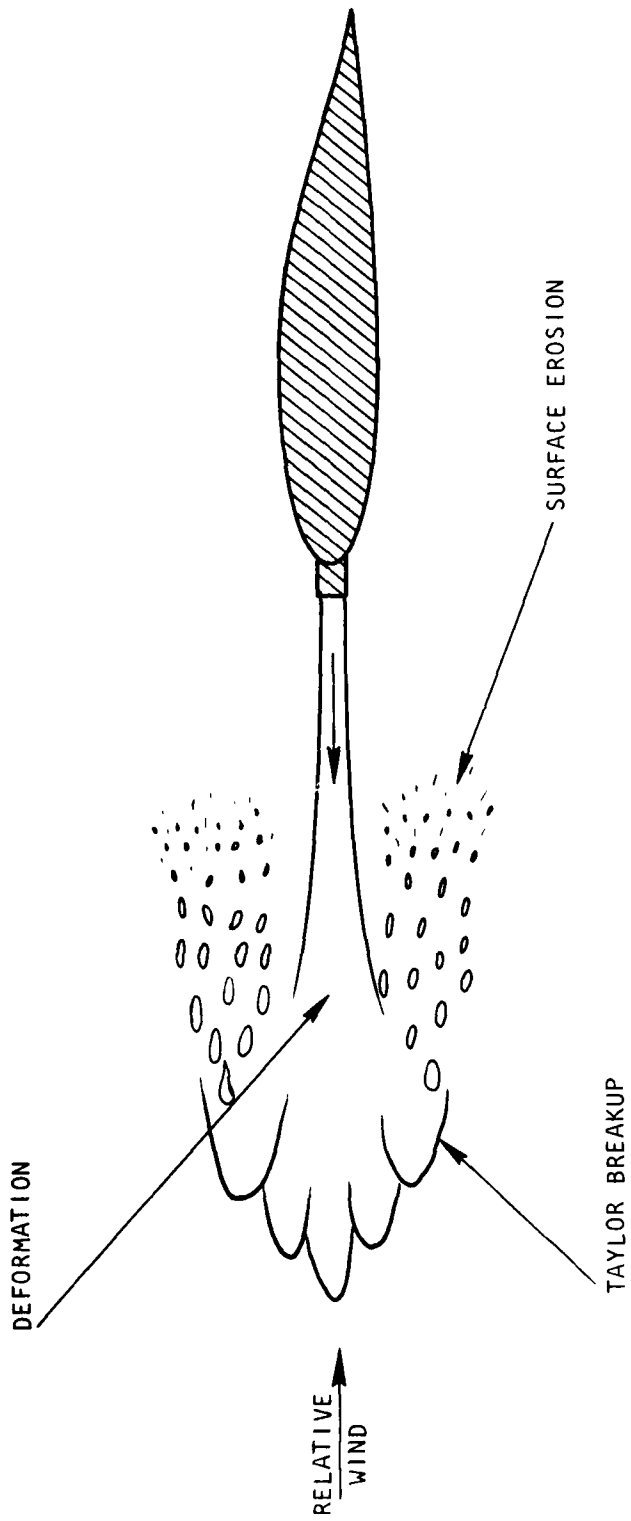


FIGURE V-4. LIQUID BREAKUP IN WING FUEL SPILLAGE CONFIGURATION

tests, the FAA Wing Fuel Spillage rig, the FAA small-scale flammability rig, and the Spinning Disc rig (at Southwest Research Institute).\*

From the nature of the phenomena involved, it is apparent that results from simple engineering tests of the type represented by the drop test at Southwest Research Institute can hardly be expected to yield information that will be useful for extrapolation, yet may still be somewhat reliable qualitative indicators of fuel flammability performance in the tested configuration. The crudeness of the tests gives little confidence that agreement which may be achieved upon extending results to other configurations is anything more than fortuitous.

#### LIQUID BREAKUP MODEL.

The incorporation of relevant breakup mechanisms and phenomena into an analytical model with the capability to calculate the resultant droplet sizes produced by the aerodynamic breakup of liquids has been accomplished only in recent years. One existing model of this type was located under the present effort. This model treats the aerodynamic stripping breakup of a Newtonian or (selected) non-Newtonian liquid injected into a subsonic airstream, accounts for primary, secondary and higher order breakup, and characterizes the complete resulting size distribution on a number and a mass basis. While moderate extensions of this model are necessary to make it fully applicable to antimisting fuel testing and analysis, current information indicates that this model is an excellent candidate for this type of modification. More importantly, once such a model is aligned with selected experimental findings, it can then be used to extrapolate limited test data to a much wider range of operating conditions and test scales, including full-scale crash tests.

The subject model is an outgrowth of Mayer's<sup>1</sup> capillary wave stripping model for estimating both stripping rate and droplet size. Mayer considered the airflow to induce small capillary waves (instabilities) on a liquid surface. When such a wave grows to an amplitude comparable to its wavelength,  $\lambda$ , the wave crest is envisioned as being eroded as a ligament, which then breaks up into droplets.

---

\* The new test configuration at the Jet Propulsion Laboratory is being fitted with a droplet size determining capability.

Adelberg<sup>70,71</sup> extended this model to incorporate the effects of aerodynamic forces as well as capillary (surface tension) forces. For an airstream moving parallel to the liquid surface, the aerodynamic forces operate mostly in a direction normal to the local average velocity of the liquid jet, as indicated earlier in connection with oscillatory type breakup of jets. The corresponding wind driven waves are referred to as acceleration waves.

The model was further extended by Andersen and coworkers<sup>46</sup> to account for primary, secondary and higher order breakup on the final droplet size distribution produced by stripping breakup of the liquid. The aerodynamic surface stripping of a liquid produces particles of various sizes, and the larger particles undergo further stripping to a stable size during their drag deceleration. This secondary breakup process also involves momentum balance between the various size classes. Emphasis here will be placed on summarizing the model equations for primary breakup; secondary breakup involves the same concepts, so nothing fundamental is omitted.

The meanings of various symbols used in this model are indicated in Table V-1.

The mass of liquid stripped aerodynamically from a liquid surface in a differential wavelength range between  $\lambda$  and  $\lambda + d\lambda$  per unit area per unit time is given by

$$\dot{M}d\lambda = K_2 \rho_\ell \lambda \frac{d\lambda}{\tau} \quad (12)$$

where  $K_2$  is a proportionality constant whose value is near unity. The quantity  $\tau$  is the time required for a relative wind to form and break a wave of wavelength  $\lambda$  from a liquid surface. It is given by

$$\frac{1}{\tau} = \frac{f}{(\lambda + a\lambda^2)^{1/2}} - \frac{g}{\lambda} \quad (13)$$

with

$$f = \left( \frac{\pi}{2\rho_\ell \sigma} \right)^{1/2} \beta \rho_g V^2 \quad (14)$$

TABLE V-1. BREAKUP MODEL NOMENCLATURE

a	= A wave acceleration parameter
A, B	= Wavelength parameters
$C_1$	= Dimensionless constant
$C_2$	= Constant parameters
$C_d$	= Drag coefficient (dimensionless)
d	= Liquid droplet diameter
$D_j$	= Initial diameter of drop or jet
e	= Dimensionless parameter that relates maximum wavelength to the liquid diameter
E	= A wavelength parameter
f	= A wind forcing parameter
F	= Dimensionless constant that determines the diameter of a droplet produced by the breaking of a wave with wavelength $\lambda$
g	= Viscous retarding parameter
k	= Dimensionless stripping constant
$K_2$	= Dimensionless mass stripping constant
$\lambda$	= Wavelength of a wind-induced wave
$\lambda_1, \lambda_2$	= Wavelength values over a wavelength increment ( $\lambda_2 - \lambda_1$ ). Also, $\lambda_1 = \lambda_{\min}$ , $\lambda_2 = \lambda_{\max}$
$\lambda_{\max}$	= Maximum wavelength that can be induced by a given wind on a liquid surface
$\lambda_{\min}$	= Minimum wavelength that can be induced by a given wind on a liquid surface
$\dot{M}$	= Mass stripping rate per unit area of liquid ( $\text{gm/cm}^2 - \text{sec}$ )
n	= Exponent of viscosity
$\dot{N}$	= Droplet formation rate per unit area of liquid (droplets/ $\text{cm}^2 - \text{sec}$ )
t	= Time (sec)
$t_b$	= Liquid breakup time (sec)
u	= Air (wind) velocity
v	= Liquid velocity
V	= Relative velocity between a liquid and an airflow

TABLE V-1. BREAKUP MODEL NOMENCLATURE (Continued)

$\beta$	= Sheltering parameter of a wind-induced wave (dimensionless)
$\dot{\gamma}$	= Shear rate of a liquid while undergoing stripping ( $\text{sec}^{-1}$ )
$\eta$	= Shear viscosity of liquid
$\rho_g$	= Gas (air) density
$\rho_l$	= Liquid density
$\sigma$	= Liquid surface tension .
$\tau$	= Time required for a relative wind to form and break a wave of wavelength $\lambda$ from a liquid surface ( $\text{sec}^{-1}$ )

$$g = \frac{8\pi^2 C_2 \eta^n}{\rho_\ell} \quad (15)$$

$$a = C_1 C_d \frac{\rho_g V^2}{4\pi^2 \sigma} \quad (16)$$

The drag coefficient  $C_d$  is given in terms of the Reynolds number

$$Re = \frac{\rho_g V D_j}{\eta_g}, \quad (17)$$

by

$$\begin{aligned} C_d &= 27(Re)^{-0.84} && \text{for } 0 \leq Re \leq 80 \\ &= .271(Re)^{0.217} && \text{for } 80 \leq Re \leq 10^4 \\ &= 2 && \text{for } 10^4 \leq Re. \end{aligned} \quad (18)$$

Integrating expression (12) using (13) gives the mass flow  $\dot{M}$  of liquid droplets ( $\text{gm}/\text{cm}^2 - \text{sec}$ ) stripped from the liquid surface by the aerodynamic growth and breaking of waves with wavelengths between  $\lambda_1$  and  $\lambda_2$ , ( $\lambda_2 > \lambda_1$ ),

$$\dot{M} = \frac{K_2 \rho_\ell}{(\lambda_2 - \lambda_1)} \left[ \frac{f}{a} (B - A) - \frac{fE}{2a^{3/2}} - g \ln \frac{\lambda_2}{\lambda_1} \right] \quad (19)$$

where

$$E = \ln \left[ \frac{B + a^{1/2} \lambda_2 + \frac{1}{2a^{1/2}}}{A + a^{1/2} \lambda_1 + \frac{1}{2a^{1/2}}} \right] \quad (20)$$

and

$$A = (\lambda_1 + a\lambda_1^2)^{1/2} \quad (21)$$

$$B = (\lambda_2 + a\lambda_2^2)^{1/2}. \quad (22)$$

In evaluating expression (19),  $\lambda_1$  is to be considered the minimum wavelength wave,  $\lambda_{\min}$ , induced on the liquid surface. This is given by the smallest positive root of the equation

$$\dot{\gamma} = \frac{2}{\tau} = \frac{2f}{(\lambda + a\lambda^2)^{1/2}} - \frac{2g}{\lambda^2}. \quad (23)$$

The maximum wavelength,  $\lambda_{\max}$ , is currently given by\*

$$\lambda_{\max} = \frac{e}{v^{4/3}} D_j. \quad (24)$$

The smallest wavelength waves formed by stripping are eroded from the liquid surface at a finite shear rate  $\dot{\gamma}$ . Unfortunately, the value of this term is not known a priori, nor is the shear dependent viscosity  $\eta(\dot{\gamma})$  in the parameter  $g$ , for a non-Newtonian liquid. To circumvent this situation a critical value of  $\tau$  equal to  $\tau_c$  is evaluated using equation (11) given earlier, i.e.,

$$\tau_c = \tau_b = k \left( \frac{D_j}{v} \right) \left( \frac{\rho_l}{\rho_g} \right)^{1/2}. \quad (25)$$

This permits a solution to be obtained for  $\lambda_{\min}$  from expression (23).

By dividing the total wavelength range  $\lambda_{\min}$  to  $\lambda_{\max}$  into zones, the corresponding mass of droplets in each zone can be obtained from (19). The droplet diameter  $d$  corresponding to a wave of wavelength  $\lambda$  is given by the simple proportionality

$$d = F\lambda. \quad (26)$$

---

\* This expression represents a modification introduced recently to obtain better agreement with small jet breakup results.

Thus by solution of the preceding equations, the mass-size distribution of droplets stripped from the liquid surface can be calculated. Likewise, corresponding expressions exist to enable calculation of the frequency distribution.

It is apparent that the model is not fully predictive, but is phenomenological and requires that certain parameters be established to align predicted results with experimental findings. On the basis of previous work with the model, approximate values of these parameters are known, so this alignment process is usually rather straightforward. The fact that the model is phenomenological in nature greatly simplifies its mathematical details. Only the most important variables affecting liquid breakup need to be incorporated in order for the model to be effective in predicting breakup results for parameter values a considerable distance away from those of the alignment point(s).

A computer coded form of this complete model has been put on-line (separate from this program) and exploratory runs for Newtonian liquids have been made to indicate its potential usefulness in antimisting fuels correlations.

An example of a mass-size distribution obtained experimentally for hot wax in a hot gas stream by Weiss and Worsham<sup>45</sup> is shown in Figure V-5. The solid curve is the complete distribution predicted with the model.

In this example the model was matched to the experimental data at a mass-median diameter (MMD) of 70  $\mu\text{m}$ . The predicted shape of the distribution results directly from the built-in uniform probability density over wavelength for wave formation.

The model was also used to calculate the expected mass-size distributions for neat Jet A fuel injected contrastream into a free airflow at different relative air velocities. The parameters adopted in this case apply to the FAA Spray Flammability Test Apparatus, but the calculated distributions do not include effects of spray impaction on the walls of the breakup chamber. This impaction is expected to be a function of droplet size, spray geometry, and fuel tested. In this case the model was aligned using a single mass-median diameter calculated using the Weiss and Worsham expression, equation (10). The calculated MMD's for the relative velocities of 40, 50, 60 and 70 m/sec were 111, 83, 65 and 53  $\mu\text{m}$ , respectively. The results are shown in Figure V-6. The curves show that the expected mass-size distributions and the MMD's are both sensitive to relative velocity. Further, there is a rather large mass fraction of droplets in small sizes where ignition sensitivity is the greatest.

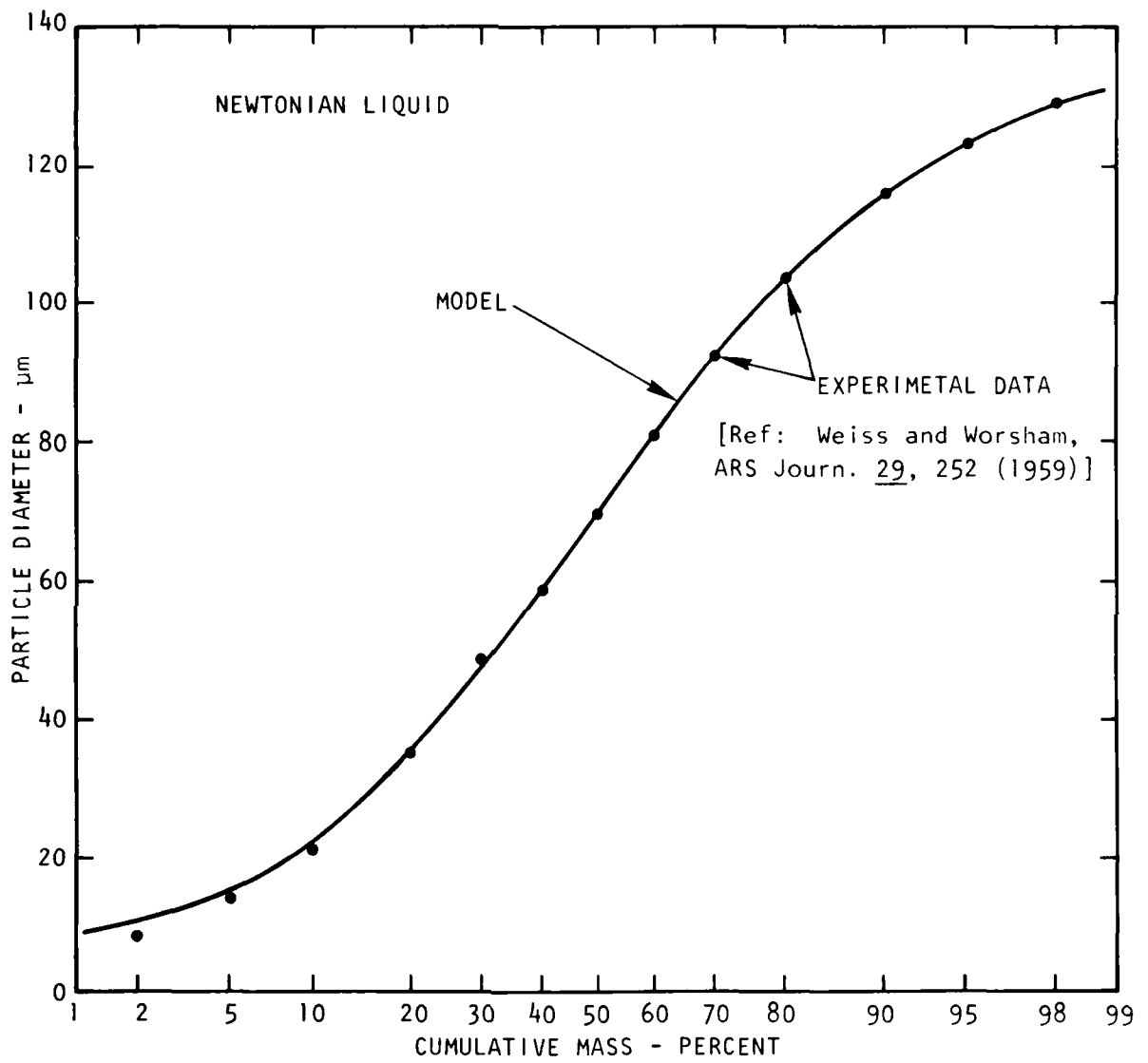


FIGURE V-5. BREAKUP MODEL PREDICTION VERSUS EXPERIMENTAL DATA

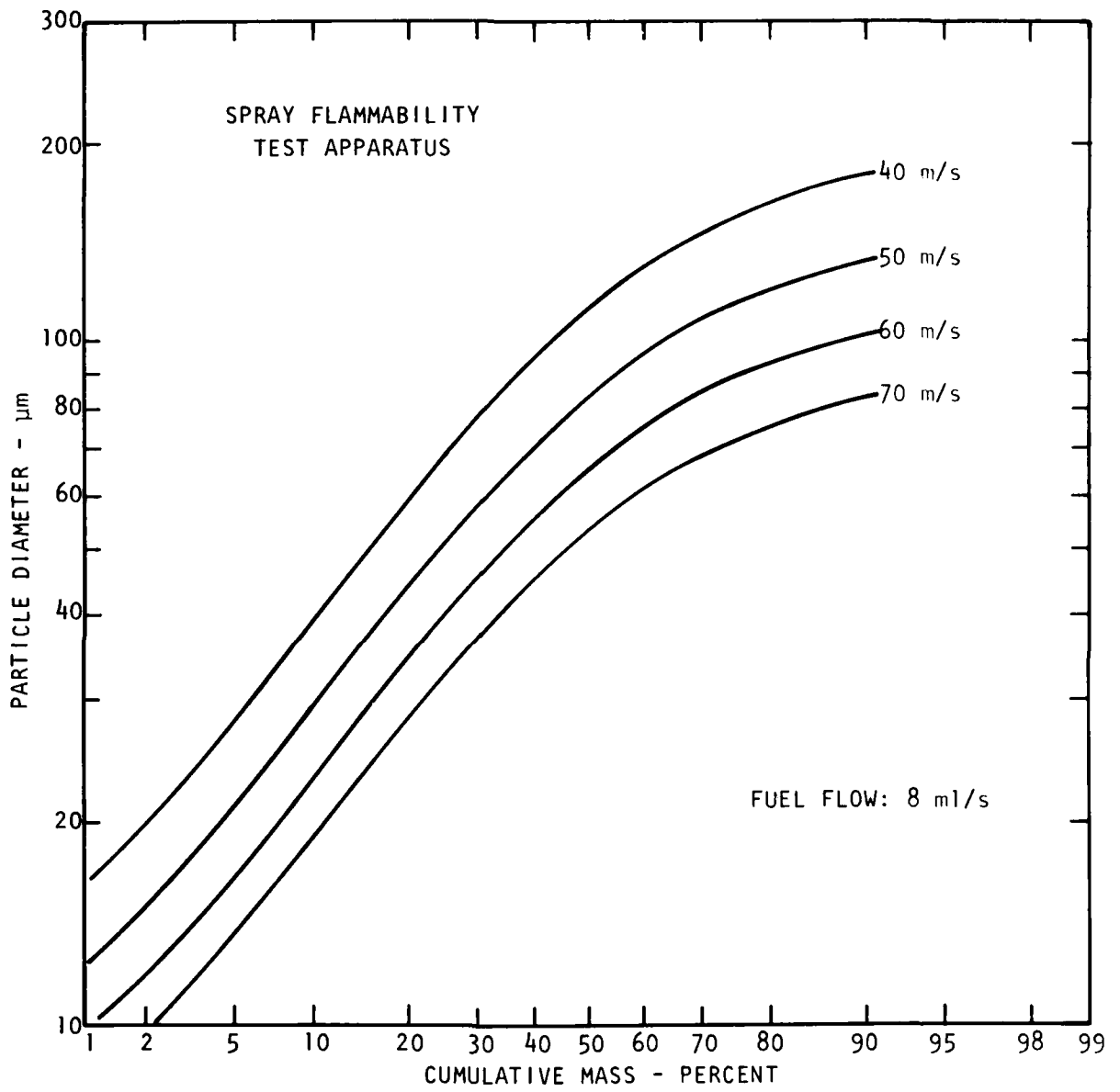


FIGURE V-6. NEAT JET A DROPLET DISTRIBUTION PREDICTIONS

Further calculations were made for neat Jet A in the same configuration to explore the sensitivity of the Spray Flammability Test Apparatus to pressure (and hence relative air-to-liquid velocity) decay during the course of single test runs. The basic information on pitot tube dynamic pressure decays and velocity decays determined experimentally at the FAA Technical Center were supplied by A. Ferrara. Simplified traces of the dynamic pressure decays for three air tank pressures are shown in Figure V-7, together with corresponding air velocity values determined at the beginning, marked central point, and end of the test runs.

The corresponding mass-size distributions for the beginning, midpoint, and of each of the test runs are shown in Figures V-8, V-9 and V-10. The relative velocities used in these calculations take into account the liquid injection velocity of 0.6 m/s. Since the air velocities change only slightly during the short time required for liquid breakup to occur, the instantaneous velocity at each time of interest was assumed to be constant for purposes of breakup computations.

The results shown in Figures V-8 through V-10 suggest that the size distribution changes during a single run may not be very significant for neat Jet A. This finding may not apply to tests conducted with antimisting fuels.

Application of the model in an illustrative sense to a full-scale crash test has also been made and these results are presented elsewhere in this report. The reader is cautioned not to place much credence in the results of calculations for that case, even though secondary breakup is taken into account, since the effects of Taylor breakup were not included.

The model is used in a final example to account for certain droplet breakup behavior actually observed in a configuration where sprays of FM-9 fuel were tested.<sup>60,67</sup> While this single example does not confirm the utility of this model in treating the breakup of a non-Newtonian liquid, we believe it is informative. Application of the model to this case has also led to findings which would be very difficult to ascertain otherwise.

The tests of interest are those conducted by Eklund<sup>60</sup> and Eklund and Cox<sup>67</sup> in which a small scale test configuration was used to form sprays of 0.3% FM-9 in Jet A. The FM-9 fuel was ejected through a 1/4 inch diameter tube (assumed to be 0.493 cm I.D.) costream into air flows of 200 mph and 285 mph in separate tests. Photographs were taken of the resulting drop sprays approximately 11-inches downstream from the liquid injection point.

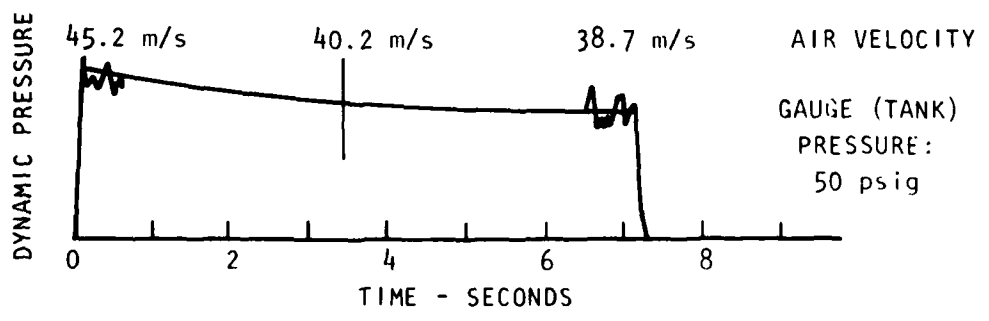
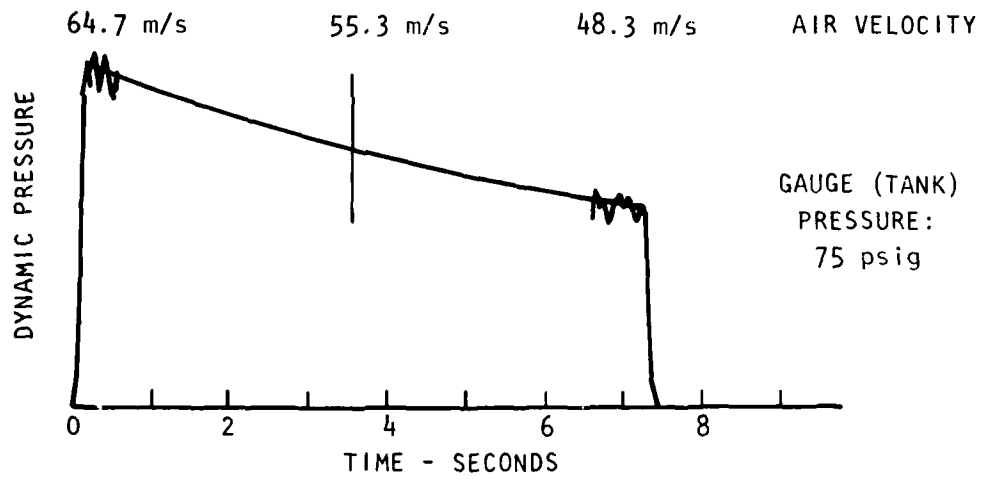
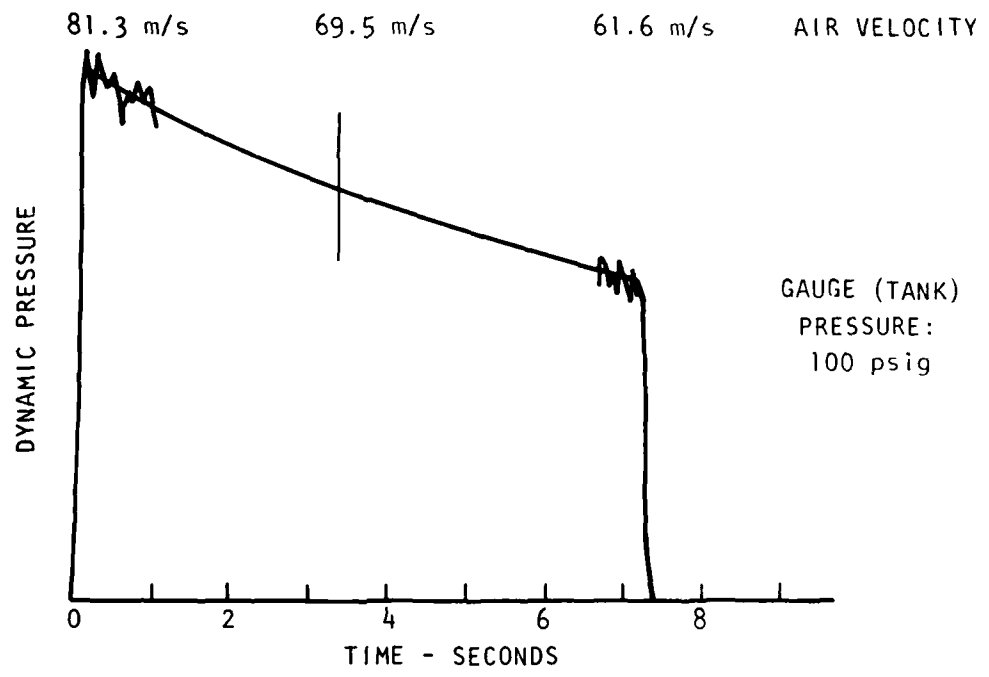


FIGURE V-7. DYNAMIC PRESSURE AND VELOCITY DECAY IN SPRAY FLAMMABILITY TEST APPARATUS

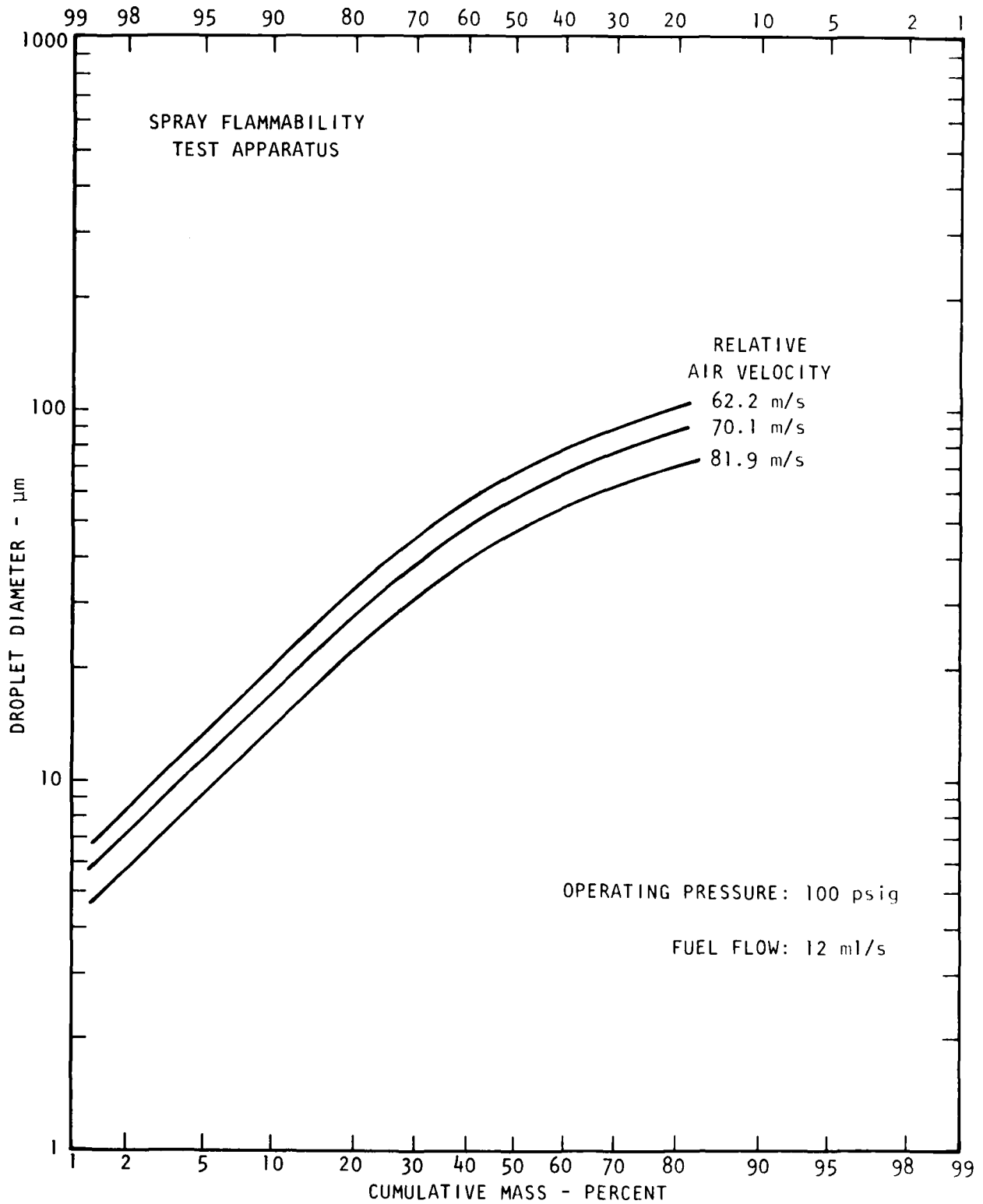


FIGURE V-8. DROPLET DISTRIBUTION DECAY PREDICTIONS FOR NEAT JET A, 100 PSIG

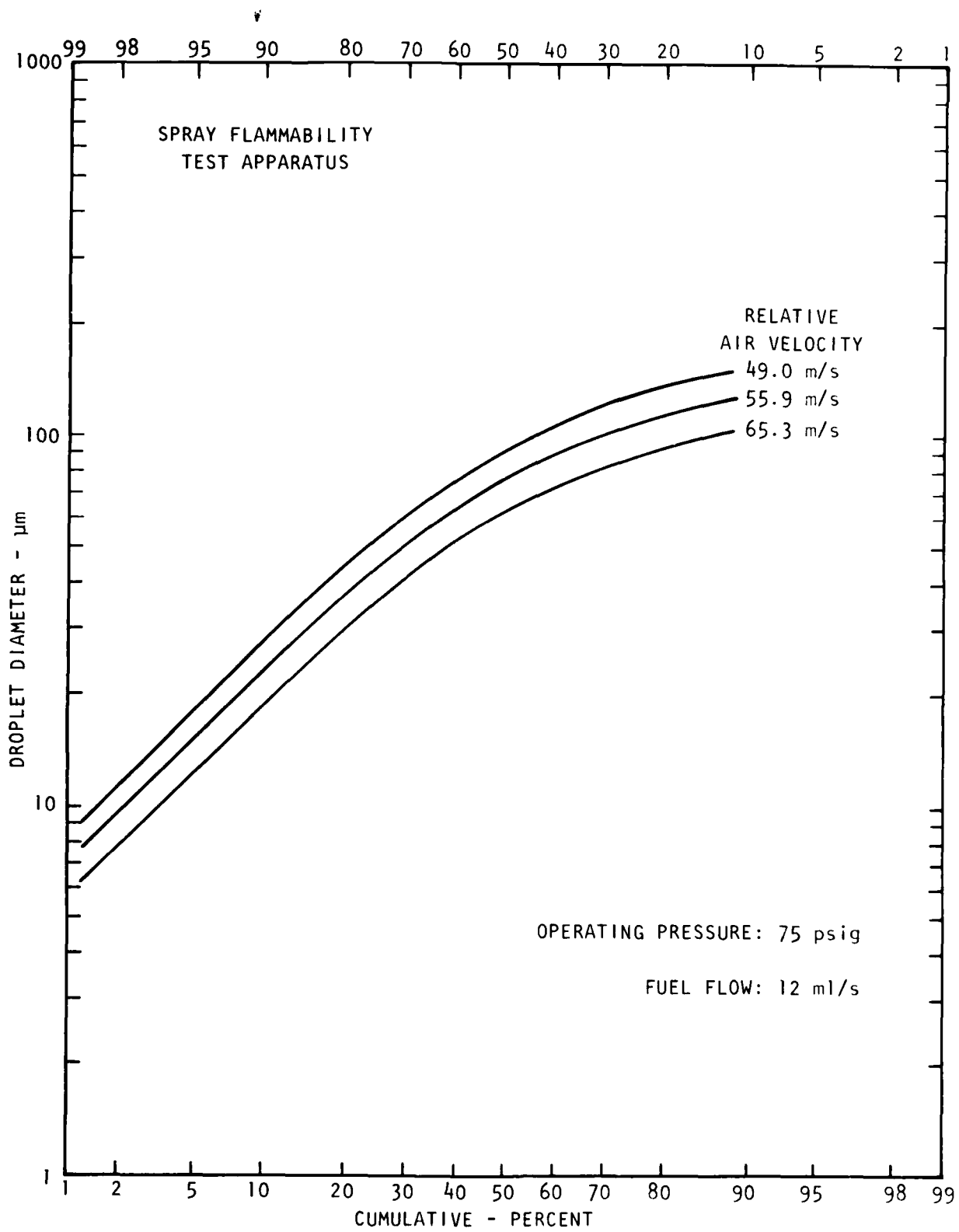


FIGURE V-9. DROPLET DISTRIBUTION DECAY PREDICTIONS FOR NEAT JET A, 75 PSIG

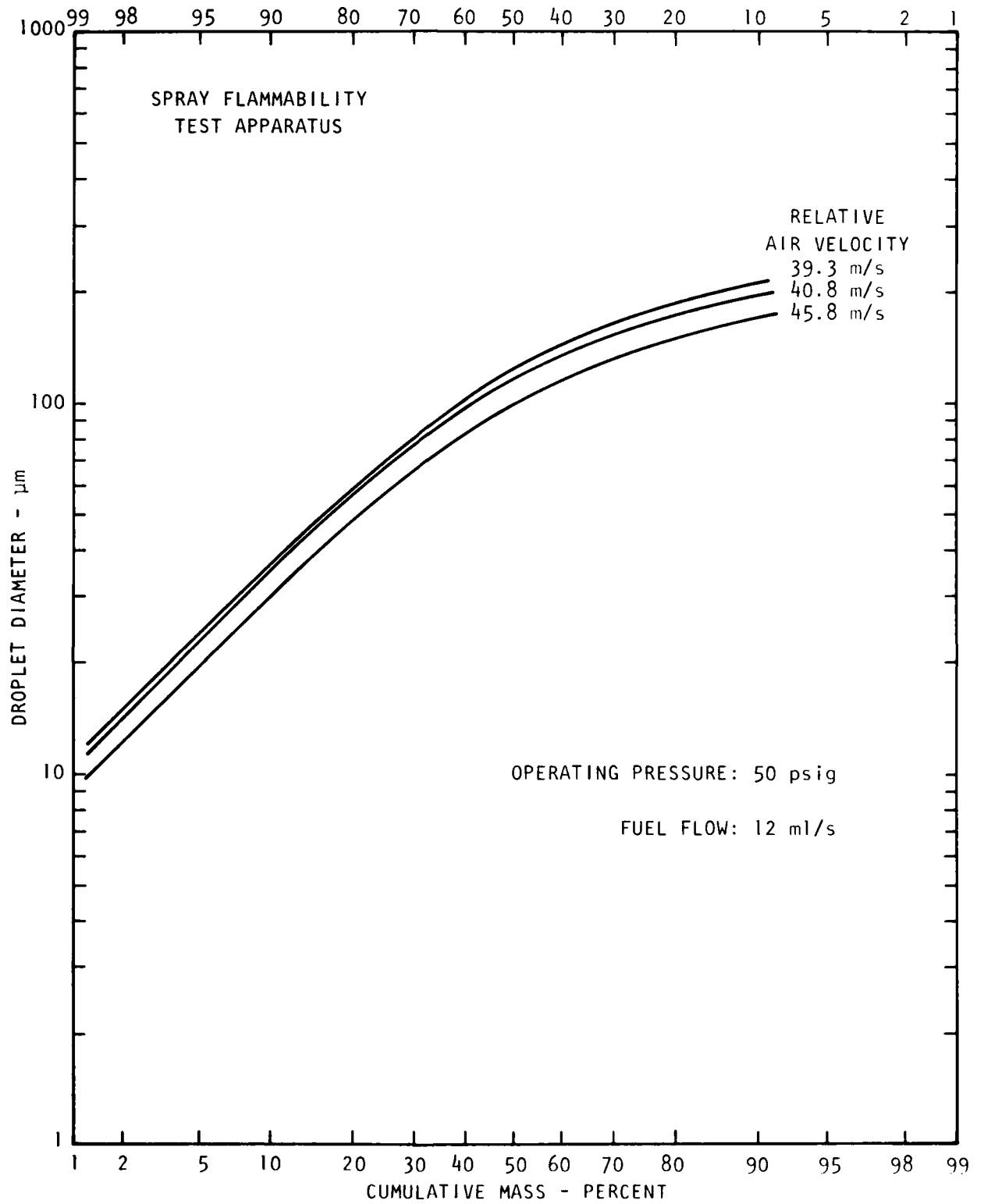


FIGURE V-10. DROPLET DISTRIBUTION DECAY  
PREDICTIONS FOR NEAT JET A, 50 PSIG

For purposes of calculations, the values of parameters assumed and used here are those given in the following table. These various quantities are defined in Table V-1, given earlier.

#### ASSUMED PARAMETER VALUES

Temperature (Fuel and Air)	T	= 75°F = 23.9°C
	$\rho_g$	= $1.189 \times 10^{-3}$ g/cm <sup>3</sup>
	$\mu_g$	= $184 \times 10^{-6}$ poise
	$\rho_f$	= .807 g/cm <sup>3</sup>
	$\sigma_f$	= 30 dynes/cm
	D <sub>j</sub>	= .493 cm
	C <sub>d</sub>	= 2.0

The apparent viscosity of the treated fuel is determined using a standard reduction technique<sup>29</sup> and the shear stress versus shear strain rate curve through points determined experimentally by Mannheimer.<sup>63</sup> The resultant shear-strain rate dependent viscosity is shown in Figure V-11. The lower critical shear strain rate point on this curve is taken as 3100 sec<sup>-1</sup> (as determined by Peng<sup>66</sup>) and the upper or second critical point (determined by Mannheimer<sup>63</sup>) is taken as about 8000 sec<sup>-1</sup>. For breakup, however, the second critical shear rate may lie anywhere in the shear rate range from the peak of the viscosity curve to the greater rate where the viscosity curve again levels out--at about 20,000 sec<sup>-1</sup> for the curve in Figure V-11. The viscosity in the low shear rate region is taken as 0.0298 poise (from Peng) and the peak viscosity at the second critical point is about 0.115 poise. After this critical point the viscosity is 0.050 poise at a shear rate of 20,000 sec<sup>-1</sup>. While the resulting viscosity curve of Figure V-11 represents a composite of experimental values, it is believed to quantitatively represent the major shear viscosity features of FM-9 fuel. Its accuracy in representing values of the fuel viscosity that were actually tested by Eklund is unknown. To proceed, it is assumed that this viscosity representation can be applied to Eklund's tests; small discrepancies may be attributable to errors in this assumption.

The general nature of the shear strain rate ( $\dot{\gamma}$ ) behavior of wind-induced instabilities of wavelength  $\lambda$  during stripping breakup of a Newtonian liquid are shown in Figure V-12. This is a plot of equation (23) for a Newtonian viscosity of 0.0298 poise and for different values of  $\lambda$ . Since the time  $t$  required for the relative wind to form and break a wave of wavelength  $\lambda$  from the surface of the jet is inversely related to  $\dot{\gamma}$ , the wavelengths for which values of  $\dot{\gamma}$  are the largest break more quickly than near the large and small wavelength

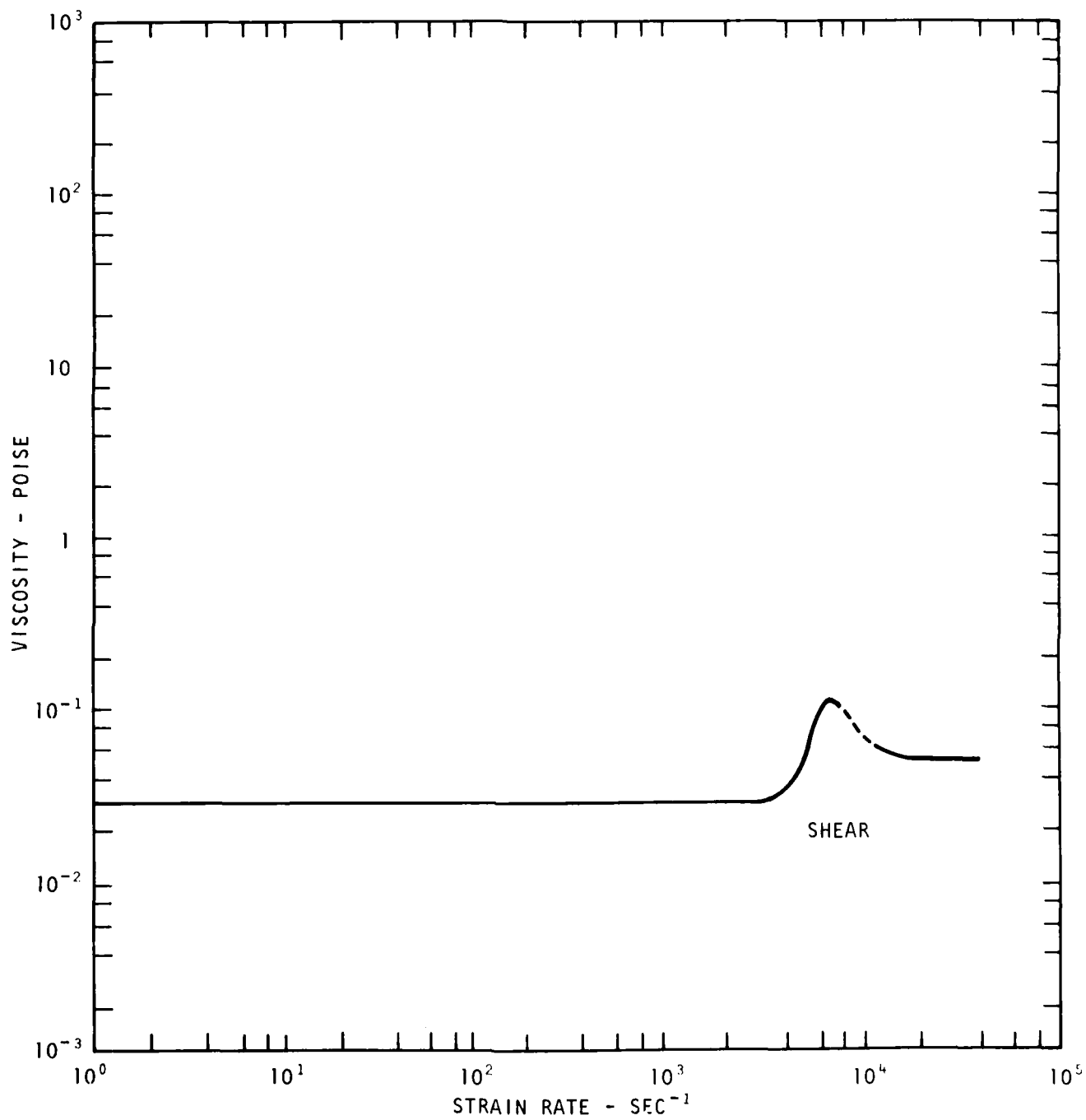
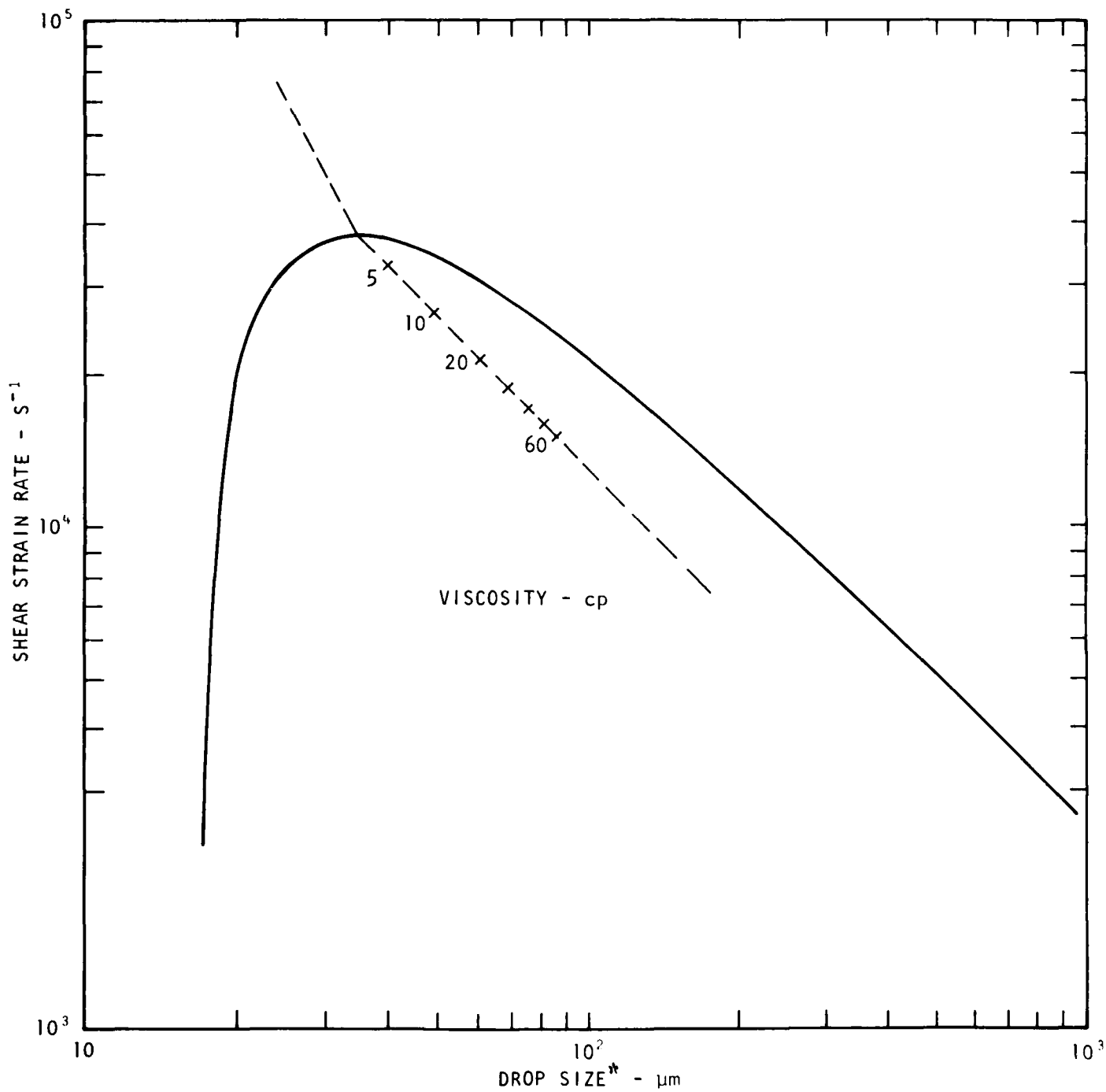


FIGURE V-11. SHEAR VISCOSITY OF 0.3% FM-9 IN JET A  
(FROM DATA OF REF. 63)



\*DROP SIZE IS DIRECTLY PROPORTIONAL TO WAVELENGTH  $\lambda$ .

FIGURE V-12. GENERAL SHEAR STRAIN RATE - DROPLET SIZE BEHAVIOR DURING STRIPPING BREAKUP OF A NEWTONIAN LIQUID

extremities of the curve. That is, the central wavelengths break first to form drops. The growth of short wavelength waves is retarded by viscous effects, whereas the growth of long wavelength waves is slowed by inertial effects.

The line with a scale emanating from the maximum of the curve indicates the locus of maxima of the curves corresponding to different viscosities. Since the shape, scale or orientation of the curve does not change appreciably when shifted in the  $\lambda$ - $\dot{\gamma}$  plane shown, a viscosity scale along the locus of maxima indicates the position of the maximum of a curve of a given viscosity.

The second line through the maximum of the curve indicates the locus of points of curves corresponding to different relative wind velocities. Points along the line for  $\dot{\gamma}$  values greater than the maximum of the curve apply to larger wind velocities than that for the curve shown.

The shear rate-wavelength behavior for the non-Newtonian FM-9 fuel involves additional considerations. The curve of Figure V-12 is based on the assumption that waves of different wavelengths grow and break independent of one another. In the case of a dilatant liquid, in particular, such as FM-9, this independence assumption needs to be tested. Currently available information on polymer treated fuels is inadequate to examine this issue, but this topic should be given consideration in future investigations.

The crux of the matter hinges on whether the fastest growing waves shear the entire surface layer of liquid exposed to the wind and hence increase the viscosity of this entire layer. If this occurs then the shorter wavelength disturbances generated on this surface might be expected to grow at a rate determined by the peak shear rate induced viscosity. On the long wavelength side of the fastest growing wavelength, some intermediate viscosity between that of the surface layer and that at a greater depth within the liquid may govern the wave growth.

The other extreme is that independence of growth of different wavelengths is maintained. In this case, the locus of possible shear states over wavelength can be determined by treating each point below the second critical point on the curve of Figure V-11 as if it were on a separate Newtonian viscosity curve at that shear strain rate.

When the wind driving force is adequate to shear FM-9 fuel at a rate in excess of the second critical rate, the shear rate-wavelength

behavior is essentially as if the liquid was near Newtonian. It is apparent, however, that a lower shear rate discontinuity exists at the value of the second critical point. As the maximum shear rate increases above this critical value, the peaks of the fixed viscosity Newtonian curves follow the upper dashed line. When the shear rate forces breakup to occur in this upper region and the time available is sufficiently long, all the liquid so sheared will break up in that region. That is, part of the liquid does not break at some lower shear strain rate below the second critical value, since the breakup time required there exceeds that at the critical value.

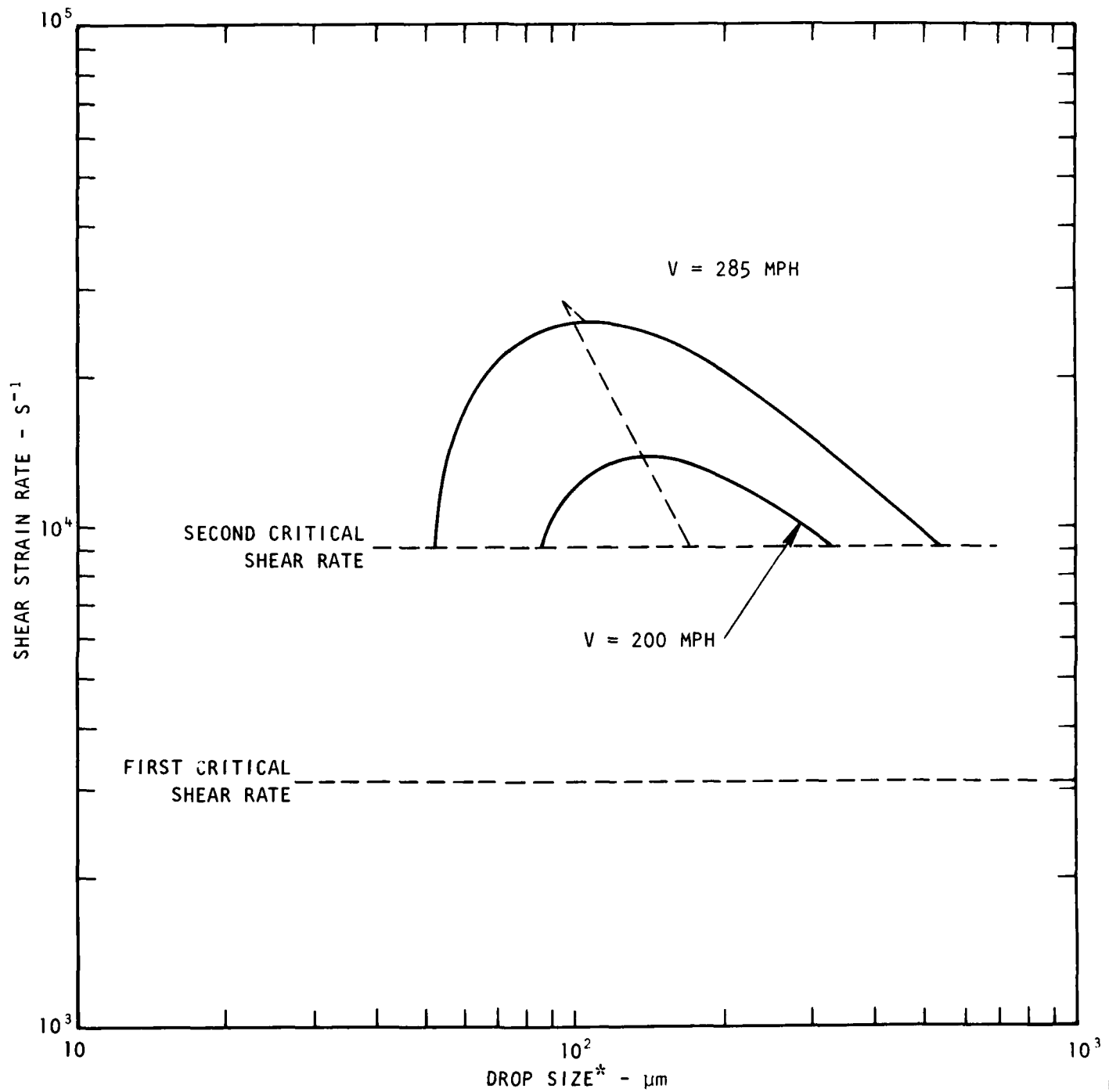
The two shear rate-wavelength curves (expressed in terms of drop size rather than wavelength by use of relation (26) with  $F = 0.08$ ) are shown in the upper region in Figure V-13. The lower curve is for a viscosity of 0.0298 poise; the upper (which is viscosity shifted) is a composite curve for a viscosity of 0.050 poise. These curves are self-consistent with each other, with the viscosity-shear rate values of Figure V-11, and with the breakup model. The location of the curves has been chosen so the model results closely represent the lower and upper limits of drop sizes produced in Eklund's tests. The situation obtained is not unique due to uncertainties in the values measured from spray photographs. The limits indicated by the curves and measured from photographs are indicated below:

Drop Size Limits	V = 200 mph		V = 285 mph	
	From Curves	From Photos	From Curves	From Photos
Lower	86 $\mu\text{m}$	90 $\mu\text{m}$	52 $\mu\text{m}$	50 $\mu\text{m}$
Upper	330 $\mu\text{m}$	350 $\mu\text{m}$	540 $\mu\text{m}$	500 $\mu\text{m}$

As can be seen, the agreement is not perfect, but it is remarkably close. It should be noted that this is not a comparison of predicted values with experiment. Rather, it is a match of theory to experiment in order to account for the experimental results.

There are several features of importance relative to this example.

1. The increase of the large drop size limit with increase of relative wind velocity is abnormal. From equations (24) and (26) the model indicates, and experiment confirms, that this upper size limit normally decreases with an increase in wind velocity. Here, however, the model itself also accounts for this abnormality; the latter arises from the discontinuity in liquid viscosity at the second critical shear strain rate.



\*DROP SIZE IS DIRECTLY PROPORTIONAL TO WAVELENGTH  $\lambda$ .

FIGURE V-13. COMPUTED BREAKUP OF 0.3% FM-9 IN JET A FOR SMALL JET EXPERIMENT OF EKLUND AND COX (REF. 67)

2. The model accounts for the breakup of the dilatant FM-9 fuel, with its peaked shear viscosity, using only shear viscosity considerations. In particular, the various effects indicated in this example and section do not indicate a need to invoke tensile or elongational viscosity to account for the breakup of FM-9 fuel. (Tensile viscosity may still be important to flow and intentional degradation aspects of FM-9 fuel, to the breakup of other types of treated fuels, and to the breakup of FM-9 fuel under prestrained conditions.)

3. The lower critical shear strain rate in the viscosity-shear rate curve is relatively unimportant insofar as representing a location where significantly different breakup effects begin to occur. The second critical shear strain rate, on the other hand, is quite important to breakup. Both actually represent key rheological parameters to be measured for a dilatant-type fuel. The upper parameter can serve to determine the drop size limits produced during liquid breakup.

4. The shear rate-wavelength behavior in the shear rate region below the second critical point is not well known at present for treated fuels, in view of uncertainties centering around wavelength independence of wave growth. This is a question of both theoretical and practical interest, as the small size portion of the spray drop spectrum is influenced by this result. This drop size regime, in turn, has a significant influence on spray ignition and flame propagation. It is expected that breakup phenomena in this region can be clarified by use of experimental data on drop size distributions, where the associated spray experiments are conducted with this goal in mind. Such experiments appear to be highly desirable in view of their potential importance to fuel spray combustion.

A final consideration before closing this example is how this explanation fits with the expected results obtained with other percentage loadings of FM-9 in Jet A fuel. Peng<sup>46</sup> has determined that the lower critical shear rate decreases with concentration increase according to the sequence: 6000 S<sup>-1</sup>, 3100 S<sup>-1</sup>, 2000 S<sup>-1</sup> and 700 S<sup>-1</sup>, corresponding to the respective concentrations 0.2%, 0.3%, 0.4%, and 0.8% of FM-9 with carrier fluid in Jet A (at 75°F). While values of the second critical shear rate are not known to have been measured as a function of concentration, it is expected that these values should increase as the concentration increases. Then, for a given air-to-liquid driving force, a sequence of increasing value of the critical shear rate would cut the shear rate-wavelength (or drop size) curve at successively higher values. The corresponding droplet size spectrum expected for breakup in the upper shear region would narrow, and the overall fire resistance of the fuel should improve.

This trend of improved fire resistance with increased value of the second critical shear rate has actually been observed and reported by Mannheimer<sup>63</sup>. He found that by introducing a suitable surfactant, both the lower and upper critical shear rate increased. The ignition resistance of the surfactant treated material was significantly improved over the 0.3% FM-9 treated Jet A without surfactant. The fact that the lower critical shear rate increased apparently had little effect--as one might now expect.

Further calculations for the purpose of data correlation of antimisting fuels were not made during this effort. There are several reasons for this. First, the computer model does not presently contain the physical model for Taylor breakup. This omission does not influence the results noted above for small jets as the Taylor breakup mechanism is not operative in these cases. Second, the existing data base of information on antimisting fuels appears inadequate regarding drop-size spectra produced in representative tests and weak in consistent rheological properties of the candidate antimisting fuels of interest. In absence of the latter, the adequacy of the model to account for the rheological behavior of various candidate antimisting fuels is not well known. The combination of data indicated could be used to ensure sufficiency of the model in terms of both rheology and breakup.

## REFERENCES

1. E. Mayer, "Theory of Liquid Atomization in High Velocity Gas Streams," ARS Journal, 31, pages 1783-1785 (1961).
2. K. J. DeJuhasz, Spray Literature Abstracts, Volumes I-IV, American Soc. Mechanical Engineers (1959-1969).
3. C. E. Lapple, J.P. Henry, and D. E. Blake, Atomization--A Survey and Critique of the Literature, Stanford Research Institute Technical Report SRI-PAU-4900 on Contract DA-18-035-AMC-122(A), Menlo Park, CA (April 1967).
4. C.C. Miesse, "Correlation of Experimental Data on the Disintegration of Liquid Jets," Ind. and Engr. Chem., 47(9), pages 1690-1701 (1955).
5. C. C. Miesse, "From Liquid Stream to Vapor Trail," Proc. Gas. Dynamics Symposium at Northwestern University, Evanston, IL, pages 7-26 (1956).
6. Lord Rayleigh, "On the Instability of Jets," Proc. London Math. Society, 10, pages 4-13 (1878); "On the Instability of a Cylinder of Viscous Liquid Under Capillary Force," Phil. Mag., 34, pages 145-154 (1882).
7. J.B. Keller, S.I. Rubinow, and Y.O. Tu, "Spatial Instability of a Jet," Phys. Fluids, 16(12), pages 2052-2055 (1973).
8. R. Betchov and W. O. Criminale, Stability of Parallel Flows, Academic Press, New York (1967).
9. C. Weber, Z. Angew, "On the Breakdown of a Fluid Jet," English Translation, Math. Mech., 11(2), pages 136-154 (1931), Ninth Progress Report, Project MX-833, Section II, University of Colorado, Boulder, CO.
10. R. P. Grant and S. Middleman, "Newtonian Jet Stability," AICHE Journal, 12(4) pages 669-678 (1966).
11. R. W. Fenn, III and S. Middleman, "Newtonian Jet Stability: The Role of Air Resistance," AICHE Journal, 15(3), pages 379-383 (1969).
12. F. W. Kroesser and S. Middleman, "Viscoelastic Jet Stability," AICHE Journal, 15(3), pages 383-386 (1969).

13. R. E. Phinney, "Stability of a Laminar Viscous Jet--The Influence of the Initial Disturbance Level," AICHE Journal, 18(2), pages 432-434 (1972).
14. M. Goldin, J. Yerushalmi, R. Pfeffer, and R. Shinnar, "Breakup of a Laminar Capillary Jet of a Viscoelastic Fluid," J. Fluid Mech., 38(4), pages 689-711 (1969).
15. M. Gordon, J. Yerushalmi, and R. Shinnar, "Instability of Jets of Non-Newtonian Fluids," Trans. Soc. Rheol., 17(2), pages 303-324 (1973).
16. A. S. Lodge, Elastic Liquids, Academic Press, New York, page 117 (1964).
17. K. Walters, Rheometry, Chapman and Hall, London, page 219 (1975).
18. W. R. Schowalter, Mechanics of Non-Newtonian Fluids, Pergamon Press, New York, page 220 (1978).
19. L. M. Milne-Thomson, Theoretical Hydrodynamics, 3rd Edition, MacMillan Co., New York (1955).
20. B. Kinsman, Wind Waves, Prentice-Hall, Englewood Cliffs, NJ (1965).
21. H. B. Squire, "Investigation of the Instability of a Moving Film," Brit. J. Appl. Phys., 4, pages 167-169 (1953).
22. W. W. Hagerty and J. F. Shea, "A Study of the Stability of Plane Fluid Sheets," J. App. Mech., 22, pages 509-514 (1955).
23. J. L. York, H. E. Stubbs, and M. R. Tek, "The Mechanism of Disintegration of Liquid Sheets," Trans. ASME, 75, pages 1279-1286 (1953).
24. N. Dombrowski and W. R. Johns, "The Aerodynamic Instability and Disintegration of Viscous Liquid Sheets," Chem. Eng. Sci., 18, pages 203-214 and 470 (1963).
25. N. Dombrowski, P. Eisenklam, and R. P. Fraser, "Flow and Disintegration of Thin Sheets of Viscoelastic Fuels," J. Inst. Fuel, 1, pages 399-406 (1957).
26. R. E. Ford and C. G. L. Furnidge, "The Formation of Drops from Viscous Water-in-Oil Emulsions Sprayed Through Fan-Jet Nozzles," Brit. J. Appl. Phys., 18, pages 491-501 (1967).

27. L. E. Nielsen, Polymer Rheology, Dekker, New York (1979).
28. R. P. Fraser, "Liquid Atomization," J. Roy. Aero. Soc., 65 pages 749-755 (1961).
29. A. H. P. Skelland, Non-Newtonian Flow and Heat Transfer, Wiley, New York (1967).
30. A. C. Merrington and E. G. Richardson, "The Breakup of Liquid Jets," Proc. Phys. Soc., London, 59(1), pages 1-13 (1947).
31. J. O. Hinze, "Forced Deformations of Viscous Liquid Globules," Appl. Sci. Res., A1, pages 263-270 (1949).
32. J. O. Hinze, "Critical Speeds and Sizes of Liquid Globules," Appl. Sci. Res., A1, pages 273-288 (1949).
33. Lord Rayleigh, Theory of Sound, Volume II, Dover, New York, page 373 (1945).
34. W. H. Andersen and H. E. Wolfe, Kinetics, Mechanism, and Resultant Droplet Sizes of the Aerodynamic Breakup of Liquid Drops, Report No. 0395-04(18)SP, Aerojet General Corp., Downey, CA (April 1964).
35. R. A. Castleman, Jr., The Mechanism of Atomization Accompanying Solid Injection, NACA Report No. 440 (1932).
36. W. R. Lane, "Shatter of Drops in Streams of Air," Ind. Eng. Chem., 43(6), pages 1312-1317 (1951).
37. G. D. Gordon, "Mechanism and Speed at Breakup of Drops," J. Appl. Phys., 30, pages 1759-1761 (1959).
38. A. R. Hanson, F. G. Domich, and H. S. Adams, "Shock Tube Investigation of the Breakup of Drops by Air Blasts," Phys. Fluids, 6, pages 1070-1080 (1963).
39. O. G. Engel, "Fragmentation of Water Drops in the Zone Behind an Air Shock," J. Res. Nat. Bur. Standards, RP 2843, 60(3), pages 245-280 (1958).
40. A. A. Ranger and J. A. Nicholls, "Aerodynamic Shattering of Liquid Drops," AIAA Journ., 7, pages 285-290 (1969).
41. B. J. Clark, Breakup of a Liquid Jet in a Transverse Flow of Gas, NASA Technical Note TN-D-2424 (August 1964).

42. G. Morrell, Rate of Liquid Jet Breakup by a Transverse Shock Wave, NASA Technical Note D-1728 (May 1963).
43. G. Morrell and F. P. Povinelli, Breakup of Various Liquid Jets by Shock Waves and Applications to Resonant Combustion, NASA Technical Note TN9-2423 (August 1964).
44. A. Sherman and J. Schetz, "Breakup of Liquid Sheets and Jets in a Supersonic Airstream," AIAA Journ., 9(4), pages 666-673 (1971).
45. M. A. Weiss and C. H. Worsham, "Atomization in High Velocity Airstreams," ARS Journal, 29, pages 252-259 (1959).
46. W. H. Andersen, N. A. Louie, and G. Ialongo, Investigation of the Aerodynamic Breakup of Viscoelastic Liquids. Phase I-- Subsonic Dissemination, Contractor Report ARCSL-CR-77037 (August 1977).
47. S. Chandrasekhar, Hydrodynamic and Hydromagnetic Stability, Clarendon Press, Oxford (1961).
48. G. I. Taylor, "The Instability of Liquid Surfaces When Accelerated in a Direction Perpendicular to Their Planes," Proc. Roy. Soc., A201, pages 192-192 (1950).
49. D. J. Lewis, "The Instability of Liquid Surfaces When Accelerated in a Direction Perpendicular to Their Planes. II," Proc. Roy. Soc., A202, pages 81-96 (1950).
50. J. B. Keller and I. Kolodner, "Instability of Liquid Surfaces and the Formation of Drops," J. Appl. Phys., 25(7), pages 918-921 (1954).
51. R. Bellman and R. H. Pennington, "Effects of Surface Tension and Viscosity on Taylor Instability," Quart. J. Appl. Math., 12(2), pages 151-162 (1954).
52. W. G. Reinecke and G. D. Waldman, A Study of Drop Breakup Behind Strong Shocks With Applications to Flight, SAMSO-TR-70-142, AVCO Systems Division (May 1970).
53. P. G. Simpkins and E. L. Bales, "Water-Drop Response to Sudden Accelerations," J. Fluid Mech., 55(4), pages 629-639, (1972).
54. E. Y. Harper, G. W. Grube, and I-Dee Chang, "On the Breakup of Accelerating Liquid Drops," J. Fluid Mech., 52(3), pages 565-591 (1972).

55. S. V. Zinn, Jr., T. I. Eklund, and W. E. Neese, Photographic Investigations of Modified Fuel Breakup and Ignition, Report No. FAA-RD-76-109, NAFEC, Atlantic City, New Jersey, September 1976.
56. R. J. Mannheimer, Rheology Study of Antimist Fuels, Report No. FAA-RD-77-10, Southwest Research Institute for FAA Systems Research and Development Service, January 1977.
57. A. F. Taylor, Notes on the Flow of Viscoelastic Fuels Through Pipes and Orifices, College of Aeronautics, Cranfield Institute of Technology, January 1973.
58. S. T. J. Peng and R. F. Landel, "Preliminary Investigation of Elongational Flow of Dilute Polymer Solutions," J. Appl. Phys., 47(10), pages 4255-4259 (1976); and Errata, J. Appl. Phys., 50(7), page 5883 (1979).
59. R. Coomber, I. Faul, and S. P. Wilford, Measurement of the Extensional Viscosity of Safety Fuels by Jet-Thrust and Triple-Jet Techniques, RAE, Technical Report No. 77157, October 1977.
60. T. I. Eklund, Experimental Scaling of Modified Fuel Breakup, Report No. FAA-RD-77-114, NAFEC, Atlantic City, New Jersey, August 1977.
61. T. I. Eklund and W. E. Neese, Design of an Apparatus for Testing the Flammability of Fuel Sprays, Report No. FAA-RD-78-54, NAFEC, Atlantic City, New Jersey, May 1978.
62. I. Faul, An Investigation Into Jet Droplet and Spray Behavior of Safety Fuels, RAE Technical Report No. 78131, November 1978.
63. R. J. Mannheimer, Influence of Surfactants on the Fuel Handling and Fire Safety Properties of Antimisting Kerosene (AMK), Southwest Research Institute for FAA Systems Research and Development Service, February 1979. (FAA-RD-79-62)
64. V. Sarohia and R. F. Landel, Influence of Antimisting Polymer in Aviation Fuel Breakup, Jet Propulsion Laboratory, AIAA/SAE/ASME, 16th Joint Propulsion Conference, June 30-July 2, 1980.
65. S. P. Wilford supplied recent data on elongational viscosities of FM-9 in Avtur prior to publication.
66. S. T. J. Peng, Rheological Behavior of AMK, Jet Propulsion Laboratory, Presentation, March 24-26, 1980.

67. T. I. Eklund and J. C. Cox, Flame Propagation Through Sprays of Antimisting Fuels, Report No. NA-78-66-LR, NAFEC, Atlantic City, New Jersey, November 1978.
68. J. W. Hoyt, J. J. Taylor, and R. L. Altman, "Drag Reduction--Jet Breakup Correlation with Kerosene-Based Additives," Journal of Rheology, 24(5), pages 685-699 (1980).
69. J. T. Davies, Turbulence Phenomena, Academic Press, New York, Chapter 7, 1972.
70. M. Adelberg, "Breakup Rate and Penetration of a Liquid Jet in a Gas Stream," AIAA Journ. 5, pages 1408-1415 (1967).
71. M. Adelberg, "Mean Drop Size Resulting from the Injection of a Liquid Jet into a High Speed Gas Stream," AIAA Journ. 6, pages 1143-1147 (1968).

## VI. CONCLUSIONS

1. The ability of certain antimisting fuels (AMF's) to minimize the post-crash fire hazard is amply supported by accumulated test data. Full- and large-scale crash simulations are highly developed, and provide essential credibility and data on a given AMF near the end of its evaluation cycle. However, the unavoidable complexity and expense of large-scale testing precludes its use in the screening of all AMF formulations and their iterations.
2. Small-scale flammability test rigs developed for screening AMF's have advantages of simplicity, high data production rate, and relatively low initial and operating costs. The data base each test rig generates is generally self-consistent and repeatable.
3. Results from the various small-scale flammability test rigs generally agree where there are substantial differences between fuels; e.g., when comparing (1) neat Jet A with an AMF, or (2) a marginal AMF with a very effective one. This is to be expected, since, in the development of a given fire test rig, intuitive aspects of the design are often adjusted based on the performance of neat fuel and "known-effective" AMF's--in effect, using these fuels as informal standards. The assumption is that wake flames or fireballs larger than those experienced with the "standard" AMF indicate a candidate that will be inferior in a real-world crash (or large-scale test).
4. Small-scale flammability test rigs have given conflicting results when comparing two AMF's lacking a wide differentiation in performance--one reversing the relative ranking of the other. Similar conflict between a small-scale and a large-scale flammability rig has also been encountered--undermining the credibility of the small-scale rig involved. It is not economically feasible to perform large-scale flammability tests every time two small-scale rigs conflict. The conclusion is evident that improvements in the resolution and consistency of small-scale flammability test rigs are highly desirable to (1) support optimization of AMF formulations, (2) confidently and consistently evaluate AMF performance versus such factors as additive concentration, storage time and degradation, and (3) minimize the need for large-scale testing for ranking AMF's.
5. The basic problem in developing small-scale flammability test rigs for AMF is the lack of design criteria related to liquid breakup phenomenology and scaling. It is only recently that preliminary understandings and models of liquid breakup have emerged. It is possible that a "dynamic bias" may inadvertently exist in a

given small-scale test rig; i.e., its peculiar combination of flow, ejection, and/or breakup dynamics may affect some AMF candidates more adversely than others--compared to their large-scale rankings.

6. Various AMF's have significantly different breakup characteristics; e.g., relative sensitivity to shear versus elongational strains and stresses. In addition, sensitivity to flow and pressure history prior to ejection can vary markedly between AMF's. It is concluded that each AMF must be thoroughly examined as to its rheological behavior under the flow and breakup conditions imposed by the flammability test rigs.

7. Based on the work presented in this report, it is now feasible and most effective to exploit current liquid breakup technology and appropriate particle measuring instrumentation in order to (a) quantitatively characterize the liquid breakup products of flammability test rigs of interest, and (b) relate the dynamic physical characteristics of a given test rig to the phenomena and products of liquid breakup. It is concluded that a semi-empirical model which addresses both large- and small-scale liquid AMF breakup would facilitate individual rig analysis and collective correlation of selected test rigs.

8. On the basis of successful liquid breakup characterization, combustion technology and related semi-empirical models can be utilized to quantitatively relate the combustion responses of small-scale flammability test rigs and their related pass/fail criteria to large-scale fireball evaluations and criteria.

**END**

**FILMED**

**6-83**

**DTIC**